Functions of the DEAH-box helicase DHX36 in type I interferon signaling

Doctoral thesis

to obtain a doctorate (PhD)

from the Faculty of Medicine

of the University of Bonn

Daniel Hilbig

from Menden (Sauerland), Germany 2023

Written with authorization of				
the Faculty of Medicine of the University of Bonn				
First reviewer:	Prof. Dr. Katrin Paeschke			
Second reviewer:	Prof. Dr. Oliver Gruss			
Day of oral examinat	ion: 27.10.22			
For the clinic and pol	For the clinic and policlinic for Translationale Onkologie, Medizinische Klinik III,			
Director: Prof. Dr. Peter Brossart				

Table of Contents

Table	of Co	ntents	3
List of	f abbr	eviations	7
1. Ir	ntrodu	ction	13
1.1	Ch	allenges of an increasing population	13
1	.1.1	Pandemics of human history	13
1.2	Vira	al life cycles	14
1.3	The	e innate immune system	15
1	.3.1	Pattern recognition receptors and adaptors	17
1	.3.2	Viral RNA-induced TLR signaling cascades	19
1	.3.3	Viral RNA-induced RLR signaling cascades	21
1	.3.4	Interferon regulatory factors (IRFs)	22
1	.3.5	Nuclear factor kappa-light-chain-enhancer of activated B-cells (NF-κB)	23
1	.3.6	Interferons and the IFN-β enhanceosome	24
1	.3.7	The type I IFN-induced JAK-STAT pathway	25
1	.3.8	Interferon-stimulated genes (ISGs)	26
1	.3.9	The distinction of self and non-self (ADAR1)	29
1.4	G-d	quadruplexes	30
1.5	The	e DEAH-box helicase DHX36	32
1	.5.1	The structure of DHX36	33
1	.5.2	G-quadruplex unwinding by DHX36	34
1	.5.3	The maintenance of homeostasis by DHX36	34
1	.5.4	Innate immunity regulation by DHX36	36
1.6	Ain	n of the study	39
2. N	/lateria	al and methods	40
2.1	Ba	cteria cell culture	40

2.1.1	Cultivation of bacteria	40
2.1.2	Cryo-conservation of bacteria	40
2.1.3	Preparation of chemical-competent E. coli	40
2.1.4	Transformation of plasmid DNA in bacteria	40
2.2 Eu	karyotic cell culture	41
2.2.1	Cultivation of adherent eukaryotic cells	41
2.2.2	Cryo-conservation of eukaryotic cells	41
2.2.3	Thawing of cryo-conserved eukaryotic cells	41
2.2.4	Generation of stable eukaryotic cell lines	42
2.2.5	Stress treatments of eukaryotic cells	42
2.2.6	CRISPR/Cas9-mediated gene knockout in eukaryotic cells	43
2.2.7	Lentiviral production for CRISPR/Cas9	43
2.2.8	Light microscopy	44
2.2.9	Growth analysis of adherent eukaryotic cells	44
2.2.10	MTT proliferation assay	44
2.2.11	FACS (Fluorescence-activated cell sorting)	44
2.3 DN	IA biochemistry	45
2.3.1	Preparation of plasmid DNA	45
2.3.2	Polymerase Chain Reaction (PCR)	45
2.3.3	Agarose gel electrophoresis	46
2.3.4	Purification of DNA from agarose gels and PCR reactions	46
2.3.5	Restriction digest of DNA	46
2.3.6	DNA ligation	46
2.3.7	Single-colony Polymerase Chain Reaction (scPCR)	46
2.3.8	DNA sequencing	47
2.4 Pro	otein biochemistry	47

	2.4	ŀ.1	Protein isolation from eukaryotic cells	47
	2.4	.2	Bradford assay	48
	2.4	1.3	Co-immunoprecipitation (Co-IP)	48
	2.4	.4	SDS-polyacrylamide gel electrophoresis (SDS-PAGE)	48
	2.4	.5	Western blot	49
	2.5	RN	A biochemistry	49
	2.5	5.1	RNA purification from human cells	49
	2.5	5.2	Reverse transcription (cDNA synthesis)	50
	2.5	5.3	Quantitative Polymerase Chain Reaction (qPCR)	50
	2.6	Oth	ners	51
	2.6	5.1	RNA-sequencing	51
	2.6	5.2	Fluorescence staining of stress granules (G3BP)	51
3.	Re	sults	3	52
	3.1	DH	X36 is necessary for the maintenance of cellular homeostasis by inhibit	ing
	an ur	ncon	trolled type I interferon response	52
	3.2	Los	ss of DHX36 results in increased type I IFN signaling	55
	3.3	DH	X36 negatively regulates type I IFN signaling	57
	3.4	The	e ablation of DHX36 augments stress tolerance and viral resistance	59
	3.5	DH	X36 acts early in type I IFN signaling	63
	3.6	DH	X36 negatively regulates PKR-induced type I IFN signaling	65
	3.7	The	e primed cell status upon the loss of DHX36 is independent of PKR	68
	3.8	DH	X36 interacts with PKR and ADAR1 in an RNA-dependent manner	69
	3.9	Inc	reased type I IFN response is mediated by DHX36 rather than by rG4s	73
4.	Dis	cus	sion	75
	4.1	Los	ss of DXH36 leads to an increased type I IFN signature	77
	4.2	DH	X36 is a negative regulator of type I IFN signaling	80

4	1.3	DHX36, a negative regulator of PKR	82	
2	1.4	PKR and ADAR1, interaction partners of DHX36	84	
4	1.5	DHX36: Stress granule functions and anti-viral effects	86	
2	1.6	The role of rG4-dependent DHX36 functions in type I IFN responses	87	
2	1.7	DHX36, a possible target for cancer therapy	89	
4	1.8	A model for DHX36 functions during viral signaling in HEK cells	91	
4	1.9	Concluding remarks	93	
5.	Ab	stract	95	
6.	Su	pplementary figures	96	
6	6.1	Supplementary figures	96	
7.	Lis	t of figures and tables	97	
8.	Tal	Гables99		
9.	Re	ferences	104	
10	А	cknowledgements	121	

List of abbreviations

2-5A 2`-5` oligoadenylates

3p-shRNA 5`-triphosphorylated short hairpin dsRNA ligand

4SU 4-thiouridine

aa Amino acid

ADAR1 Adenosine deaminase acting on RNA 1

AIDS Acquired immunodeficiency syndrome

APOBEC Apolipoprotein B mRNA editing enzyme catalytic subunit

AP Activator protein

ARE AU-rich element

ATP Adenosine triphosphate

avSG Anti-viral stress granule

CARD Caspase activation and recruitment domain

ChIP Chromatin immunoprecipitation

CLR C-type lectin receptor

CoIP Co-immunoprecipitation

CSV Chum salmon reovirus

CTE C-terminal extension

CXCL10 C-X-C motif chemokine ligand 10

DBD DNA-binding domain

DC Dendritic cell

DEAD Aspartate-glutamate-alanine-aspartate

DEAH Aspartate-glutamate-alanine-histidine

DDX DEAD-box helicase

DHX DEAH-box helicase

dG4 DNA G-quadruplex

DNA Deoxyribonucleic acid

ds Double-stranded

DSM DHX36 specific motif

EBOV Ebola virus

ELAVL1 embryonic lethal and abnormal vision-like protein 1

eIF2α Eukaryotic translation initiation factor 2 subunit

EMCV Encephalomyocarditis virus

FACS Fluorescence activated cell sorting

G3BP1 Ras GTPase-activating protein-binding protein 1

G4 G-quadruplex

HCV Hepatitis C virus

HEK Human embryonic kidney

HIV Human immunodeficiency virus

hnRNP Heterogeneous nuclear ribonucleoproteins

HSV Herpes simplex virus

hTERC Human telomerase RNA component

IAD IRF association domain

IAV/IBV influenza A or B virus

IFIT Tetratricopeptide repeats

IFN Interferon

IFNAR IFN-α/β receptor

IFNGR IFN-γ receptors

IkB Inhibitor of kB

IKK inhibitor of kB kinase-related kinase

IL Interleukin

ILF3 Interleukin enhancer binding factor 3

IRAK Interleukin-1 receptor-associated kinase

IRF Interferon-regulatory factor

IRF-E IRF binding element

ISG Interferon stimulated gene

ISGF Interferon stimulated gene factor

ISRE Interferon-stimulated response element

JAK Janus kinase

JNK c-Jun N-terminal kinase

KO Knockout

LGP2 Laboratory of genetics and physiology 2

IncRNA Long non-coding RNA

LRR Leucine-rich repeat

MAPK Mitogen-activated protein kinases

MAVS Mitochondrial antiviral signaling proteins

MDA5 Melanoma differentiation-associated protein 5

mDC Myeloid dendritic cells

MEF Mouse embryonic fibroblasts

miRNA Micro RNA

mRNA Messenger ribonucleic acid

MV Measles virus

MyD88 Myeloid differentiation primary response 88

NF-kB Nuclear factor kappa-light-chain enhancer of activated B cells

NAP NF-κB-activating kinase-associated protein

NDV Newcastle disease virus

NEMO NF-κB essential modifier

NLR Nucleotide-binding domain, leucine-rich repeat containing receptors

NLS Nuclear localization site

NPC Neuronal progenitor cells

OAS Oligoadenylate synthetase

OASL OAS-like

OB Oligonucleotide and oligosaccharide-binding-fold-like

PAM Porcine primary pulmonary macrophages

PAMP Pathogen-associated molecular pattern

PAR CLIP Photoactivatable-ribonucleoside-enhanced crosslinking and immune-

precipitation

pDC Plasmacytoid dendritic cells

PhpC Phenylpyrrolocytosine

PKR Protein kinase R

Pol-II Polymerase II

pp Diphosphate

ppp Triphosphate

Poly (I:C) Polyriboinosinic:polyribocytidylic acid

PRD Positive regulatory domains

PRR Pattern recognition receptors

PRRSV Respiratory syndrome virus

RBP RNA binding protein

RD Repressor domain

RHD Rel-homology domain

RIG-I Retinoic acid-inducible gene I

RIP Receptor-interacting protein

rG4 RNA G-quadruplex

RHAU RNA helicase associated with AU-rich elements

RL Ratchet-like

RLR RIG-I-like receptors

RNA Ribonucleic acid

RNAi RNA interference

RNase L Ribonuclease L

RNA-seq Next generation RNA sequencing

RNU6 RNA, U6 small nuclear 1

RSAD2 Radical S-adenosyl methionine domain-containing protein 2

SARS-CoV Respiratory syndrome coronavirus variant

SeV Sendai virus

SF Superfamiliy

SFV Semliki Forest virus

SG Stress granule

siRNA Small interfering RNA

SOCS Suppressor of cytokine signaling

ss Single-stranded

STAT Signal transducer and activator of transcription

SVCV Spring viremia of carp virus

TANK TRAF family member-associated NF-kB activator

TAK Transforming growth factor-β activated kinase

TBK1 TRAF family member-associated NF-kB activator binding kinase

TGF Transforming growth factor

TIR Toll/IL-1 receptor

TLR Toll-like receptor

TMEV Theiler's murine encephalomyelitis virus

TNF Tumor necrosis factor

TRAF Tumor necrosis factor receptor-associated factor

TRIF Toll/IL-1 receptor domain-containing adaptor-inducing interferon-β

TYK Tyrosine kinase

UTR Untranslated region

WH Degenerate-winged-helix

WT Wild type

YFV Yellow fever virus

1. Introduction

1.1 Challenges of an increasing population

The exponential increase of the human population will pose new challenges in almost every conceivable field. One major problem that comes with an increasing population density are infectious pathogens that spread with apparent ease and lead to endemic or pandemic outbreaks¹. Many important conclusions can be drawn from former outbreaks but, nevertheless, this ongoing evolutionary battle between pathogens and their hosts poses a constant threat to mankind. Therefore, the inevitable emergence of new deadly agents can only be faced and solved by constant development and improvement in medicine, which in turn presupposes a profound comprehension of the underlying molecular mechanisms of immunity.

1.1.1 Pandemics of human history

Over time, humanity has seen devastating diseases diminishing the population in a tremendous way. First reports of pandemics go back to 542-546 AD. The gram-negative bacterium *Yersinia pestis*, the causative agent of the plague, transferred most likely from fleas of rats to humans and has led to millions of deaths by causing a flu-like illness. Almost one thousand years later in 1347, the reoccurrence of this disease, the notorious "Black Death", reshaped mankind again in an obliterating way leading up to two hundred million deaths on earth over time².

At the end of the 19th century, the world witnessed the first outbreak of influenza A. This virus caused many pandemics over hundreds of years called the "Russian Flu" or "Asiatic flu"^{3,4}. Near the end of World War I, the subtype H1N1 of influenza A gave rise to another calamity in human history⁵. The so-called "Spanish flu" caused up to fifty million deaths with a very high case fatality rate of more than 2.5%⁴.

Another type of virus, the human immunodeficiency virus (HIV), showed up for the first time in 1960^{6,7}. The underlying disease called acquired immunodeficiency syndrome (AIDS), even though highly treatable nowadays, still spreads continuously and leads to many deaths^{8–10}.

The latest example of viral pandemics is the severe acute respiratory syndrome coronavirus (SARS-CoV-1), which leads to a disease with flu-like symptoms referred to as SARS^{11,12}. The virus of the family *Coronaviridae* has an assumed zoonotic origin and

was most likely transmitted from bats to humans¹³. While the first pandemic outbreak in 2002 has led to less than 1000 deaths, another newly identified strain called SARS-CoV-2 has been threatening the world¹⁴. SARS-CoV-2 is a possibly bat-borne coronavirus that, like SARS-COV-1, transmitted to humans and is leading to millions of infections and thousands of deaths^{15,16}.

With increasing effort in scientific understanding of factors such as disease origin, transmission and distribution many deadly agents have been repulsed and almost eradicated. For instance, bacterial diseases like the bubonic plague or cholera that rely on manmade circumstances such as poor living conditions with bad sanitation are on decline. Nevertheless, viral pathogens with their high mutation frequencies that give rise to genetic drifts and shifts constantly lead to increased fitness and re-emergence of new and deadlier strains.

The following chapters will provide an overview of viruses in general and their strategies of infection and replication in humans as well as the evolved mammalian immune system.

1.2 Viral life cycles

Viruses are considered as organisms "at the edge of life" because they possess several properties of living organisms like an own genome or that they evolve under natural selection¹⁷. Nevertheless, the lack of a cellular structure, a missing metabolism and the fact that their reproduction is dependent on host organisms are several aspects indicating that viruses are more like organic structures rather than a form of life¹⁸.

Generally, a virus particle is composed of a nucleic acid, either positive or negative sensed single-stranded (ss) or double-stranded (ds) RNA or DNA, and a protecting coat consisting of several proteins referred to as capsid¹⁹. Variations of virus structures evolved over time as for instances an additional outer envelope that can protect the virus. All these variations give rise to many different morphologies such as simple helical and icosahedral forms or more complex structures as well as distinctive sizes ranging from 20 nanometers (nm) in diameters to 1400 nm in length.

The life cycle of viruses differs greatly between species, but several basic steps can be described. The first stage of virus replication starts with the attachment of the virus to a host cell. Proteins at the outer part of the virus bind to surface proteins on the cell and in turn, the virus entry takes place via membrane fusion and endocytosis or by penetration

of the cell membrane^{20–22}. The uncoating and removal of the viral capsid leads to the release of the viral nucleic acid inside the host cell. The entry of the viral genome eventually leads to the expression of early viral proteins, either directly in the case of positive-sense ssRNA viruses or indirectly via the synthesis of viral messenger RNAs (mRNA) for negative-sense ssRNA/ssDNA and dsRNA/dsDNA^{23–26}. These proteins in turn give rise to several rounds of replication of the viral genome and also enable the assembly of the virus particle^{27,28}. The last stage is the release of the virus in which the host cell membrane opens by lysis and the virus gets released²⁹. Some viruses integrate their genome into the host genome and undergo a lysogenic cycle as a so-called provirus. The provirus replicates passively during the replication of the host genome and stays in its latent phase. At some point and upon different kinds of triggers the provirus leaves this latent phase and enters its active form which eventually give rise to the replication and release of the virus.

1.3 The innate immune system

The vast plethora of viruses have developed diverse strategies to infect and manipulate their hosts for replication and propagation. In turn, these constant threats have led to the establishment of a sophisticated multi-layered immune system in the hosts that challenges the pathogenic attacks³⁰. The immune system comprises two branches, the innate and the adaptive immunity. After a virus has successfully passed through the first mechanic barriers of defense the invader faces a new cellular environment. In this early stage, leukocytes of the innate immune system come in contact with the pathogens and start an immediate response to inhibit further spreading of the invaders³¹. Additionally, these and other white blood cells start a cascade of recruiting more immune cells to amplify the immune reaction. In the late phase of infection, cells of the adaptive immune system get attracted to the place of attack that eventually leads to a directed response via selection and amplifications of specific antibody producing lymphocytes³².

Innate immunity and all its complexity has evolved over millions of years in many organisms^{33,34}. This part of the immune system is considered as the older form of defense compared to the adaptive immune system and is conserved from primitive multicellular species over plants, fungi and insects to all vertebrates. The overall function of the innate immune system is the orchestration of responses to non-self and danger signals of invasive microbes and tissue injuries.

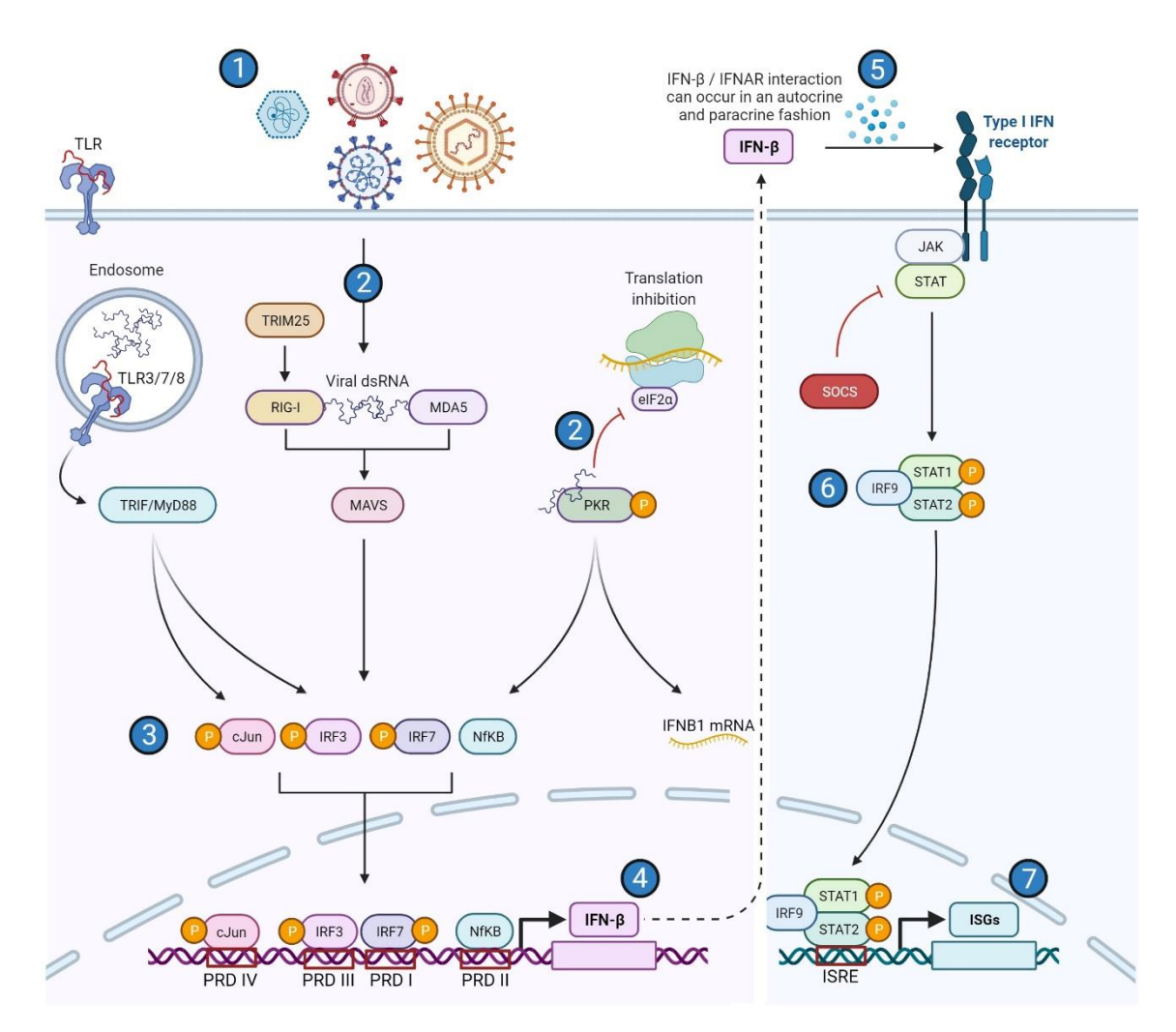


Figure 1.3.1 The type I interferon (IFN-I) response during RNA virus infection

(1) Released viral RNAs activate pattern recognition receptors (2) in the cytoplasm (RIG-I, MDA5, PKR) or in the endosomal compartments (TLR3, TLR7, TLR8). The phosphorylation of PKR inhibits overall translation (2), whereas the others bind and activate specific adapter proteins (TRIF, MyD88, MAVS) to transmit the information. The activated signaling cascade leads to the activation of transcription factors (3), which translocate into the nucleus to bind the *IFNB1* promoter at distinct PRD domains. Expressed IFN- β (4) is released and binds in an autocrine and paracrine fashion to type I IFN receptors (IFNAR1, IFNAR2). Subsequent intracellular phosphorylation of JAKs lead to the formation and translocation of the ISGF3 complex (IRF9, STAT1, STAT2) into the nucleus to drive interferon stimulated gene expression by binding to ISRE promoter sites. Figure created with BioRender.

Mechanical and chemical barriers constitute first defense mechanisms to ward off most microbes³⁵. This includes physical components like the skin, mucus or saliva as well as soluble recognition molecules such as clotting factors, natural antibodies and the complement system³⁶. Another part are the cellular components, consisting of phagocytic cells as for instance macrophages, antigen presenting cells like dendritic cells (DCs) and cells that eliminate damaged or infected cells such as natural killer cells. Additionally, many other non-immune cells belong to the innate immune system such as epithelial cells, which act as a physical barrier in different organs like the lung and usually face pathogens first^{37,38}. Intriguingly, these cells are also capable of chemokine and cytokine production and the processing of other danger signals^{39,40}.

The innate immune system has to respond quickly to invading pathogens which possess superior replication times and rapid distribution properties in order to adequately defend the host organism. This complexity of fast responses against thousands of different pathogens is possible because of a highly sophisticated network of receptors.

1.3.1 Pattern recognition receptors and adaptors

Evolution has given rise to a plethora of species, each endowed with specific traits to serve their own survival strategies and lifestyles. In the case of pathogens, our body leverages some of these diverse traits to distinguish between self and non-self molecules in order to defend the body by an induced immune response⁴¹. The recognition of these so-called pathogen-associated molecular patterns (PAMPs) occurs at the extracellular or intracellular space by specific pattern recognition receptors (PRRs). Extracellular PRRs are localized at the cell membrane and recognize for example lipopolysaccharides of the outer membrane of gram-negative bacteria or fungal cell wall components such as β-glucans or chitin^{42,43}. On the other hand, intracellular PRRs find their targets like viral nucleic acids inside the cell in the cytoplasm or distinct vesicles like endosomes^{44–46}. Dependent on their structural homology, protein domains as well as their specific targets most PRRs can be classified into 5 families (Table 1.1)⁴¹.

Table 1.1 Families of pattern-recognition receptors

Family	Members	Domains	Sites of
			action
Toll-like receptors (TLR)	TLR 1-10	LRR, TIR	Cell surface,
			endosomes
C-type lectin receptors	Dectin-1, etc.	C-type lectin	Cell surface
(CLR)			
Nucleotide-binding	NOD1-2, NLRC3-5,	Nucleotide	Cytoplasm,
domain, leucine-rich	NLRP1-9 and 11-14,	binding, LRR	endosomal
repeat (LRR)-containing	NAIP1, 2, 5, 6		membrane
(or NOD-like) receptors			
(NLR)			
RIG-I-like receptors	RIG-I, MDA5, LGP2	DExD/H	Cytoplasm
(RLR)		helicase,	
		CARD	
AIM2-like receptors	AIM2, IFI16	PYRIN, HIN-	Cytoplasm,
(ALR)		200	nucleus

The hallmark of PRR activation is the production of interferons (IFNs) and proinflammatory cytokines, which directly hamper pathogenic progression and activate and/or attract other cells in a paracrine manner (Figure 1.3.1)⁴⁷. Additionally, constitutively expressed antiviral proteins are activated and lead to an immediate pathogenic inhibition by diverse processes. Other responses comprise the activation of phagocytosis, autophagy, cell death and cytokine processing^{48,49}.

In the majority of cases, the binding of a pathogenic ligand to its corresponding PRR results in the attachment of adaptor proteins to the PRR. Most adaptor proteins contain several protein domains that allow the binding to the PRR and proteins downstream in the signaling cascade at the same time. Furthermore, adaptors integrate signals of not only one PRR but several and thus, display an important hub in the coordinated interferon response. Their classification into distinct groups depends on the respective protein domain that allows PRR interaction as well as on the signaling domain enabling the binding to downstream proteins (Table 1.2)⁴¹.

Table 1.2 Adaptor proteins of PRRs

Adaptor	PRR	Signaling	Sites of action
proteins	interaction	domain	
TIRAP/MyD88	TIR	Death	Cell surface,
			endosomes
TRAM/TRIF	TIR	TRAF-binding,	Cell surface,
		RHIM	endosomes
MAVS	CARD	Proline-rich	Mitochondrial and
		region, TRAF-	peroxisomal membrane
		binding	
ASC	PYRIN	CARD	Cytoplasm,
			mitochondria

Different pathogenic threats presuppose a dynamic and versatile orchestration of PRR signaling that specifically inhibits only the invader with minimal or appropriate self-inflicted damage. In case of RNA viruses, the human innate immune system uses specific PRRs of the group of TLRs and RLRs. Additionally, proteins of other families exhibit anti-viral functions as well and support the actions against the viral threat.

1.3.2 Viral RNA-induced TLR signaling cascades

First traces of Toll-like receptors (TLRs) were initially discovered in 1985. Initially described as a gene involved in embryonic development of *Drosophila melanogaster* by the lab of Christiane Nüsslein-Volhard, Eric Wieschaus and colleagues, TLR4's ability to function as an antibacterial protein was fully elucidated in 1998^{50,51}. Charles Janeway and Ruslan Medzhitov showed that a human orthologue of the fruit fly gene was able to induce an immune response by the activation of certain genes. To date, 10 genes have been described in the human genome that encode for TLRs⁴².

TLRs are single-pass membrane receptors that are expressed on many different cells as for instance circulating immune surveillance cells like macrophages, dendritic cells and T- and B-cells as well as non-immune cells like epithelial or endothelial cells or fibroblasts.

Whereas TLR1, TLR2, TLR4, TLR5, TLR6 and TLR10 are localized on the cell membrane and detect PAMPs in the extracellular space, TLR3, TLR7, TLR8 and TLR9 are located to the membrane of intracellular vesicles for the detection of foreign nucleic acids^{52,53}. When activated by binding to their ligands most TLRs form homodimers or heterodimers and some TLRs translocate from their initial site of action like the membrane to other locations such as endosomes^{54,55}.

In the case of TLR3 activation by double-stranded RNA or its synthetic analogue polyriboinosinic:polyribocytidylic acid (poly(I:C)), the adaptor protein Toll/IL-1 receptor (TIR) domain-containing adaptor-inducing interferon- β (TRIF) binds to a TLR3 homodimer^{56,57}. This recruitment gives rise to three different downstream signaling pathways⁵⁸.

First, the interaction of TLR3 and TRIF leads to the activation of tumor necrosis factor (TNF) receptor-associated factor 3 (TRAF3) and TRAF6. This triggers the following interaction of TRAF3 with NF- κ B-activating kinase-associated protein 1 (NAP1), TRAF family member-associated NF- κ B activator (TANK)-binding kinase 1 (TBK1) and inhibitor of kB (I κ B) kinase-related kinase- ϵ (IKK- ϵ). Eventually, this leads to the phosphorylation and thus, activation of the transcription factors IFN-regulatory factor 3/7 (IRF3 and IRF7). Afterwards, the homodimer IRF3/IRF3 and/or heterodimer IRF3/IRF7 translocate into the nucleus to mainly drive the transcription of *IFNB1*⁵⁹.

The second signaling cascade involves the induction of two different downstream transcription factors. After the binding of TRIF to TLR3, TRAF6 and receptor-interacting protein 1 (RIP-1) engage and bind to transforming growth factor- β (TGF- β) -activated kinase 1 (TAK1)^{60,61}. Subsequently, TAK1 autophosphorylation leads to the activation of the IkB kinase complex as well as the phosphorylation of mitogen-activated protein kinases (MAPKs)⁶². The former consists of the scaffold protein NF-kB essential modifier (NEMO) and the two kinases IKK- α and IKK- β . Ultimately, the IkB complex gives rise to the activation of the NF-kB transcription factor and its translocation to the nucleus to drive the expression of proinflammatory cytokines. The MAPK signaling transduction finally leads to the activator protein 1 (AP1)-mediated stimulation of chemokines⁵⁹.

Given the fact that dsRNA is either the form of genetic material or synthesized as an intermediate during virus replication it was postulated to be the major PAMP recognized by PRRs. However, advances in technology in the RNA field enabled the identification of

TLR7 and TLR8 as PRRs that primarily recognize ssRNA⁶³. The expression of TLR7 and TLR8 is mainly restricted to a different subset of immune cells like plasmacytoid dendritic cells (pDCs) and B-cells or monocytes, myeloid DCs and macrophages, respectively. In contrast to TLR3, which exclusively binds to TRIF, TLR7/8 recruit the adapter protein myeloid differentiation primary response 88 (MyD88) after ligand binding and homodimerization. Subsequently, a complex consisting of MyD88, Interleukin-1 receptor-associated kinase 1 (IRAK1), IRAK4 and TRAF6 forms and dependent on the cell type induces the activation of NF-κB and AP-1, and/or IRF7 to finally drive TNFα and type I IFN expression, respectively⁶³.

The major PAMP recognition sites of TLR3, TLR7 and TLR8 comprise the endosomal space while the cytoplasmic compartment is monitored by receptor proteins of other families.

1.3.3 Viral RNA-induced RLR signaling cascades

The cytoplasmic space is the major location for viral nucleic acid release as well as viral synthesis and replication. Thus, several RNA sensing PAMPs monitor the cytoplasm for foreign RNA moieties. One family are RLRs encompassing three members; namely retinoic acid-inducible gene-I (RIG-I), melanoma differentiation-associated protein 5 (MDA5) and laboratory of genetics and physiology 2 (LGP2)⁶⁴. All three proteins belong to the family of DEAD/H-box helicases each harboring 9 conserved protein motifs, including motif II with the amino acid sequence of aspartate-glutamate-alanine-aspartate/histidine (DEAD/DEAH), also known as the Walker B domain ⁶⁵. Together, the upstream localized characteristic motif called Walker A domain and the Walker B domain function in adenosine triphosphate (ATP) binding and hydrolysis, respectively, to enable energy-driven processes.

Structurally, RIG-I, MDA5 and LGP2 possess similar protein domains with a central helicase core consisting of two helicase domains (HeI1/2) as well as a C-terminal repressor domain (RD) involved in ATP hydrolysis ligand binding, respectively. However, only RIG-I and MDA5 harbor an N-terminal caspase activation and recruitment domain (CARD) which enables protein-protein interactions⁶⁶. On one hand, LGP2 was believed to be non-functional in signal transduction because of the missing CARD, but on the other hand several studies implied a regulatory role of LGP2 on RIG-I by direct binding via its RD^{67,68}.

The main ligands that lead to RIG-I or MDA5 activation are short and long dsRNA fragments, respectively, with a triphosphate (ppp) at the 5'end. However, it was shown that short 5'-pp dsRNA is also sufficient to activate RIG-I⁶⁹⁻⁷². Both, 5'-ppp and 5'-pp dsRNAs are leveraged by many different viruses like influenza A and B (IAV, IBV), measles virus (MV), Newcastle disease virus, Ebola Virus (EBOV) and reoviruses, respectively. Additionally, the synthetic viral dsRNA analogue poly (I:C) is able to bind and activate RIG-I and MDA5 in a length-dependent manner of the nucleic acid chain⁷³. In the ligand-free state of RIG-I the RD domain represses the CARD and helicase domains by folding back and binding to it in order to prevent RIG-I from uncontrolled activation in a stress-free environment⁷⁴. The attachment of dsRNA to the RD releases this steric hindrance and opens the CARD for protein-protein interaction and the helicase domain for ATP hydrolysis. In contrast, MDA5 is constitutively phosphorylated and binding to its ligand induces desphosphorylation for its activation. Subsequently, the translocation of RIG-I and MDA5 along the dsRNA promotes their homo-oligomerization via CARD-CARD interactions leading to a filamentous complex, which facilitates the CARD-mediated interactions with mitochondrial antiviral signaling proteins (MAVSs)^{75–78}. At this point, the complex which is located at the mitochondrial membrane serves as a scaffold for the binding of several proteins resulting in the dichotomy of the signaling pathway. On one hand, binding of TRAF2/6 activates the IKK complex that eventually leads to NF-kB activation^{79,80}. On the other hand, interaction with TRAF3 promotes a complex consisting of TANK, IKKy, IKKs and TBK1 to induce IRF3 and IRF7 phosphorylation and dimerization. Both, IRF3/7 and NF-kB translocate to the nucleus and coordinate the IFN and pro-inflammatory gene expression^{81,82}.

1.3.4 Interferon regulatory factors (IRFs)

The family of IRFs comprises 9 different members from which IRF1, IRF2, IRF3, IRF5, IRF7 and IRF9 have been directly implicated in anti-viral responses⁸³. All these proteins share a well-conserved N-terminal amino acid sequence including 5 consecutive tryptophan repeats in its DNA binding domain (DBD)⁸⁴. Crystal structure and promoter analyzes revealed that the DBD forms a helix-turn-helix domain and binds to a consensus DNA sequence which is common for all IRF family members referred to as IRF binding element (IRF-E)^{85,86}. However, the consensus sequence slightly differs between the IRF family members and thus, each IRF can lead to a subtle change in

gene expression patterns with different outcomes for the relevant cellular processes. For instance, the binding of IRF3 to an IRF-E depends on an 8-nucleotide sequence and the substitution of any nucleotide renders the binding site unrecognizable^{87,88}. In contrast, IRF7 has a broader IRF-E recognition spectrum and can still interact even if the IRF-E has up to 3 nucleotide changes in the consensus sequence. Additionally, most IRFs with the exception of IRF1 and IRF2 harbor an IRF association domain (IAD) that allows binding to different IRFs mediating homo- or heterodimerization^{89–92}.

Among all IRFs the two highly homologous proteins IRF3 and IRF7 gained most attention because of their key regulatory roles in type I IFN expression in virus infected cells. Even though IRF3 and IRF7 share similar structures both highly differ in their expression pattern. IRF3 is constitutively expressed and localizes to the cytoplasm in a latent form⁹³. Upon viral infection IRF3 undergoes phosphorylation, which in turn leads to the formation of a homo- or heterodimer with IRF3 or IRF7 and drives type I IFN gene expression after translocation into the nucleus⁹⁴. In contrast, IRF7 has a low basal expression level, which strongly increases after the induction of the type I IFN-mediated signaling as for instance *IFNB1* induction⁹⁵. Similar to IRF3, IRF7 phosphorylation leads to the formation of a homo- or heterodimer with IRF3 to drive type I IFN gene expression. The variation of type I IFN gene expression depends on the different binding affinities of IRF3 and IRF7 to their promoters. For example, IRF3 is very potent in the induction of *IFNB1* whereas IRF7 induces both *IFNB1* and several genes for IFN- $\alpha^{96,97}$. Furthermore, due to the susceptibility to ubiquitin-dependent degradation, and thereby it's very short half-life time of roughly 1 hour, IRF7 may represent a key player in the transient orchestration of type I IFN gene induction and feedback loop control to prevent uncontrolled overshooting⁹⁵.

Apart from the stimulation of type I IFNs, IRF3 and IRF7 are capable of binding to promoters of some ISGs and directly affect their expression⁹⁸.

1.3.5 Nuclear factor kappa-light-chain-enhancer of activated B-cells (NF-kB)

The NF-κB family of transcription factors plays a pivotal role in diverse cellular processes such as cell survival, proliferation or the orchestration of stress responses to a plethora of stimuli⁹⁹. In the case of innate immunity, NF-κB leads to the activation of type I IFNs and is critical for the appropriate regulation of cell death by inducing anti-apoptotic factors¹⁰⁰. All NF-κB proteins, namely NF-κB1, NF-κB2, ReIA, ReIB and

c-Rel, harbor an N-terminal Rel-homology domain (RHD) which comprises a DBD, a nuclear localization site (NLS) as well as a domain necessary for protein-protein interactions^{101–104}. To bind the DNA consensus sequence referred to as kB site the NF-κB proteins form homo- or heterodimers, however, only RelA, RelB and c-Rel possess a transactivation domain to initiate transcription¹⁰⁵. In contrast, NF-κB1 and NF-κB2 are translated as precursors, p105 and p100, which undergo posttranslational processing to form p50 and p52, respectively, and miss a transactivation domain^{106–108}. Owing to the missing transactivation domain, NF-κB1 and NF-κB2 homodimers are believed to bind to kB sites and compete with the other dimers to repress transcription initiation.

In a stress free environment NF- κ B proteins are sequestered by the IkB proteins I κ B α , I κ B β , I κ B relocation into the nucleus 109,110. Upon stress, as for instance viral stress, IkB proteins are phosphorylated by the IKK complex consisting of IKK α , IKK β and IKK γ that leads to ubiquitination and subsequent degradation of the inhibitors 111. As a consequence, the NF- κ B proteins translocate to the nucleus and bind kB sites on the DNA to drive transcription of for instance IFNB1112.

1.3.6 Interferons and the IFN-β enhanceosome

In 1957, an unknown factor was described as a positive regulator of immunity which "interferes" with viral replication 113. Nowadays, several of these factors, referred to as interferons (IFNs), have been described and classified into type I, II and III IFNs dependent on their homology, actions and signaling pathways 114. In humans, type I IFNs are expressed by almost every cell type and comprise the proteins IFN- α , IFN- β , IFN- ϵ , IFN- ϵ and IFN- ϵ which are all located in a cluster on chromosome 9. However, IFN- α has 13 subtypes each expressed from a different *IFNA* gene, whereas the others exist as single copy genes 115–118. Once expressed and released, type I IFNs bind in a paracrine and autocrine fashion to the receptors IFN- α/β receptor 1 (IFNAR1) and IFNAR2 to activate an anti-viral signaling cascade 119–121. In contrast, IFN- γ is the only member of type II IFNs and its expression is restricted to immune cells such as T-cells and natural killer cells. In addition, IFN- γ induction is interleukin-12 (IL12) dependent and it binds to the IFN- γ receptors 1 (IFNGR1) and IFNGR2 to stimulated downstream signaling 122–124. The last group comprises IFN- λ 1, IFN- λ 2, IFN- λ 3 and IFN- λ 4 referred to

as type III IFNs, which were more recently discovered compared to type I IFNs. Even though both classes are expressed in almost all cells and play a role in anti-viral immunity, type III IFNs differ in their receptor signaling by binding to IL10R2 and IFNLR1¹²⁵.

The expression of type I IFNs is mainly controlled at the transcriptional level and the enhancer of the IFN-β gene is one of the best characterized higher eukaryotic cis-regulatory elements. Under normal conditions, the IFNB1 transcription is sterically blocked by nucleosomes, which prevent the assembly of the pre-initiation complex at its promoter¹²⁶. Upon viral infection, *IFNB1* gene expression is a highly coordinated process induced by the enhanceosome consisting of the transcription factors AP-1, IRF3/7 and NF-kB as well as a scaffolding protein high mobility group AT-hook 1 (HMGA1)¹²⁷. Once activated, protein complexes of the aforementioned transcription factors bind to four positive regulatory domains (PRD I-IV) at the position -102 to -47 upstream of the transcription start site in the IFNB1 enhancer. Crystal structure analyzes showed that AP-1 together in a complex with two IRF3s cover PRD III-IV, whereas NF-kB in combination with IRF3 and IRF7 bind to PRD I-II¹²⁸⁻¹³⁰. While necessary for the proper assembly of the enhanceosome, HMAD1 is dispensable for its later function⁹⁷. Only the combined action of all transcription factors results in the displacement of the nucleosomes that eventually leads to the uncovering of the TATA-box and recruitment of the other transcription factors to activate RNA polymerase II dependent transcription 126. Missing of a single component of the enhanceosome abrogates IFNB1 transcription, which highlights the importance of each of these proteins. Interestingly, the role of IRF7 in the enhanceosome is less clear since its low basal expression levels hint to a role later in viral infections.

1.3.7 The type I IFN-induced JAK-STAT pathway

The expression of type I IFNs and its binding to the IFNARs at the cell membrane give rise to the activation of the Janus kinase- signal transducer and activator of transcription (JAK-STAT) signaling cascade¹³¹. In humans, there are four members including JAK1, JAK2, JAK3 and tyrosine kinase 2 (TYK2) which all feature 7 specific homology regions including a receptor binding domain as well as a kinase domain^{132–134}. Upon ligand binding to IFN receptors associated JAKs undergo conformational changes which lead to their auto- or transphosphorylation¹³⁵. In turn, phosphorylated receptors allow the

binding of the STAT family members STAT1, STAT2, STAT3, STAT4, STAT5A, STAT5B and STAT6 to JAKs that results in their phosphorylation ^{136–142}. Eventually, homo- and heterodimers are formed that translocate into the nucleus to drive anti-viral gene expression. In the case of IFNAR activation by type I IFNs, STAT1 and STAT2 interact with IRF9 and form the interferon stimulated gene factor 3 (ISGF3) complex ^{143–145}. Binding of ISGF3 to specific regulatory sequences in the genome referred to as interferon stimulated response elements (ISREs) drives the expression of hundreds of interferon stimulated genes (ISGs) ^{146,147}. Additionally, STAT1 and STAT4 homodimers are induced upon type I IFN signaling as well. All signaling cascades certainly result in a combined response to interfere with and counteract viral replication and spread.

Since the autoactivation of the JAK-STAT pathway is a common feature of autoimmune diseases, the tight regulation after stress induction is indispensable. Therefore, several negative feedback loops exist such as phosphorylation-mediated inhibition of JAKs, decrease of IFNAR proteins at the cell surface and competition between different STATs each with their own binding spectrum and strength. Another control mechanism is the ISGF3 dependent expression of suppressor of cytokine signaling (SOCS) proteins, which can directly bind phosphorylated receptors and inhibit STAT recruitment as well as lead to E3-uibiquitin dependent degradation of STATs^{148–150}.

1.3.8 Interferon-stimulated genes (ISGs)

The final step of IFN signaling is the sophisticated orchestration of ISG expression and modulation during viral stress as well as their regulation after stress relief. Profound investigations utilizing distinct doses of IFNs and varying treatment times in different cell types revealed 50-1000 upregulated genes considered ISGs^{151,152}. Comparisons of micro array data showed that roughly 200 ISGs are commonly expressed in most cell types upon IFN induction, however, the characterization of bona fide ISGs remains elusive due to the lack of knock out studies and other molecular analyzes^{153,154}.

Considering the fact that the viral life cycle can be divided into different steps, many ISGs fulfil diverse functions in a temporal and spatial manner to hamper viral attachment, entry, localization, replication and particle formation. Additionally, whereas the expression of most ISGs is induced after IFN signaling several ISGs are constitutively expressed at low levels to act early in the anti-viral response¹⁴⁷. In this

regard, the appropriate amount of latent ISGs is highly important to prevent autoimmune signaling which critically impairs cellular homeostasis.

Upon viral nucleic acid entry, the foreign RNA is detected by PRRs and additionally by the several present ISGs to directly disturb viral expansion. One main cytosolic ISG that binds viral RNA is the protein kinase R (PKR)¹⁵⁵.

PKR In the early infection phase many RNA viruses rely almost completely on the host translation machinery to drive the expression of their own RNA. Thus, one major counteraction of host cells is the translational shutdown of all RNAs to prevent further viral expression. A rapid response to this is accomplished by the protein product of the gene EIF2AK2 namely PKR, which is able to directly bind viral dsRNA or poly (I:C) via its N-terminal binding domain¹⁵⁶. This triggers the autophosphorylation of PKR and in turn, induces the phosphorylation of the eukaryotic translation initiation factor 2 subunit 1 (elF2α)^{157–159}. The eukaryotic translation initiation complex consists of several proteins and the phosphorylation of elF2α leads to the complete abolishment of ribosomal cap-dependent translation¹⁶⁰. Concomitantly, the preferential initiation of cap-independent translation takes place to specifically express vital proteins that promote the anti-viral response¹⁶¹. In addition to its direct action on translation, PKR is implicated in other pathways including the activation of c-Jun N-terminal kinase (JNK), p38 mitogen-activated protein kinase (MAPK), STAT1 and STAT3 as well as the tumor suppressor p53^{162,163}. Moreover, there is evidence that PKR also indirectly activates NF-κB, which is capable of inducing type I IFN signaling^{164,165}. The role of type I IFN induction was further validated by PKR knock down studies which revealed a regulatory role in transcription of IFNB1 and IFN-β production^{166–169}. Intriguingly, the increased transcription of IFNB1 is not necessarily accompanied by enhanced translation and protein production of IFN-β, which was shown in PKR deficient cells upon encephalomyocarditis virus (ECMV) or Semliki Forest virus (SFV) infections¹⁷⁰. This implied a post-transcriptional role of PKR on IFNB1 transcripts itself rather than the regulation of the *IFNB1* transcription. Furthermore, the production of IFN- α/β PKR is independent of the phosphorylation of eIF2α indicating a bipartite role in type I IFN signaling and translation¹⁷⁰. Controversially, the discovery of RIG-I and MDA5 as the major cytoplasmic PRRs complicated the picture of PKR-dependent type I IFN signaling. In this context, knock out mice studies demonstrated a crucial role for RIG-I and MDA5

in the response to several viruses such as influenza virus or picornavirus, respectively¹⁷¹.

OAS Early viral RNA detection induces gene expression of many ISGs including the oligoadenylate synthetase (OAS) family members OAS1, OAS2, OAS3 and OAS-like (OASL)^{172–176}. Besides its induction via type I IFNs, OAS transcription is IRF dependent. which directly binds to OAS promoters in its dimerized form and leads to its early expression in the anti-viral response 177,178. All OAS proteins consist of an N-terminal and C-terminal domain connected by a linker region and all share parts necessary for ATP binding as well as for viral dsRNA detection 179. With the exception of OASL, which exhibits substantial divergence in the N-terminal domain, all OAS proteins possess enzymatic activity. Binding to viral dsRNA leads to the allosteric activation of OASs, which results in the connection of a donor (ATP) molecule and an acceptor ATP¹⁸⁰. The consecutive addition of ATP to the growing ATP chain results in 2`-5` oligoadenylates (2-5A), which serve as ligands for the latent form of ribonuclease L (RNase L)^{173,181–183}. Upon binding of 2-5A, RNase L dimerizes in order to execute overall RNA degradation including viral RNA as well as cellular RNA and thus, inhibits RNA translation and protein synthesis¹⁸⁴. Furthermore, OASL is incapable of RNase L activation due to its missing active site, however, its upregulation during IFN signaling implies an active role as an ISG¹⁸⁵. In line with this, OASL sensitizes virally infected cells by enhancing the sensitivity of RIG-I activation in the absence of TRIM25¹⁸⁶. Ultimately, RNase L induced RNA degradation gives rise to a positive feedback loop inducing further type I IFN signaling by activating other RNA sensing PRRs.

IFIT Other rapidly induced proteins are from the IFN-induced protein with tetratricopeptide repeats (IFIT) family¹⁸⁷. In humans, this family is composed of IFIT1, IFIT2, IFIT3 and IFIT5 and all have a specific number of tetratricopeptide repeat domains in common, which are necessary for protein-protein interactions^{188–194}. Even though all IFITs ostensibly lack enzymatic activity there is clear evidence of their action in type I IFN signaling upon viral RNA sensing. Under normal conditions, their expression levels are minor or shut off completely, however, type I IFNs and IRFs lead to their induction^{195,196}. Several studies described a broad range of anti-viral activity of the IFIT family including general translation inhibition, recognition and sequestration of

uncapped 5`-ppp RNA and mRNA lacking a 5`cap 2`-O methylation at position N1 as well as direct binding to viral proteins for their inhibition 197-200.

RSAD2 Viral infection studies revealed Radical S-Adenosyl Methionine Domain-Containing Protein 2 (RSAD2) as another gene that inhibits viral infection¹⁴⁷. Upon viral RNA sensing, RSAD2 expression is strongly induced by type I IFN and alternatively by IRF3^{201–206}. Induction of the anti-viral activity depends on its N-terminal amphipathic domain and numerous knock out and overexpression studies described a broad spectrum of the underlying mechanisms as for example the inhibition of lipid rafts necessary for viral budding^{207–209}.

PRRs Important PRRs such as RIG-I, MDA5 or PKR are described as ISGs and their expression is additionally induced by type I INFs^{210–213}. This induces a positive feedback loop to amplify the initial signaling cascade in an autocrine manner as well as in a paracrine fashion for the priming of cells in close proximity.

1.3.9 The distinction of self and non-self (ADAR1)

The plethora of functions of PRRs and ISGs include the sensing of a diversity of PAMPs. This includes obvious properties of pathogenic molecules such as β -glucans of bacteria or chitin of fungi which are absent and dispensable in human cells. In contrast, RNA molecules are of fundamental necessity for cellular function and life and thus, it comes as no surprise that cells have evolved another strategy to detect foreign nucleic acids²¹⁴. There are three basic criteria in vertebrates to distinguish self from non-self-nucleic acids. First, the concentration of nucleic acids as defined by nucleic acid synthesis, degradation or availability influenced by shielding factors like proteins. Second, the localization of nucleic acids as for instance the absence of RNA in the endosomal compartment^{215,216}. Third, the presence of pathogenic nucleic acid structures non-existing in the host such as sequence motifs, specific structures or modifications like 5`-ppp cap or 5`-cap-0 structures of RNA^{70,73,217–219}.

In cellular conditions, the combined orchestration and monitoring of all aspects leads to a defined immune response in cases of non-self-signal detection. Interestingly, there is emerging evidence of endogenous RNAs that possess similar features to viral RNA. The existence and transcription of retrotransposons in the genome results in viral-like dsRNA moieties, however, the cells circumvent autoimmunity²²⁰. One possible process is the editing of RNAs as seen in mammals by the two proteins apolipoprotein B mRNA editing

enzyme catalytic subunit (APOBEC) and adenosine deaminase acting on RNA 1 (ADAR1)²²¹. The former enzymatically catalyzes the deamination of cytosine to uracil, whereas the latter deaminates adenosine to inosine (A to I editing)^{222–225}. The nucleoside inosine is detected as guanosine by the translation machinery, which can lead to substitutions in the amino acid code²²⁶. Moreover, the A to I editing results in the destabilization of complementary strands of dsRNA structures, which is critical in the maintenance of self-tolerance. In this context, it has been shown that ADAR1 prevents translational shutdown during type I IFN signaling and additionally, autoactivation of PKR by endogenous RNA elements²²⁷.

Interestingly, a full knock out of the DEAH-box helicase DHX36 in human embryonic kidney (HEK) cells shows a similar phenotype indicated by the autophosphorylation of PKR without a viral trigger. It was hypothesized that secondary structures, referred to as G-quadruplexes, within mature mRNAs lead to their stabilization and accumulation and hence, induce uncontrolled activation of PRRs by endogenous dysregulated RNAs²²⁸.

1.4 G-quadruplexes

The central dogma of a linear transmission of genetic information from DNA to RNA and eventually to protein was challenged by the existence of several processes as for instance reverse transcription or RNA replication. First flourishing in obscurity and later on coming to light, RNA emerged as a new bioactive molecule as shown in a myriad of publications. The existence of micro RNA (miRNA) or long non-coding RNAs (IncRNAs) as regulators of expression underlined these observations, however, the structural properties of RNA possess similar regulatory features and still remain unclear.

RNA stably forms secondary structures as for instance loops, helices, bulges, junctions, pseudoknots or combinations of these. Interestingly, the existence of several non-canonical DNA structures, among them a structure referred to as G-quadruplex (dG4) was followed by the discovery of such G4s in RNA (rG4s).

In general, on DNA and RNA, guanine-rich sequences can assemble into G4 structures²²⁹. Hoogsteen hydrogen bonding of four guanines assist the formation of a planar G-quartet and π -stacking of at least two G-quartets results in the assembly of a mature G4^{230,231}. The stacked G-quartets are connected by variable loops resulting in diverse G4 conformations on DNA such as parallel, anti-parallel or hybrid G4s, while the charged hydroxyl group of the sugar in RNA favors the parallel G4 conformation²³². The

steric repulsion of negative charges in the center of the G4 are stabilized by mono- or bivalent cations as in the physiological context by potassium (K+) or sodium (Na+)²³³⁻²³⁵. High-throughput studies confirmed previous *in silico* analyzes of canonical G4s represented by the consensus sequence G_x-N₁₋₇-G_x-N₁₋₇-G_x-N₁₋₇-G_x, where x is 3-6 and N denotes any nucleotide, and revealed more than 700.000 potential dG4s sites within the genome²³⁶⁻²³⁸. Interestingly, *in cellulo* chromatin immunoprecipitation (ChIP) experiments with a G4 specific antibody called BG4 showed only 10.000 potential dG4 sites indicating a temporal formation of G4s^{239,240}.

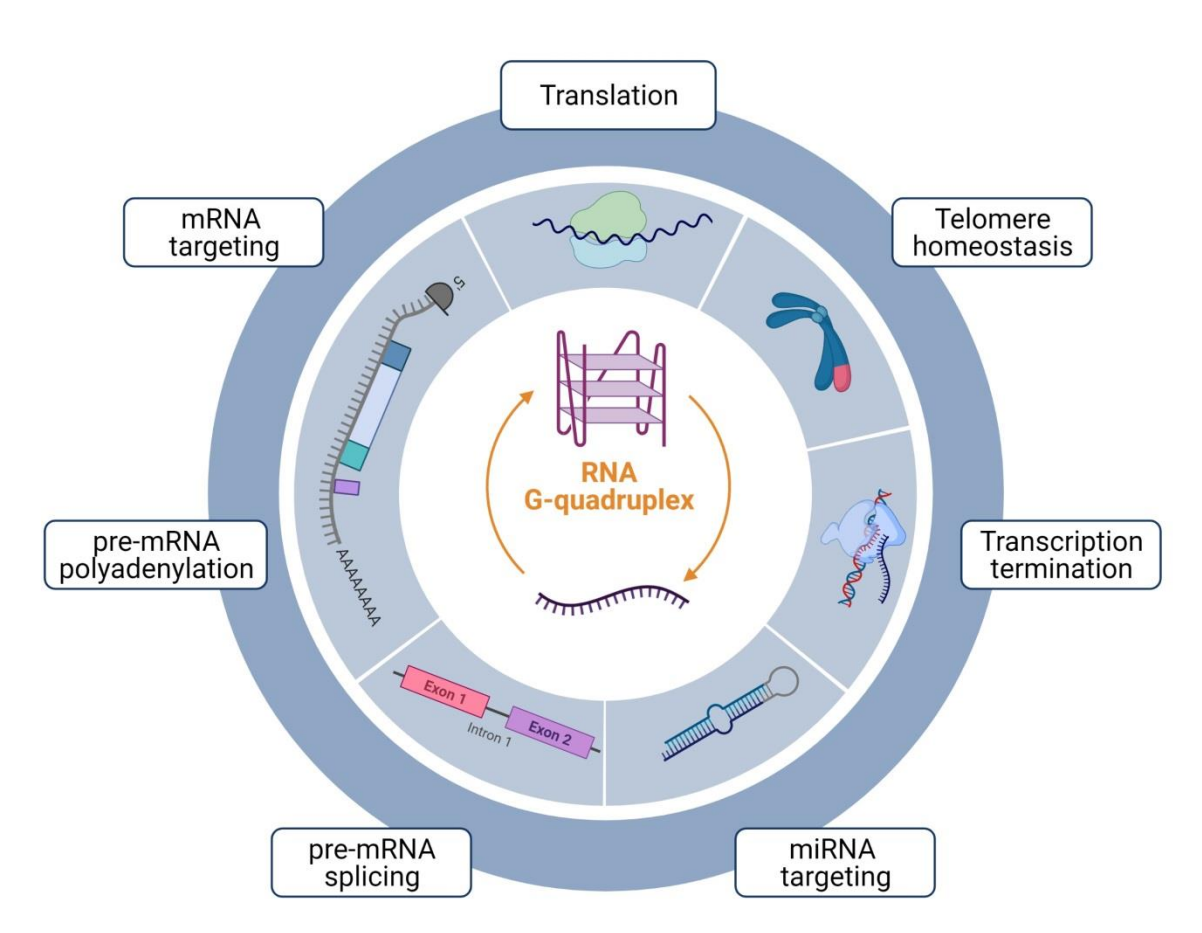


Figure 1.4.1 Cellular functions of RNA G quadruplexes (rG4s)

The formation of rG4s positively or negatively influence translation by serving as a protein loading platform or by blocking ribosomal entry, respectively. The exact mechanism during transcription termination is unclear, whereas the formation of rG4s in TERC decrease telomerase activity. The folding of rG4s in pre-mRNA influences splicing as well as polyadenylation. Generally, rG4s enable the targeting of mRNAs and miRNAs by proteins. Figure created with BioRender.

On the RNA level, reverse transcription stalling experiments combined with next generation sequencing methods identified 13.000 putative rG4 structures within the transcriptome and several investigations highlighted their importance in diverse biological processes²⁴¹. In contrast to dG4s, which are highly evolutionary conserved among species ranging from bacteria, yeast, plants and mammals, rG4s are almost depleted in bacteria²⁴². Interestingly, the genomic localization of dG4s is strongly increased in regulatory regions such as promoters or telomeres pointing again to a positive evolutionary pressure²⁴³. The presence of rG4s in 5` untranslated regions (5`UTRs), splicing sites, coding sequences or 3`UTRs gives evidence for their implications in almost all biological processes of the RNA`s life journey including transcription, splicing, translation and degradation^{244–248}.

The formation of G4s and their regulatory roles are evident, however, uncontrolled G4 folding gives rise to for example replication fork stalling, genomic instability, telomere malfunction or transcription block, which eventually leads to critical cellular damage. It comes as no surprise that several diseases such as autoimmunity or cancer are accompanied by G4 dysregulation²⁴⁹.

Owing to the highly thermostable conformations of G4s, which can outcompete canonical DNA or RNA structures, the need of a regulatory cellular machinery is indispensable.

1.5 The DEAH-box helicase DHX36

Helicases are described as modulators of nucleic acids and are classified into 6 superfamilies (SFs) dependent on the absence (SF1-SF2) or appearance of a ring like protein structure (SF3-SF6)²⁵⁰. Most helicases belong to SF2, which form the largest group and are characterized by the presence of 9 highly conserved protein motifs necessary for ATP binding and hydrolysis, molecular rearrangements as well as nucleic acid binding²⁵¹. Further subdivisions include proteins referred to as DEAD/DEAH-box helicases²⁵².

The human DEAH-box helicase DHX36 is encoded on chromosome 3 in the genome and expressed in at least two different isoforms in HeLa cells. The full length isoform 1 (DHX36iso1) is made of 1010 amino acids with the size of 114,76 kDa and predominantly localizes to the nucleus, whereas isoform 2 misses the amino acids 517-530 and remains mainly in the cytoplasm^{253,254}. However, DHX36iso1 exhibits a

strong accumulation in the cytoplasmic space in HEK cells and thus, indicates cell type specific localization differences²²⁸.

Similar discrepancies are observed in the functions of DHX36. Firstly, described as an RNA helicase associated with AU-rich elements (RHAU) and secondly indicated as a G4 resolvase 1 (G4R1) clearly show the versatility of this protein and its involvement in various cellular processes encompassing replication, transcription, splicing and translation as well as immunity^{253,255}.

1.5.1 The structure of DHX36

Several structure specific motifs and domains of DHX36 render it a multifaceted protein with diverse functions.

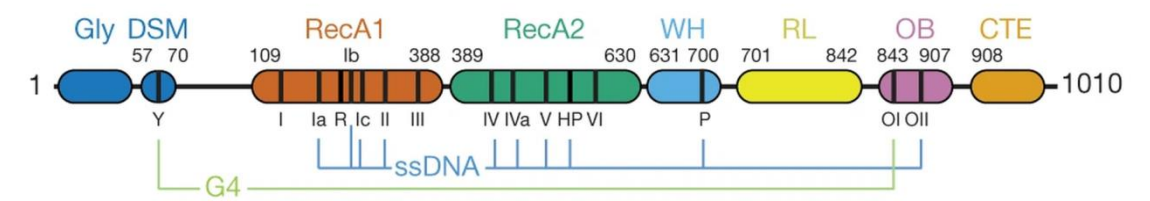


Figure 1.5.1 Schematic structure of DHX36

Individual domains (Glycine-rich element (Gly), DHX36-specific motif (DSM), helicase domains RecA1 and RecA2, degenerate-winged-helix (WH), ratchetlike (RL), oligonucleotide and oligosaccharide-binding-fold-like (OB) subdomains (OI and OII), C-terminal extension (CTE)) are depicted in different colors. Drawn lines indicate binding sites for G4 structures or ssDNA. The walker B domain including the DEIH motif of DHX36 is located in RecA2 II (not displayed). DHX36 isoform1 is composed of 1010 amino acids (aa), whereas DXH36 isoform2 misses a 14 aa sequence (not displayed). Numbers indicate positions of domains in the full length polypeptide.

At the N-terminus two domains, a glycine-rich element followed by a DHX36 specific motif (DSM) are in close proximity^{254,256,257}. The glycine-rich element plays a role in the stress granule localization whereas the DSM is necessary, but not sufficient for the binding to specific secondary nucleic acid structures on DNA and RNA referred to as DNA G-quadruplexes (dG4s) or RNA G4s (rG4s)^{258–260}. Subsequently, two central RecA domains, RecA1 and RecA2, form the core and include the walker B domain with an amino acid sequence substitution from alanine to isoleucine; aspartate-glutamate-isoleucine-histidine (DEAH→DEIH)²⁶¹. Both RecA domains are involved in the binding and hydrolysis of ATP to fulfil energy-driven processes like nucleic acid unwinding. The

C-terminal end is composed of 4 motifs namely degenerate-winged-helix (WH), ratchet-like (RL), and two oligonucleotide and oligosaccharide-binding-fold-like (OB) subdomains (OI and OII) followed by a C-terminal extension (CTE)^{257,262}. Implications for single-stranded nucleic acid binding were described for the former 3 domains, whereas only the subdomain OI showed an involvement in G4 binding^{255,263,264}. Nevertheless, the CTE functions remain elusive and underlying studies are missing.

1.5.2 G-quadruplex unwinding by DHX36

The helicase DHX36 showed strong binding to dG4 and rG4 *in vitro* with picomolar (pM) affinities of 77 pM and 39 pM, respectively²⁶⁰. In accordance with this, the ability of dG4 and rG4 unwinding of DHX36 is vastly superior compared to other DNA or RNA structures like duplexes, 5′ overhang duplexes, 3′ overhang duplexes or Y-form duplexes^{255,265}.

The crystal structure and resolution studies of DHX36 indicate slightly different mechanisms of dG4 and rG4 unwinding²⁵⁷. On DNA, DHX36 requires binding to a parallel dG4 structure as well as a single stranded tail of 8-9 nucleotides, which induces steric translocations of the RecA and OB subdomains. The subsequent ATP-independent execution of a repetitive tug and release leads to the unhinging and resetting of one guanine from the dG4²⁶³. This partial unfolding and refolding process can continue for many cycles and is sufficient for the initiation of complementary strand annealing. Noteworthy, there are ATP-dependent as well as ATP-independent mechanisms described for dG4 unwinding of DHX36, which can be explained by the versatile nature of each dG4 structure used in the different studies.

On RNA, the binding of a monomeric DHX36 molecule to the rG4 leads to its disruption in an ATP-independent fashion. Subsequent refolding of the rG4 is an energy-driven process resulting in ATP to ADP conversion and occurs in similar successive repetitions like on DNA level²⁶⁶. Taking place in the cellular environment, binding of DHX36 to a rG4 results in a steady dynamic modulation of the rG4 until it encounters for instance a ribosome, which leads to the dislocation of DHX36 to leave the rG4 resolved.

1.5.3 The maintenance of homeostasis by DHX36

The ability of DHX36 to regulate overall G4 formation implicates its importance in the maintenance of cellular homeostasis. On DNA level, the uncontrolled formation of dG4s

is implicated in the internal arrest of DNA polymerase II (Pol-II), which negatively impacts genome stability by a topoisomerase 2-dependent mechanism²⁶⁷⁻²⁶⁹. Furthermore, the modulation of dG4s at promoters or coding regions affects gene transcription in various manners, however, the underlying mechanisms are not completely understood. dG4s formation in promoters can either sterically block transcription or support transcription by providing a loading platform for other proteins and transcription factors²⁶⁹. Additionally, whether transcription is positively or negatively influenced depends on the dG4 formation on the sense or antisense strand. The location of the dG4 in the antisense strand of DNA can lead to transcription stalling by blocking RNA Pol-II, whereas dG4 formation in the sense strand is believed to disrupt annealing of the two ssDNA strands, hence supporting transcription rendering the template strand accessible for RNA Pol-II. In line with this, mouse model experiments showed that a conditional knock out of DHX36 is lethal²⁷⁰. Additionally, tissue-specific depletion in the hematopoietic system results in several developmental defects as for instance differentiation problems at the proerythroblast stage or causes hemolytic anemia. Furthermore, ablation in germ cells is accompanied by diminished spermatogonial differentiation²⁷¹. Nevertheless, the specific role of DHX36-dependent dG4 dysregulation in the observed phenotypes remains elusive and evidence is missing.

In contrast, *DHX36* deletion in the cardiac system results in defective heart development and growth retardation, which was directly dependent on the rG4 formed in the 5`UTR of the Nkx2-5 mRNA²⁷². Similarly, the interaction of DHX36 with the rG4 in the 3`UTR of the *TP53* pre-mRNA upon UV-damage maintains correct 3`end-processing leading to steady protein expression²⁷³. Based on telomere studies, DHX36 is implicated in 5` located rG4 resolution of the human telomerase RNA component (hTERC) to facilitate telomerase holoenzyme functions^{256,259,274,275}. This was validated by the observation of shortened telomeres upon small interference RNA (siRNA) knock down of *DHX36* in HEK cells²⁷⁶.

The rG4 interactions of DHX36 were further analyzes by two independent studies that demonstrated the global impact of DHX36 on mature mRNAs^{228,277}. In HEK cells, a combined approach of 4-thiouridine (4SU)-assisted photoactivatable-ribonucleoside-enhanced crosslinking and immunoprecipitation (PAR CLIP) and ribosome profiling revealed ~20.000 binding sites of DHX36 on RNA of which 4500 sites were located in

the exons of different mRNAs. Intriguingly, *in situ* analyzes showed an overlap of the DHX36 binding sites with putative rG4 forming sequences as well as a set of AU-rich elements. Furthermore, comparison of the PAR CLIP results with RNA-seq data of *DHX36* knock out cells revealed an rG4-dependent reduction of translation of DHX36 mRNA targets. The observation of stress granule formation (SG) in *DHX36* knock out cells as well as the detection of autophosphorylation of the anti-viral protein PKR implies that the accumulation of translation incompetent rG4 harboring mRNAs can lead to autoimmune dysfunctions²²⁸. Interestingly, *DHX36* overexpression is generally observed in many cancer types again pointing to a global function in maintaining cellular homeostasis²⁷⁸.

1.5.4 Innate immunity regulation by DHX36

The detection of viral nucleic acids by PRRs is a major function during innate immunity. While the non-self character of viral nucleic acids plays an important role in recognition, different viruses possess evolutionary conserved dG4 and/or rG4 structures in their genome indicating a possible role in their life cycle^{279,280}. Interestingly, another G4 binding protein referred to as nucleolin interacts with an rG4 in the genome of the hepatitis C virus (HCV) and suppresses its replication²⁸¹. Even though a direct implication of DHX36 with viral G4s is missing, a role in viral regulation is postulated due to its interaction with the several Influenza A genome or human immunodeficiency virus (HIV) segments as well as viral proteins^{282–284}.

On the other hand, several studies showed a direct role of DHX36 in viral nucleic acid induced innate immunity. A common consequence of viral infections is the accumulation of anti-viral stress granules (avSG), which constitute a critical step in the immune response²⁸⁵. avSG emerge from liquid-liquid phase separation and store mRNAs and diverse proteins^{286,287}. Their specific role is still elusive, however, it has been shown that subsequent stress relief leads to the graduate disassembly of avSG and the release of their components, thus render avSG a temporal and spatial storage for proteins and mRNA. Interestingly, DHX36 locates via its N-terminus to SG upon stress and its loss attenuates avSG formation²⁵⁴. In addition, a constitutive physical interaction of DHX36 with RIG-I as well as a complex formation of DHX36, RIG-I and PKR upon viral infection was reported²⁸⁸. However, the direct binding of DHX36 to PKR remained uncertain. In the context of PRRs, DHX36 was described to associates with viral RNA, though the

experimental setup cannot exclude RIG-I bridging of DHX36 to the viral RNA, which was also detected. In line with this, another study reported DHX36 indirectly connects with poly (I:C) in a complex composed of DDX1, DDX21, DHX36 and TRIF, in which DDX1 is the direct binder of poly (I:C)²⁸⁹.

After viral infection endogenous DHX36 expression is upregulated and overexpression approaches indicate a repressive role in viral replication²⁹⁰. In line with this, a decrease in *IFNB1* expression as well as diminished IRF3 dimerization was observed after infection with Newcastle disease virus (NDV) or poly (I:C) in tamoxifen-induced *DHX36* knock out mouse embryonic fibroblasts (MEFs)²⁸⁸. However, the treatment with a RIG-I specific ligand showed no significant differences and even gave rise to increased *IFNB1* transcripts in *DHX36* knock out MEFs. Additionally, the NDV replication remained unchanged up to 12 hours after infection in siRNA induced *DHX36* knock down HEK cells. These effects depend on the ATPase function of DHX36, which facilitates PKR phosphorylation upon viral infection.

All these observations clearly demonstrate a specific role of DHX36 in innate immunity, however, the precise mechanism of DHX36 remains still elusive and many data show contradictory results. Moreover, viral studies on real *DHX36* knock out cells are missing, since former experimental setups only used tamoxifen-induced deletion or RNAi-mediated knock down of *DHX36*.

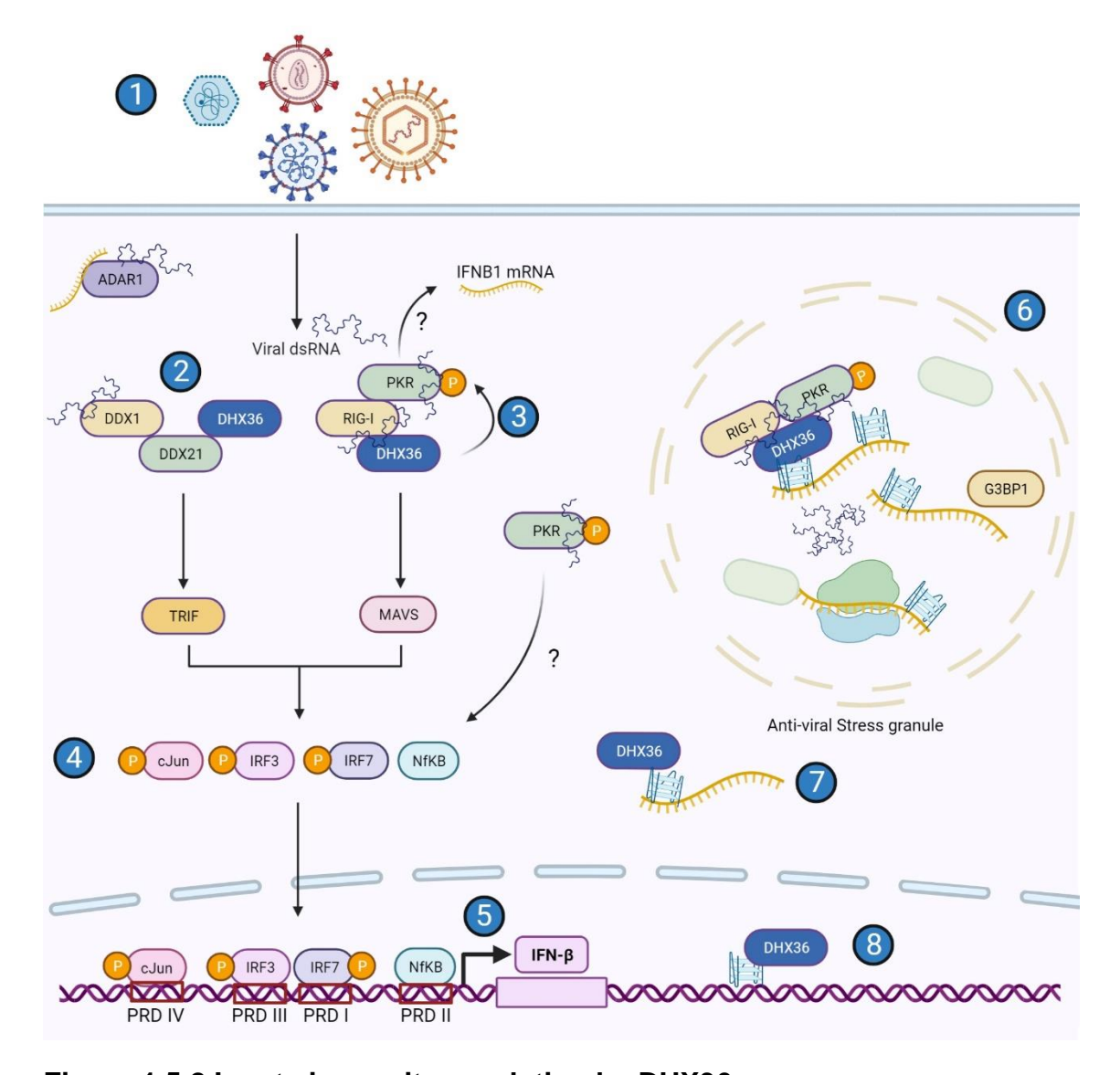


Figure 1.5.2 Innate immunity regulation by DHX36

(1) In myeloid dendritic cells, virus injected RNA binds intracellularly to a (2) complex consisting of DHX36, DDX21, and DDX1, in which the latter binds directly to the nucleic acids and DDX21 bridges the interaction of DHX36 and DDX1. (4) All three proteins bind to TRIF to stimulate the expression of interferons (5). DXH36 is also in complex with RIG-I and PKR and all three proteins bind to viral RNA in mouse embryonic fibroblasts. (3) DHX36 enhances PKR phosphorylation to inhibit viral infection. (6) In HeLa cells, the proteins of this complex localize to stress granules and loss of *DHX36* leads to reduced stress granule (SG) formation in virus infection. Moreover, *DHX36* depletion in human embryonic kidney cells leads to induction of SG formation without a viral trigger, most likely induced by the accumulation of RNA G-quadruplexes (G4s) harboring mRNAs. (7) In this regard, DHX36 binds to RNA G4s on mRNAs in a global fashion and destabilize those to render the mRNA accessible for the translation machinery. Furthermore, DHX36 is the major helicase, which unwinds G4 on (7) RNA and (8) DNA in HeLa cell lysates. Figure created with BioRender.

1.6 Aim of the study

Uncertain times and fear of the unknown drives us further and further. Beyond basic research, this study was a small contribution to face and fight global viral threats yet to come. Despite this, the overall aim of this thesis is to shed light on the proposed main functions of the DEAH-box helicase DHX36 in anti-viral immune responses.

To address this question, transcriptome-wide studies coupled with biochemical analyzes of differently regulated mRNAs in *DHX36* knock out cells with and without viral stress were pinpointed to a set of genes. Based on these results, implications in the regulation of the interferon I response was further examined in order to identify the specific signaling cascade of DHX36 as well as interaction partners. Finally, the dependence of DHX36 on general cellular metabolism and viral replication was confirmed with additional experimental data.

In order to accomplish these aims, next-generation sequencing of the transcriptome was performed in *DHX36* knock out cells. Viral stress treatments were performed to further validate the obtained results by the analyzes of mRNA and protein accumulations. Additionally, loss of function and overexpression experiments were conducted with a special focus on the identified interferon stimulated gene sets. Finally, potential models were based on protein-protein interactions of DHX36 as well as CRISPR-Cas9 mediated double knock out studies to identify epistatic mechanisms.

2. Material and methods

2.1 Bacteria cell culture

2.1.1 Cultivation of bacteria

All used or generated *E. coli* strains were grown on LB agar plates at 37°C in a bacterial incubator. Liquid growth cultures were inoculated from a single-grown colony and in 5 mL of liquid media incubated at 37°C and 200 rpm agitation overnight (~16 hours).

If necessary, solid and liquid bacterial growth media were supplemented with the appropriate amounts of antibiotics compatible to resistances of each bacteria strain (100 μ g ml⁻¹ ampicillin, 50 μ g ml⁻¹ kanamycin, 30 μ g ml⁻¹ chloramphenicol). The OD600 was measured using a spectrophotometer.

2.1.2 Cryo-conservation of bacteria

Bacteria stocks were prepared from a fresh overnight culture (liquid) by mixing 800 µl bacterial culture with 50% sterile glycerol for cryo-conservation. Snap-freezing was performed in liquid nitrogen and stocks were afterwards stored at -80°C.

2.1.3 Preparation of chemical-competent E. coli

A single colony of *E. coli* DH5 α was inoculated in LB liquid media and grown overnight at 37°C and 200 rpm agitation. On the next morning 250 mL SOB media were inoculated with 2 mL of the overnight culture and grown at 18°C and 180 rpm agitation until the culture reached OD600 = 0.6 The bacterial suspension culture was chilled on ice for 10 min and afterwards centrifuged at 4°C and 2000 rpm for 10 min. The bacteria pellet was resuspended in 80 mL ice-cold TB buffer, incubated for 10 min on ice and again centrifuged at 4°C and 2000 rpm for 10 min. The pellet was carefully resuspended in 20 mL fresh ice-cold TB buffer by agitation. DMSO (f.c. 7%) was added and the suspension was incubated in ice for 10 min. Finally, the cells were aliquoted (100 μ L), snap-frozen in liquid nitrogen and stored at -80°C.

2.1.4 Transformation of plasmid DNA in bacteria

An amount of 50 μ L chemical-competent *E. coli* DH5 α cells was thawed on ice. The bacterial suspension was supplemented with 1 to 10 ng of cold plasmid DNA and afterwards incubated for 30 min on ice. A heat shock was performed at 42°C for 50 sec and were put back immediately on ice for 5 min. A volume of 450 μ L of pre-warmed SOC medium was added to the suspension and incubated for 1 h at 37°C and 500 rpm

agitation in a heat block. After collecting the bacteria by centrifugation for 1 min at 8000 xg the pellet was resuspended in 150 μ L SOC medium. The bacterial suspension was spread on a respective selective LB agar plate (100 μ g ml⁻¹ ampicillin, 50 μ g ml⁻¹ kanamycin, or 30 μ g ml⁻¹ chloramphenicol) and incubated at 37°C over night.

2.2 Eukaryotic cell culture

2.2.1 Cultivation of adherent eukaryotic cells

Adherent HEK293 cells were cultured in DMEM medium supplemented with 10% FBS (v/v) and 1% Penicillin/Streptomycin (v/v) in sterile cell culture petri dishes in a cell incubator at 37°C and 5% CO₂. Media for "wildtype" cells were additionally supplemented with 100 μg ml⁻¹ Zeocin and 10 μg ml⁻¹ Blasticidin. Selection media for stable transfected cells contained 100 μg ml⁻¹ Hygromycin B instead of Zeocin.

Cells were passaged regularly after reaching 70% of confluence. Passaging was performed by washing the cells with pre-warmed sterile PBS. Afterwards, the cells were incubated with a Trypsin-EDTA solution and incubated for 5 to 8 min at 37°C with 5% CO₂. The detachment reaction was stopped by adding the respective DMEM medium. After counting the cell amount by using a hemocytometer the cells were seeded in a new cell culture petri dish and incubated further at 37°C and 5% CO₂. After maximal 15 passages the cells were discarded and a new aliquot of fresh cells was thawed.

2.2.2 Cryo-conservation of eukaryotic cells

Long term storage of eukaryotic cells was achieved by cryo-conservation. A cell suspension was prepared as in 6.2.2.1. The collected cell pellet was dissolved in freezing media (standard DMEM medium additionally supplemented with 10% FBS and 10% DMSO) to achieve a cell density of 3*10⁶ cells/mL. Each vial was filled with 1 mL of cell suspension and frozen in a cell freezing container at -80°C enabling a steady decrease in temperature. After 3 days at -80°C the cryo vials were transferred to a -150°C freezer for long term storage.

2.2.3 Thawing of cryo-conserved eukaryotic cells

Frozen cryo-conserved eukaryotic cell stocks were thawed in a water bath at 37°C and transferred to a 15 mL reaction tube filled with pre-warmed standard DMEM medium. The cell suspension was centrifuged for 3 min at 200 xg and the supernatant was discarded. The cell pellet was resuspended in 5 mL standard DMEM medium and

transferred to a 10 cm cell culture petri dish filled with 10 mL standard DMEM medium. The cells were incubated at 37°C and 5% CO₂.

2.2.4 Generation of stable eukaryotic cell lines

All stable HEK293 cell lines were generated by Dr. Markus Sauer and colleagues (Sauer et al., 2019). In short, HEK Flip-In™ T-REx™ 293 cells were grown in DMEM medium until ~40-50% confluency. 9 µg of the pFRT plasmid with the integrated gene of interest and 1 µg of the helper plasmid pOG44 (Flp recombinase) were diluted in 440 µL sterile ddH₂O. An amount of 50 µL sterile 2.5 M CaCl₂ solution was added to the plasmid mixture. In the meanwhile, the cells in the petri dish were treated with 40 µM (f.c.) chloroquine for 5 min. Afterwards, 500 µL 2x HBS buffer were dropwise added to the plasmid solution and carefully mixed after each drop. After a 5 min incubation step at RT the mixture was added to the cells in the petri dish and incubated for 5 h at 37°C and 5% CO₂. Next, the medium was exchanged with standard DMEM medium and the cells were further incubated for 2,5 days at 37°C and 5% CO₂. Collection of transfected clones was achieved by adding DMEM selection medium supplemented with hygromycin and blasticidin until single clone colonies were possible for further expansion.

2.2.5 Stress treatments of eukaryotic cells

Transient transfection of HEK293 or HeLa cells was performed according to the LipofectaminTM 2000 transfection reagent protocol from Thermo Fisher Scientific. For transfections in a single well of a 6-well plate 48 μ L of Opti-MEM medium were mixed with 2 μ L Poly I:C (HMW) of a 1 μ g/ μ L stock solution (f.c. 1 μ g/mL) in a reaction tube. A second reaction tube was filled with 46 μ L Opti-MEM medium and 4 μ L LipofectaminTM 2000 (twice the amount of the μ g of the used nucleic acid) were added. Afterwards, the Poly I:C containing solution was added dropwise to the reaction tube containing LipofectaminTM 2000. The mixture was incubated for 5 min at RT and subsequently, 100 μ L of the solution were added dropwise to the well of the 6-well plate containing 2 mL of normal growth medium and the cells.

The RIG-I ligand IVT4 (*in-vitro* transcript 4) was transfected the same way like Poly I:C but with a f.c. of 100 ng/mL medium and the appropriate amount of LipofectaminTM 2000.

The chemical compound INF α was added directly to the medium of the cells in a concentration of 10.000 U/mL.

2.2.6 CRISPR/Cas9-mediated gene knockout in eukaryotic cells

The stable knockout of DHX36 in HEK Flip-In[™] T-REx[™] 293 cells was performed by Dr. Stefan Juranek (Sauer et al., 2019). In short, 4x 10⁵ Flp-In T-REx HEK293 cells were grown over night in a 6-well plate. On the next morning, 100 pmol DHX36 crRNA and 100 pmol tracrRNA-ATTO 550 complementary to the crRNA were solved together in Nuclease-Free Duplex Buffer. After incubation at 95°C for 5 min the reaction was cooled at RT for 15 min. 125 µl Opti-MEM mixed with 7.5 µl CRISPRMAX Transfection Reagent and 15 pmol annealed RNA was mixed with 15 pmol Cas9 protein and 5 µl Cas9+reagent (IDT) in Opti-MEM. Both solutions were incubated for 5 min at RT. The RNA mix was carefully added to the Transfection Reagent solution and afterwards transferred dropwise to the HEK Flip-In[™] T-REx[™] 293 cells in the 6-well plate. Selection of positive transfected cells was achieved by single cell flow cytometry in a 96-well plate. The DHX36 knock out was validated by western blot and on DNA sequencing.

2.2.7 Lentiviral production for CRISPR/Cas9

An amount of 3.8 x106 293 LentiX cells were cultured in DMEM medium supplemented with 10% FBS (v/v) and 1% Penicillin/Streptomycin (v/v) in sterile cell culture 10 cm petri dishes in a cell incubator at 37°C and 5% CO₂. After one day and 5 h before transfection, the medium was exchanged to normal DMEM with 10% FBS and 1% PS and additional 25 μ M chloroquine. The vector plasmid (pLenti/pRRL) with integrated guide RNA, 2 μ g packaging vector (psPAX2/dr81.9) and 1 μ g of the viral envelop vector (pMD2G/VSVG) were combined in 1 mL Opti-MEM at room temperature. 21 μ L Polyethylenimine 25 kDa (PEI) were added to the transfection mix (3:1 ratio of PEI to total DNA) and incubated for 15 min at room temperature. Afterwards, the transfection mix was added drop-wise to the cells. On the next morning, the medium was exchanged to normal DMEM with 10% FBS and 1% PS. The supernatant was harvested and filter through a 0.45 μ m syringe and kept at -80°C for long term storage.

2.2.8 Light microscopy

Microscopic images were taken after indicated time points of treatments (see always the specific treatments) using an EVOS FL cell imaging system.

2.2.9 Growth analysis of adherent eukaryotic cells

The growth rate of the different HEK cell lines under Poly I:C conditions was analyzed by counting over a time period of 10 days. The starting cell number for all cell lines was 0.1 x10⁶ in a single well of a 6-well plate in technical triplicates. Cell number analysis was calculated by counting with a Bürker hemocytometer.

2.2.10 MTT proliferation assay

Cell proliferation of different HEK cell lines after Poly I:C treatment was analyzed by a commercial MTT-based proliferation approach. HEK Flip-In™ T-REx™ 293 "wildtype" cells and HEK Flip-In™ T-REx™ 293 DHX36 KO cells were seeded 0.7 x10⁴ or 1 x10⁴, respectively, in triplicates in a 96-well plate. After the Poly I:C treatments the medium was discarded and 100 µL of a 0.5 mg/mL MTT solution was carefully added to the cells. The cells were incubated for 4 h at 37°C and 5% CO₂. Afterwards, 100 µL DMSO was added to each well and incubated for 1 h at RT and 100 rpm in the dark. The solution was thoroughly mixed with a pipette and the absorbance was measured at 570 nm with a Tecan Infinite®200 plate reader.

2.2.11 FACS (Fluorescence-activated cell sorting)

Trypsinized single eukaryotic cells (in FACS tubes) were washed two times with 2 mL cold PBS (centrifugation at 500 xg for 3 min) and collected in 100 μL Fixable Viability Dye eFluor 780 (diluted 1:1000 in 1xPBS buffer) in a concentration of 500.000 cells/mL. After brief vortexing the cells suspension was incubated for 30 min at 4°C in the dark. Subsequently, the cells were washed two times with 2 mL cold PBS (centrifugation at 500 xg for 3 min). The cells were resuspended in 1 mL cold PBS and 1 drop of Hoechst 33342 Ready Flow Reagent was added and incubated for 60 min at 37°C while shaking at 200 rpm in the dark. Afterwards, the cells were washed two times with 2 mL PBS and the cells were finally collected in 400 μL PBS. After filtration through a filter paper the cells were ready for analysis with the BD FACSCantoTM II Cell Analyzer. All experiments were later on further analyzed using the FlowJo software (FlowJo LLC).

2.3 DNA biochemistry

2.3.1 Preparation of plasmid DNA

Isolation of DNA plasmids from bacteria was performed with the innuPREP Plasmid Mini Kit (Analytik Jena) and according to the supplier's instructions.

2.3.2 Polymerase Chain Reaction (PCR)

PCRs were performed by preparing a mix out of all reagents listed in the table below. For analytical PCRs the homemade Taq polymerase was used. PCRs for cloning were performed with the commercial ExTaq polymerase.

Reagent	Homemade Taq	ExTaq
10x PCR buffer for homemade Taq	1x	-/-
10x ExTaq Buffer	-/-	1x
dNTP mix	200 μΜ	200 μΜ
Each primer	0.5 μΜ	0.5 μM
Template DNA	10 – 50 ng	10 – 50 ng
Homemade Taq	1 µl	-/-
ExTaq	-/-	1 U
ddH ₂ O	To 50 μl	To 50 μl

After combining all reagents, the PCR reaction tube was placed in a PCR cycler with the conditions shown in the table below.

Step	Time	Temperature	Cycle	
Initial denaturation	5 min	95°C	1x	
Denaturation	20 s	95°C		
Annealing	15 s	53 - 58°C*	30x - 36x	
Elongation	1 min/kb	72°C		
Final elongation	5 min	72°C	1x	
* depending on melting temperature of primer sets				

2.3.3 Agarose gel electrophoresis

Agarose powder (1 - 2%) was melted in 1x TAE buffer in a microwave and after 5 min of cooling in agitation 0,01% ethidium bromide was added to the gel solution and distributed by further stirring. The solution was poured into a gel tray and dried for 30 min at RT. The solidified gel was set up in an electrophoresis chamber filled with 1x TAE buffer and the DNA or RNA samples were loaded. Under standard conditions the voltage was set to 120 V for 120 min at RT. Detection of the nucleic acid signals was performed with a ChemiDOC XRS+ Imaging System.

2.3.4 Purification of DNA from agarose gels and PCR reactions

Plasmid and PCR fragment isolations from agarose gels were performed using the innuPREP Gel Extraction Kit (Analytik Jena) and innuPREP PCRpure Kit (Analytik Jena), respectively, according to the supplier's instructions.

2.3.5 Restriction digest of DNA

Restriction enzymes were purchased from Thermo Fisher Scientific and used according to the supplier's instructions. Restriction digestions were carried out for 2 - 3 hours at 37°C and afterwards analyzed by gel electrophoresis.

2.3.6 DNA ligation

Nucleic acid fragments from plasmid as well as PCR fragment digestions were ligated with the T4 DNA ligase in a molar ratio of 1:5 and with a total amount of 200 ng of total nucleic acid. The ligation was performed over night at 16°C.

2.3.7 Single-colony Polymerase Chain Reaction (scPCR)

Screening of positive transformed bacteria that carried the right plasmid was performed by PCR. Plasmids were isolated (see 6.2.3.1), digested with different restriction enzymes and afterwards analyzed by gel electrophoresis with following sequencing.

Reagent	Amount	
10x PCR buffer for homemade Taq	1x	
dNTP mix	200 μΜ	
Each primer	0.5 μΜ	
Template	Single colony	
Homemade Taq	0.5 μΙ	
ddH ₂ O	Το 20 μΙ	

The PCR cycler conditions are listed in the table below.

Step	Time	Temperature	Cycle
Initial denaturation	10 min	95°C	1x
Denaturation	20 s	95°C	
Annealing	15 s	53 - 58°C*	30x
Elongation	1 min/kb	72°C	
Final elongation	5 min	72°C	1x
* damagda an migray ant			
* depends on primer set			

2.3.8 DNA sequencing

Isolated plasmids from bacteria or eukaryotic DNA were sequenced by the Eurofins company. The samples were sent as pre-mixed in reaction tubes according to the companies' instructions. The sequencing results were analyzed with the Serial Cloner software.

2.4 Protein biochemistry

2.4.1 Protein isolation from eukaryotic cells

Eukaryotic cells were collected in a 1.5 mL tube after trypsinization (see 6.2.2.1). The cells were centrifuged at 200 xg for 5 min at RT and afterwards washed with cold PBS. After another centrifugation at 200 xg for 5 min at 4°C the cells were resuspended in NP40 lysis buffer and incubated for 15 min on ice. Subsequently, the cell suspension was centrifuged at 14.000 xg for 15 min at 4°C. At the end, the supernatant was

transferred to a new 1.5 mL tube and the protein concentration was measured by the Bradford assay.

2.4.2 Bradford assay

Protein concentrations were determined by the Bradford assay by combining 998 μ L 1x Bradford solution with 2 μ L of protein lysate. The solution was incubated for 5 min at RT in the dark and the absorbance at 595 nm was measured in a photometer.

2.4.3 Co-immunoprecipitation (Co-IP)

HEK293 DHX36 overexpression cells were treated with tetracycline overnight to induce the DHX36-FLAG protein. The cells were harvested on the next morning at 80-90% confluency. For this, the cells were washed 3 times with 5 mL cold 1x PBS and harvested with a cell scraper and transferred to a 1.5 mL tube. After centrifugation at 4°C with 200 rpm for 5 min the supernatant was discarded and the cell pellet was resuspended in 500 µL cold NP40 lysis buffer. The solution was incubated for 15 min on ice and afterwards centrifuged at 4°C with 14.000 xg for 15 min. The supernatant was transferred to a 2 mL tube and 50 µL were taken for the input sample and mixed with 10 µL 6x SDS loading buffer. The input was boiled for 5 min at 95°C and then stored at -20°C. The remaining 450 µL sample was filled up to 950 µL with NP40 lysis buffer and 50 μL αFLAG magnetic beads (washed once with NP40 lysis buffer on a magnetic rack) were added. The sample was incubated at 4°C on a head over tail rotator overnight. On the next day, the beads were washed 5 times on a magnetic rack with cold NP40 lysis buffer and subsequent 5 min rotation on a nutator on ice. After the last washing step, the remaining NP40 lysis buffer was discarded and the beads were resuspended in 35 µL 1x SDS loading dye and boiled for 10 min at 95°C. Subsequently, the beads were removed with the magnetic rack and the sample was transferred to a new reaction tube and was stored at -20°C for further analysis.

2.4.4 SDS-polyacrylamide gel electrophoresis (SDS-PAGE)

Protein separation was achieved by denaturating discontinuous sodium dodecyl sulphate polyacrylamide (PAA) gel electrophoresis (SDS-PAGE). Proteins were separated by size using a 12% SDS-PAA separating and a 4% SDS-PAA stacking gel containing 0.1% SDS and that were both polymerized by addition of 1:100 ammonium persulfate (APS) and 1:1000 tetramethylethylendiamin (TEMED). The isolated protein

samples were mixed with a 6x SDS protein loading dye (f.c. 1x SDS protein loading dye) and 20 μ L of the protein solution was loaded to each well of the SDS gel with a total concentration of 20 μ g of proteins per well. The SDS-PAGE chambers (Biorad) were assembled and the gel was run for 2 h at 80-120 V in 1x SDS running buffer.

2.4.5 Western blot

After protein separation by SDS-PAGE (see 6.2.4.4) the gel was transferred to the blotting chamber. All used items were soaked in blotting buffer and were placed in the blotting chamber in the following order (from bottom to top): Whatman paper, nitrocellulose membrane, the gel, Whatman paper. Remaining bubbles were removed by carful rolling with a small glass rod over the top Whatman paper. Semi-dry blotting for 1 h with 2 mA per cm² of the gel size (5x8 cm → 80 mA per gel) was performed. Afterwards, the membrane was transferred to 1x TBS-T containing 5% milk and incubated for 1 h at RT while rotating. The membrane was briefly washed with 1x TBS-T and transferred to a 50 mL tube containing 1x TBS-T with 2% milk and with the corresponding first antibody. The first antibody incubation was performed over night at 4°C on a rotator.

On the next morning, the first antibody solution was discarded and the membrane was washed three times for 10 min with 1x TBS-T. Subsequently, the membrane was incubated for 2 h at RT in a 50 mL tube with 1x TBS-T with 2% milk and with the corresponding secondary antibody. The membrane was afterwards washed three times with 1x TBS-T and the transferred to a plastic sheet. The membrane was incubated with 300 µL PierceTM ECL Western Blotting Substrates (1:1 ratio) and the reaction was detected with the Molecular Imager ChemiDOC XRS Imaging System. Detection times were calculated automatically by the device. Protein intensities were further analyzed and calculated with ImageJ (Fiji).

2.5 RNA biochemistry

2.5.1 RNA purification from human cells

Cells were harvested by adding 500 μ L TRIzol reagent to a single 6-well. After breaking of the cells by stirring the solution was transferred to a 1.5 mL reaction tube and 100 μ L chloroform were added. The solution was vortexed for 10 seconds and afterwards incubated for 10 min at room temperature. Subsequently, the phase separation was

achieved by centrifugation at 14.000 xg for 15 min at 4°C. The aqueous phase (contains the RNA) was transferred to a new 1.5 mL reaction tube and 1 Volume of ice-cold isopropanol was added for RNA precipitation. The solution was incubated for 30 min on ice and then centrifuged at 14.000 xg for 30 min at 4°C. The supernatant was discarded and the RNA pellet was vigorously washed with 70% ethanol. After centrifugation at 14.000 xg for 5 min at 4°C the supernatant was discarded and the remaining ethanol was spun down by a brief centrifugation at 14.000 xg at 4°C. The remaining ethanol was removed by carful pipetting and the pellet was dried for 5 min at room temperature. Finally, the dried pellet was resolved in 30 – 50 μ L RNase free ddH₂O. The RNA concentration was determined with a Nanodrop.

2.5.2 Reverse transcription (cDNA synthesis)

The SuperScriptTM III Reverse Transcriptase kit was used according to the supplier's instructions. In brief, 500 ng of isolated RNA (see 6.2.5.1) was diluted in 4 μ L of ddH₂O and 0.5 μ L Oligo d(T) primer and 0.5 μ L dNTPs (each 2.5 mmol). The solution was incubated at 65°C for 5 min and then placed on ice for 1 min. Afterwards, a mastermix of 2 μ L 5x First Strand buffer, 0.5 μ L DTT and 0.5 μ L SuperScript Reverse Transcriptase III was added to the RNA solution and incubated at 50°C for 50 min. The reverse transcription was terminated with a subsequent heat inactivation at 85°C for 5 min.

2.5.3 Quantitative Polymerase Chain Reaction (qPCR)

The collected cDNA (see 6.2.5.2) was diluted in 190 μ L ddH₂O. For a single qPCR reaction an amount of 3 μ L of the cDNA was mixed with 6 μ L IQ SYBR Green 2x Mastermix and 3 μ L primer mix (1 μ M forward and reverse primer). The subsequent qPCR was carried out in triplicates in a 96-well plate on a CFX96 RealTime System.

Step	Time	Temperature	Cycle
Initial denaturation	3 min	95°C	1x
Denaturation	15 s	95°C	
Annealing	15 s	57.5°C	40x
Elongation	15 s	72°C	

2.6 Others

2.6.1 RNA-sequencing

For RNA-sequencing, complementary DNA preparation of the resulting RNA was done with the NEBnext Ultra Directional RNA Library Prep Kit for Illumina. Enrichment of the cDNA was performed using indexed primers of the NEBNext Multiplex Oligos for Illumina and sequencing was performed on a HiSeq 2500 platform. Sequencing reads were aligned to the hg19 human genome using Tophat 2²⁹¹. Cufflinks was used to quantify reads on the UCSC hg19 annotation set differential expression was determined by Cuffdiff²⁹¹.

2.6.2 Fluorescence staining of stress granules (G3BP)

Sterile coverslips were coated with a 100 µg ml⁻¹ poly-D lysine solution for 1 h at 37°C. HEK293 "WT" and DHX36 KO cells were seeded in a density of 500.000 cells and 700.000 cells per well in a 6-well plate, respectively. The cells were grown until 60% confluency and then transfected with 1 µg/mL Poly I:C (see 6.2.2.5). After incubation at 37°C for the indicated time points, the cells were briefly washed 2 times with 1x PBS and then fixed in a 4% formaldehyde (PFA) solution diluted in 1x PBS for 10 min. Afterwards, the cells were washed once with 1x PBS and then permeabilized in 1x PBS supplemented with 1% BSA and 0,2% Triton X-100 for 30 min at 4°C. Afterwards, the cells were washed 2 times with cold 1x PBS. The coverslips were subsequently transferred to a 24-well plate and 200 μL of a f.c. 5 μg/mL αG3BP antibody solution diluted in 1x PBS with 2% milk was added. The samples were incubated at 4°C overnight. The next morning, the samples were washed 3 times for 5 min at 100 rpm at RT. Afterwards, the samples were incubated with 200 µL of a 1:1000 dilution of the Anti-Mouse Alexa Fluor 488 secondary antibody in 1x PBS with 2% milk for 2 h at RT. Finally, the coverslips were washed 3 times with 1x PBS and mounted with 10 µL Fluoroshield containing DAPI on a glass slide. The samples were analyzed by using a Leica fluorescence microscope.

3. Results

Previous studies described the role of the DEAH-box helicase DHX36 in anti-viral stress responses particularly in type I interferon (IFN) signaling. However, differences in the observations of *in cellulo* RNA recognition as well as several different protein-protein interactions gives rise to conflicting information about the real DHX36 function. Therefore, a system-wide analysis of DHX36 followed by in-depth biochemical approaches with regard to viral infections is indispensable for the full comprehension of its functions in type I IFN signaling.

For that reason, my PhD thesis is structured in 3 different sections: First, the analysis of consequences of the loss and overexpression of DHX36 on viral responses. Second, the investigation of DHX36 on cellular metabolism as well as viral replication and third, the understanding of molecular mechanisms of DXH36 in the type I IFN signaling cascade.

3.1 DHX36 is necessary for the maintenance of cellular homeostasis by inhibiting an uncontrolled type I interferon response

Our previous studies showed an accumulation of stress granules (SG) upon the loss of DHX36 as well as the phosphorylation of the viral RNA sensor PKR²²⁸. The human clustered regularly interspaced short palindromic repeats associated 9 (CRISPR/Cas9) generated DHX36 knockout (KO) human embryonic kidney (HEK) cells (Flp-In™ System of Thermo Fisher Scientific) were used to validate the former results²²⁸. In the following chapters the HEK Flp-In™ cells will referred to as wild type (WT) cells and HEK Flp-In™ DHX36 KO cells solely as DHX36 KO cells. Additionally, all discussed experiments in this thesis were performed in at least 3 biological replicates. Immunofluorescence staining of the SG localizing protein Ras GTPase-activating protein-binding protein 1 (G3BP1) was performed to visualize SG formation and the amount of SG-positive cells were counted using Image J (Figure 3.1.1 A). A significant increase in the detection of SG-positive cells of 6% in DHX36 KO cells compared to WT cells was observed (Figure 3.1.1 B). Furthermore, the phosphorylation of PKR is an indicator of its activation usually after sensing viral RNA. For this reason, proteins of untreated WT and DHX36 KO cells were extracted and further processed by immunoblotting (western blot). The detection was accomplished by the use of a specific antibody against the phosphorylated version of PKR. No phosphorylation of PKR was observed in WT cells, whereas the DXH36 KO

cells showed a slight increase in PKR phosphorylation (Figure 3.1.1 C). Both experiments confirmed the results of our initial study. The observed phenotypes of increased SG formation and enhanced PKR phosphorylation was speculated to be a result of accumulating endogenous RNA, harboring G-quadruplexes (rG4s) eliciting an uncontrolled immune response²²⁸. To test the hypothesis, RNA isolation of WT and DHX36 KO cells was performed and further processed by next generation sequencing (RNA-seq) to identify changes in transcription. As aforementioned, the phosphorylation of PKR takes place after foreign RNA sensing, which determined the focus on type I IFN induced signals including genes of the JAK-STAT signaling pathway and ISGs (Figure 3.1.1 D). A slight increase of the IFN- α/β receptors IFNAR1/2, as well as the downstream acting genes JAK1/2, was observed in the DHX36 KO cells comparted to WT cells. Moreover, two genes implicated in IFN signaling, STAT2/5b, as well as several JAK-STAT inhibitors SOCS2/5/6 were highly upregulated in DHX36 KO cells. On the other hand, several genes were below the detection threshold in the RNA-seg analysis, especially ISGs (Figure 2 A). For this reason, reverse transcription quantitative polymerase chain reaction (RT-qPCR; short qPCR) was performed for in-depth analysis and confirmation of the RNA-seq results. All the subsequent displayed qPCR results in this thesis were initially normalized to the house keeping gene RNU6 (for all following data not explicitly mentioned). Under normal conditions, the basal expression levels of IRF7 are low and strongly induced after type I IFN signaling and thus, display a good indicator of cellular viral stress⁹⁵. Indeed, the DHX36 KO cells exhibit increased IRF7 transcript levels compared to WT cells (Figure 3.1.1 E). Further analyzes of early (IFNB1) as well as late expressed genes (IFIT1, RSAD2 and ADAR1) induced by viral RNA sensing showed a similar pattern with a significant 2-fold increase in transcripts for DHX36 KO cells compared to WT cells (Figure 3.1.1 F-J). DDX58 (RIG-I) levels displayed a slight upregulation, yet not significant. To exclude a differential uptake of nucleic acids, induced by the DHX36 mutation, a plasmid transfection was conducted expressing green fluorescent protein (GFP) under a constitutively expressed promoter. As expected, there was no significant difference in the amount of GFP positive cells (Supplementary Figure 1 A).

Taken together, these results confirm the initial hypothesis of an induced type I interferon response without a viral trigger upon the loss of *DHX36*.

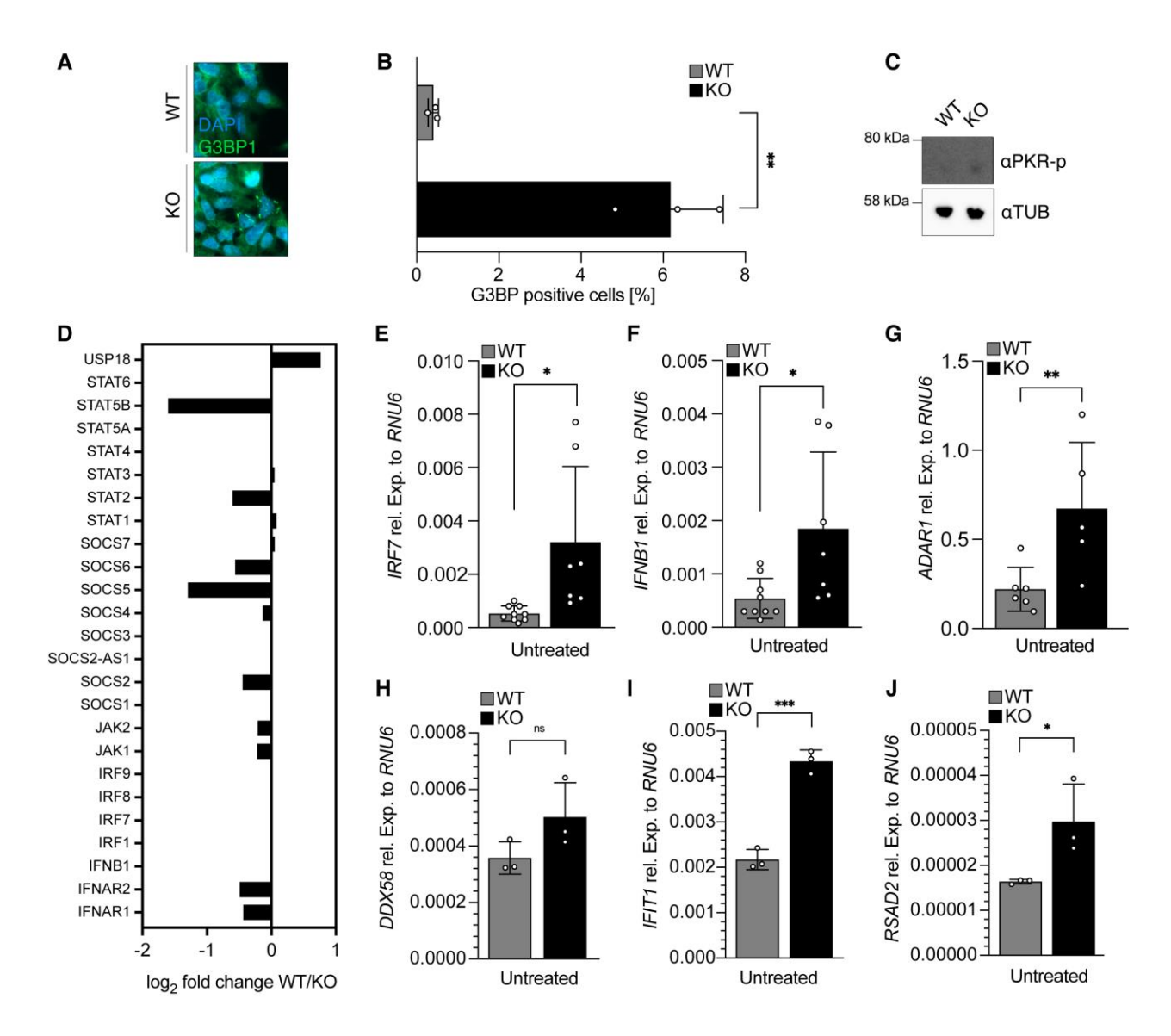


Figure 3.1.1 The knockout of DHX36 induces anti-viral stress conditions

A) Immunofluorescence staining of SG localizing protein G3BP1 in WT and *DHX36* KO cells. DAPI was used as a DNA/nucleus marker. B) Quantifications of G3PB1 positive cells in WT and *DHX36* KO cells. C) Immunoblot (western blot) analysis of WT and *DHX36* KO cells using antibodies against phosphorylated PKR and α-tubulin after protein size separation by SDS-PAGE. D) RNA-seq analysis of the JAK-STAT pathway comparing transcript levels of WT and *DHX36* KO cells. Differences of gene transcript levels are indicated as log₂ fold changes of reads per kilobase of transcript per million mapped reads (RPKM). E) - J) Transcript quantifications by RT-qPCR of the indicated genes in untreated conditions comparing WT and *DHX36* KO cells normalized to mRNA levels of *RNU6*. Significances were determined by Students t-test (n≥3). Significance levels: *p < 0.05, **p < 0.01, ***p < 0.001, ns = not significant. Error bars represent standard deviations of at least 3 biological replicates.

3.2 Loss of DHX36 results in increased type I IFN signaling

The observation of increased type I IFN signaling genes indicates a primed state of cells in the absence of DHX36 (Figure 3.2.1 A-J). To test this assumption, WT and DHX36 KO cells were treated with the RNA nucleic acid analogue poly (I:C) for 12 h and 24 h mediated by Lipofectamin 2000 transfection. Subsequently, RNA isolation and RNA-seq analysis with a focus on the JAK-STAT pathway and ISGs revealed a strong increase in transcript levels of most of the investigated genes after 12 h administration of poly (I:C) with a peak at 24 h post treatment (Figure 3.2.1 A). To further strengthen the RNA-seq data, a timeline of poly (I:C) treatment with the indicated time points was performed in WT and DHX36 KO cells and isolated RNA was analyzed by qPCR. Fold changes to WT untreated levels for the 4 target genes IFNB1 and DDX58 as well as IFIT1 and RSAD2 covering early and late IFN pathway genes, respectively, showed a clear phenotype. The transcript levels of IFNB1 started to increase after 6h post poly (I:C) incubation and peaked after 24 h (Figure 3.2.1 B). Interestingly, DHX36 KO cells display a 2.5-fold increase compared to WT cells. Similarly, DDX58 transcription was already observed after 3 h poly (I:C) treatment. However, the peaks of transcript levels at 6 h and 12 h differed between WT and DHX36 KO cells, respectively (Figure 3.2.1 C). Moreover, an almost 4-fold change after 12 h treatment was observed for the DHX36 KO cells in comparison to WT cells. A decrease in transcription of DDX58 was observed in the DHX36 KO cells from 12 h to 24 h, whereas the DDX58 levels almost remained at a steady state from 12 h to 24 h in WT cells. In case of IFIT1 and RSAD2, the transcription slightly increased from 3 h to 12 h after poly (I:C) treatment and was highest at 24 h in WT and DHX36 KO cells (Figure 3.2.1 C-D). In line with the previous results, the expression levels of both genes showed a 5-fold increase in the DHX36 KO cells in relation to WT cells.

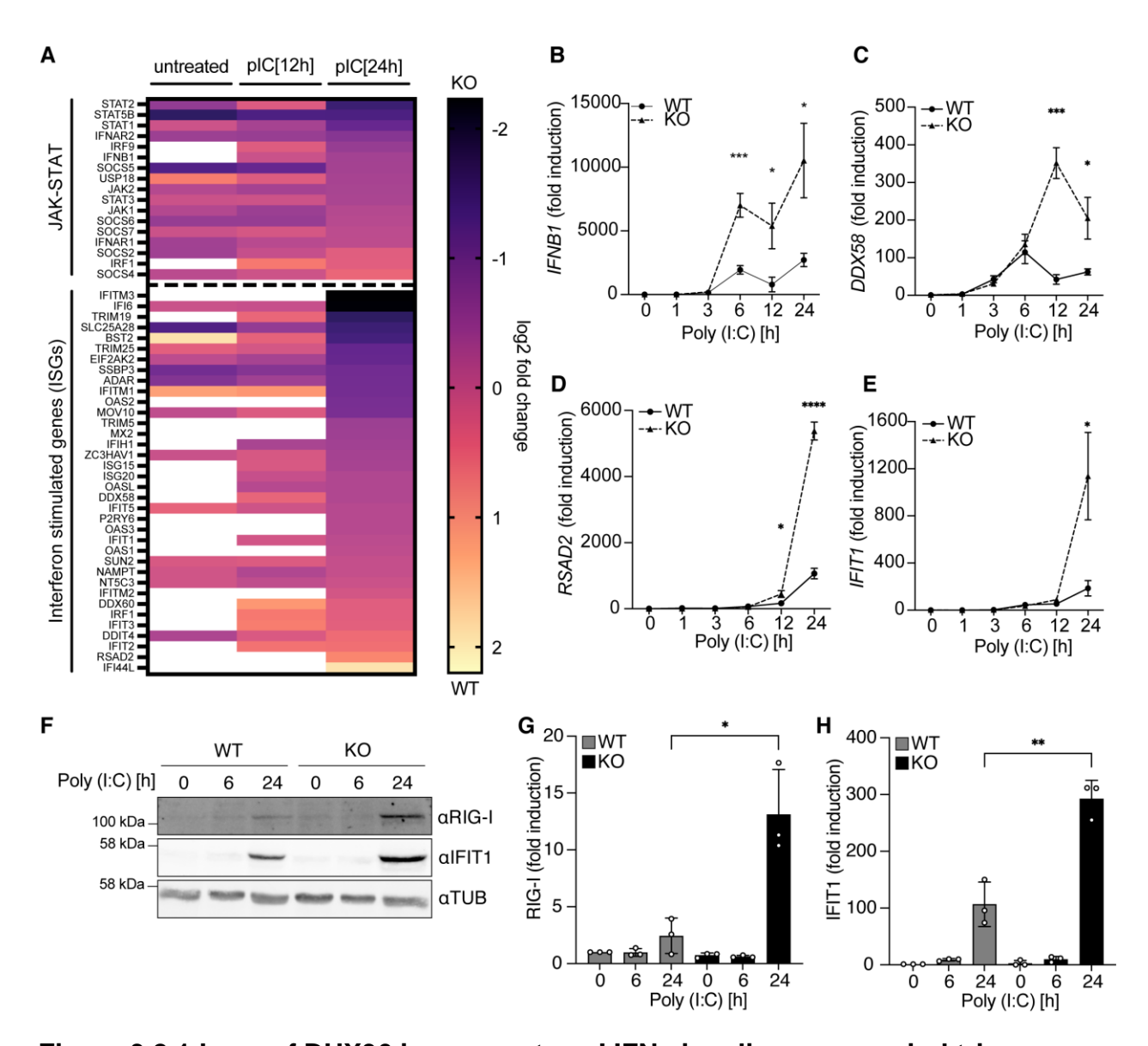


Figure 3.2.1 Loss of DHX36 increases type I IFN signaling upon a viral trigger

A) RNA-seq analysis of the JAK-STAT pathway and interferon stimulated genes (ISGs) of WT and DHX36 KO cells after 0 h, 12 h and 24 h treatment with poly (I:C). Differences of gene transcript levels are shown as \log_2 fold changes of RPKM values. White blocks indicate low expression levels excluded by a cut off set at RPKM = 5. B) - E) Transcript quantifications by RT-qPCR of the indicated genes after different time points of poly (I:C) treatment comparing WT and DHX36 KO cells. Gene transcripts are displayed after normalization to mRNA levels of RNU6. Fold changes were calculated to WT untreated conditions. F) Immunoblot analysis of WT and DHX36 KO cells upon poly (I:C) treatment using antibodies against RIG-I, IFIT1 and α -tubulin after size separation via SDS-PAG. G-H) Protein signal intensities were quantified by measuring the densitometry using ImageJ and were normalized to the α -tubulin signal. Fold changes are displayed in comparison to WT untreated levels. Significances were determined by Students t-test (n \geq 3). Significance levels: *p < 0.05, **p < 0.01, and ****p < 0.001. Error bars represent standard deviations of at least 3 biological replicates.

DHX36 plays an important role in the stability and translation of mRNAs and loss of this helicase leads to the accumulation of translationally incompetent mRNAs 228 . To address the question whether increased mRNA levels of type I IFN genes eventually lead to elevated protein outputs, proteins of WT and *DHX36* KO cells after poly (I:C) treatment were extracted and analyzed by immunoblotting. Detection of the proteins was accomplished by the use of specific primary antibodies and the corresponding fluorescently labelled secondary antibodies. Afterwards, the protein levels of RIG-I and IFIT1 were normalized to the housekeeping gene α -Tubulin. At a steady state, both proteins show minor protein levels below the detection limit, however, a high induction was observed after 24 h after poly (I:C) treatment (Figure 3.2.1 F). Moreover, the results clearly showed a significant 3 to 4-fold increase for IFIT1 and RIG-I, respectively, in *DHX36* KO cells relatively to WT cells (Figure 3.2.1 G-H).

These results confirmed the hypothesis of an anti-viral primed cell state of cells upon the loss of *DHX36* as well as an increased type I IFN response upon a viral trigger.

3.3 DHX36 negatively regulates type I IFN signaling

The collected data strongly suggests a negative regulation of type I IFN signaling by DHX36. To test this assumption, a timeline of WT cells treated with poly (I:C) for the indicated time point was performed to check for the transcription of *DHX36*. Isolated RNA samples were reverse transcribed into complementary DNA (cDNA), analyzed by qPCR and the results are displayed after normalization to untreated WT cells. Already after 1 h a slight decrease of *DHX36* transcript levels was observed, which further reduced at 3 h and 6 h post treatment (Figure 3.3.1 A). At 12 h of poly (I:C) treatment, the transcript levels raised and returned to a similar level as detected in untreated conditions. In order to strengthen these results, protein lysates were generated for the same conditions and analyzed by immunoblotting using a DHX36 monoclonal antibody. Interestingly, the protein expression of DHX36 differed in a temporal manner compared to the qPCR results. Here, DHX36 protein levels remained unchanged until 6 h after the application of poly (I:C). Only after 24 h, a significantly strong decline was observed comparable to a complete vanishing of DHX36 protein levels as seen in *DHX36* KO cells (Figure 3.3.1 B-C).

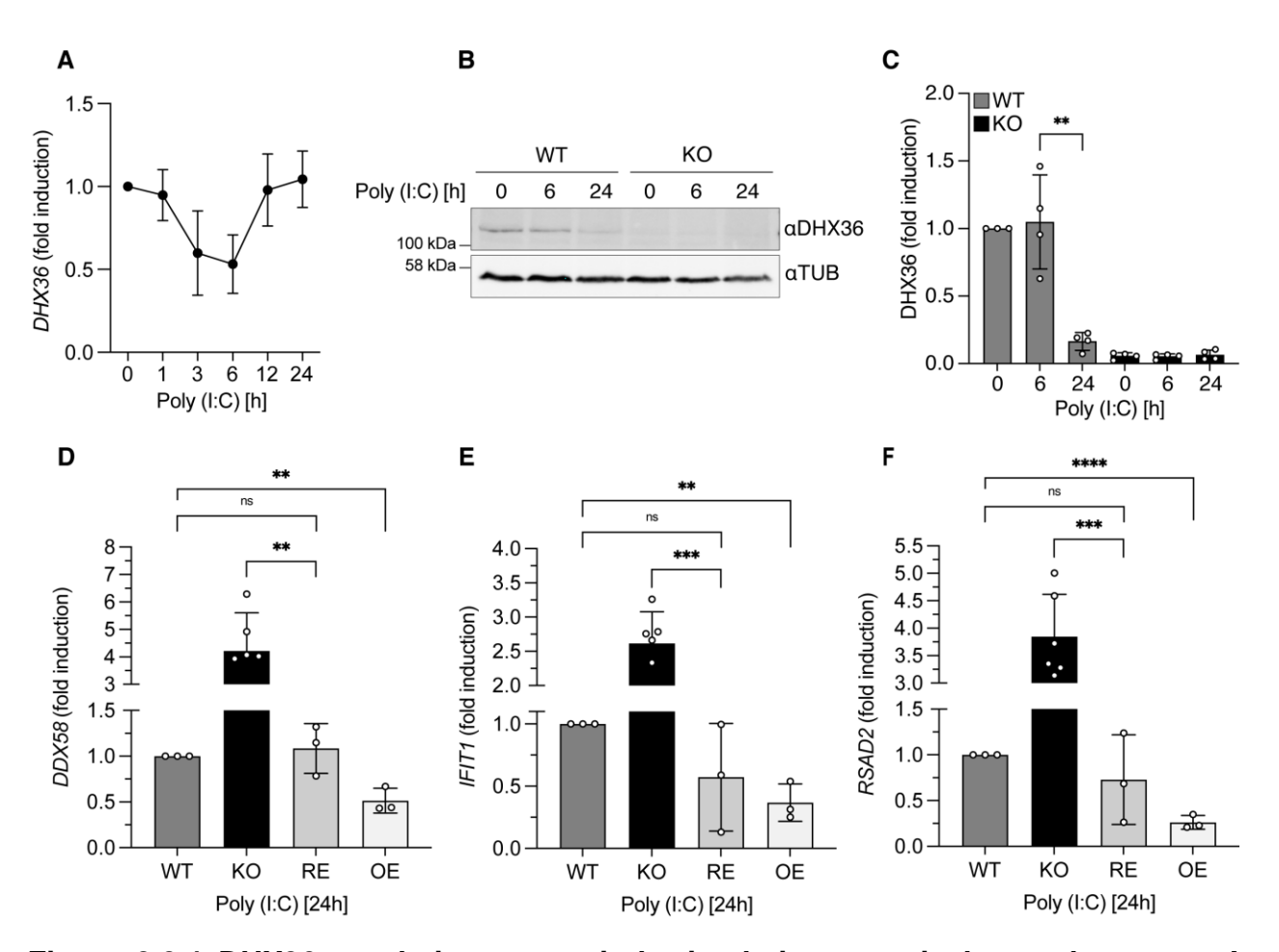


Figure 3.3.1 DHX36 regulation upon viral stimulation negatively regulates type I IFN signaling

A) Transcript quantifications by RT-qPCR of *DHX36* during a time course of poly (I:C) treatment in WT cells. *DHX36* transcripts are displayed after normalization to mRNA levels of *RNU6*. Fold changes were calculated to WT untreated conditions. B) Immunoblot analysis of WT and *DHX36* KO cells upon poly (I:C) treatment using antibodies against DHX36 and α-tubulin after size separation via SDS-PAG. C) Protein signal intensities were quantified by measuring the densitometry using ImageJ and were normalized to the α-tubulin signal. Fold changes are displayed in comparison to WT untreated levels. D) - F) Transcript quantifications by RT-qPCR of the indicated genes after ectopic integration of *DHX36*isoform1 into *DXH36* KO cells (RE = rescue) and WT cells (OE = overexpression) following poly (I:C) treatment for 24 h. Signals were normalized to RNU6 and fold changes were calculated to WT cells after 24 h poly (I:C) treatment. Significances were determined by Students t-test (n≥3). Significance levels: *p < 0.05, **p < 0.01, ***p < 0.001, ns = not significant. Error bars represent standard deviations of at least 3 biological replicates.

Since the strong downregulation in expression of DHX36 after a viral trigger resembles the cellular conditions upon loss of DHX36, the question was whether this decline of DHX36 is necessary to induce a type I IFN response. To this end, HEK (Flp-In™ System of Thermo Fisher Scientific) cells with a stable ectopic integration of N-terminally FLAG/HA tagged DHX36 isoform1 (DHX36iso1) at the Flip In site were deployed (referred to as DHX36 OE hereafter). Moreover, the same reporter construct was applied to the DHX36 KO cells in order to rescue the observed phenotypes of enhanced ISG levels and thus, exclude any off-target effects caused by the CRISPR/Cas9 evoked genetic mutation (referred to as DHX36 RE hereafter). The temporal transgenic expression of the DHX36 OE cells was induced by the application of tetracycline for 16 h. Afterwards, all conditions were treated for 24 h with poly (I:C) and RNA samples were taken, reverse transcribed and finally analyzed by qPCR. The results were normalized to WT conditions after 24 h of treatment. In case of all analyzed genes, DDX58, IFIT1 and RSAD2, the DHX36 RE showed no significant differences to the transcript levels of the WT cells (Figure 3.3.1 D-E). The comparison of DHX36 KO to DHX36 RE cells confirmed the previous observed phenotype of increased levels of all 3 examined genes. Intriguingly, the DHX36 overexpression cell line showed the opposite effect with a significant decrease of roughly 2-fold of all tested ISGs after 24 h poly (I:C) treatment (Figure 3.3.1 D-E).

Taken together, the downregulation of DHX36 protein levels upon poly (I:C) treatment as well as the observed decrease in ISG transcripts after preventing this downregulation point to a negative regulation of type I IFN signaling by DHX36.

3.4 The ablation of DHX36 augments stress tolerance and viral resistance

Increased levels of ISGs as observed in the *DHX36* KO cells suggest an augmented resistance to viral stress (Figure 3.1-3.2). In order to check this hypothesis, WT cells and *DHX36* KO cells were treated for 24 h with poly (I:C) and analyzed by light microscopy for phenotypic alterations. Generally, the loss of *DHX36* leads to a reduction in duplication time of cells as well as formation of cell clusters (Figure 3.4.1 A)²²⁸. After administration of poly (I:C) the WT cells detached from the surface of the dish and remained in the supernatant in a spherical form resembling dead cells. In contrast, the *DHX36* KO cells remained mainly attached to the surface after the 24 h treatment with poly (I:C). To test whether the detached cells undergo cell death after poly (I:C)

treatment, fluorescence activated cell sorting (FACS) with specific dyes to distinguish live from dead cells was performed. Unexpectedly, no increase in cell death was observed after the poly (I:C) administration in the cases of WT cells and *DHX36* KO cells indicating the spherical detached cells remain live for the time of treatment (Figure 3.4.1 B). Furthermore, the clear phenotype of the *DHX36* KO cells in light microscopy could hint to an increased fitness of the cells. To test this hypothesis, a colorimetric assay referred to as MTT for assessing the cell metabolic activity was conducted in untreated and 24 h poly (I:C) treated conditions. In this case, the poly (I:C) treatments were normalized to the regarding cell conditions, either WT or *DHX36* KO, to exclude observed changes caused by the cellular growth defects in the *DHX36* KO cells. The addition of poly (I:C) reduced the WT cells metabolic activity by 50%, whereas the *DHX36* KO cells showed only a 30% reduction in metabolism (Figure 3.4.1 C).

61

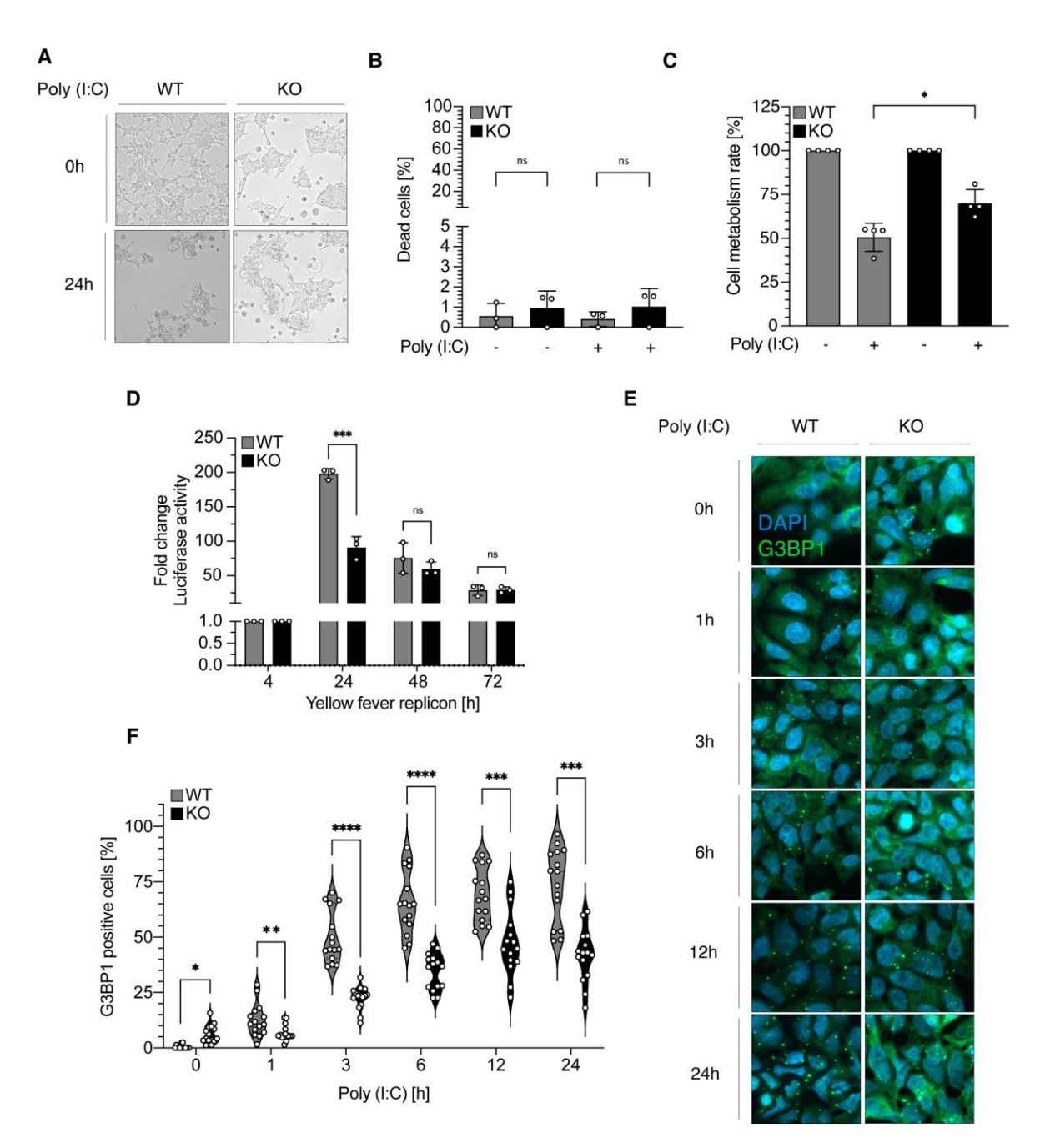


Figure 3.4.1 Loss of DHX36 gives rise to enhanced anti-viral responses and increased cell metabolism

A) Microscopic analysis of the WT and DHX36 KO cell phenotypes upon poly (I:C) treatment. B) Cell death after the application of poly (I:C) was determined by the dye eFluor 780 incorporating only into dead cells via FACS. Percentages of three times 100.000 positive cells are presented of WT and DHX36 KO cells. C) The cell metabolic rate was analyzed by MTT assay. Normalization of the 24 h poly (I:C) treated samples to the respective untreated conditions are displayed for WT and DHX36 KO cells. D) Differences of luciferase activity that is concomitantly connected with yellow fever virus replicon replication was analyzed by measuring the absorption. Fold changes of luciferase levels of WT and DHX36 KO levels normalized to the treatment after 4 h are

displayed. E) Immunofluorescence staining of G3BP1 in WT and DHX36 KO cells after poly (I:C) treatments for the indicated time points. DAPI was used as a DNA/nucleus marker. F) Quantifications of G3PB1 positive cells in WT and DHX36 KO cells. Significances were determined by Students t-test (n \geq 3). Significance levels: *p < 0.05, **p < 0.01, ***p < 0.001, ns = not significant. Error bars represent standard deviations of at least 3 biological replicates.

The previous data show an augmented stress tolerance under artificial viral infection conditions using the RNA analogue poly (I:C) (Figure 3.4.1 A-C). To further challenge the aforementioned hypothesis, a viral replicon of the yellow fever virus (YFV) was used to investigate differences in viral replication. This replicon harbors all viral proteins necessary for replication, however, is incapable of the production of viral particles caused by the lack of structural core proteins. Additionally, a Renilla luciferase is located upstream of the viral genes and is used as a fluorescent read out for the amount of replicon inside of the cells analyzed by absorption after cell lysis. The YFV replicon was transfected to WT and DHX36 KO cells by electroporation and samples were taken on 3 consecutive days. The measured absorption of all WT and KO DHX36 cells were normalized to WT or DHX36 KO cells samples taken at 4 h after transfection, respectively. In both cases, a strong increase in Renilla luciferase activity was observed after 24 h post treatment with a subsequent decrease after 48 h and 72 h (Figure 3.4.1 D). Intriguingly, the DHX36 KO cells exhibit a significant 2-fold reduction in the Renilla luciferase signal intensity 24 h after the transfection. However, this difference was undetectable afterwards.

In general, viral stress responses are accompanied by the prerequisite formation of avSGs representing a platform for the interaction of proteins and RNAs of the host²⁸⁵. The observation of increased type I IFN signaling and improved viral resistance in *DXH36* KO cells suggests changes in avSG formation as well. For this reason, a timeline of WT and *DHX36* KO cells under poly (I:C) conditions was performed and analyzed by immunofluorescence using the SG localizing protein G3BP1. As expected, from 1 h to 6 h after poly (I:C) treatment the WT cells showed a strong increase in the accumulation of SG and reach a plateau with no observation of a decrease after 12 h or 24 h (Figure 3.4.1 E). As previously shown, the *DHX36* KO exhibits more SG positive cells than the WT cells without stress. Even though the *DHX36* KO cells were able to form SG after poly (I:C) application, a significant reduction compared to WT cells was

observed for all tested time points during the application of the compound (Figure 3.4.1 F).

Taken together and despite of reduced SG formation, the data of increased metabolism after poly (I:C) treatment and diminished viral replication of the YFV replicon clearly point to an augmented viral resistance upon the loss of *DHX36*.

3.5 DHX36 acts early in type I IFN signaling

Previous studies examined the potential pathways in which DHX36 executes its function with regard to anti-viral responses^{288,289}. In order to investigate the underlying signaling cascade of DHX36 which leads to the observed phenotype described in this thesis, several compounds were used that activate the type I IFN pathway at different stages and by different proteins. INF-α was deployed as a ligand for the cell surface receptors IFNAR1/2 to activate downstream the JAK/STAT pathway and hence, stimulate the expression of ISGs. Additionally, a more specific 5'-triphosphorylated short hairpin dsRNA ligand (3p-shRNA) was applied that solely activates RIG-I and its signaling cascade including type I IFN expression, as well as subsequent ISG expression induced by the IFNs. The IFN-α was directly applied to the supernatant, whereas the 3p-shRNA ligand and the control poly (I:C) were transfected by using Lipofectamine 2000. Both, WT and DHX36 KO cells were treated for 24 h with the 3 different compounds and RNA samples were taken. After cDNA synthesis and qPCR analysis for the 3 genes DDX58, IFIT1, and RSAD2 all data was normalized to the WT cells conditions for the respective treatment after 24 h. All analyzed genes showed the formerly described phenotype of enhanced transcript levels after the application of poly (I:C) in DHX36 KO cells compared to WT cells (Figure 3.5.1 A-C). Interestingly, the treatment with INF-α caused similar levels of DDX58 or IFIT1 in WT and DHX36 KO cells or even less levels in the case of RSAD2 (Figure 3.5.1 C). A different observation was made after adding 3p-shRNA for the stimulation of RIG-I. The transcript levels of DDX58 in the DHX36 KO cells were comparable to the levels after INF-α treatment and showed no increase in relation to WT cells (Figure 3.5.1 A). On the other hand, IFIT1 and RSAD2 showed elevated transcript levels in *DHX36* KO cells in comparison to the INF-α treated samples (Figure 3.5.1 B-C). However, the levels of *IFIT1* and *RSAD2* were significantly lower than the poly (I:C) levels.

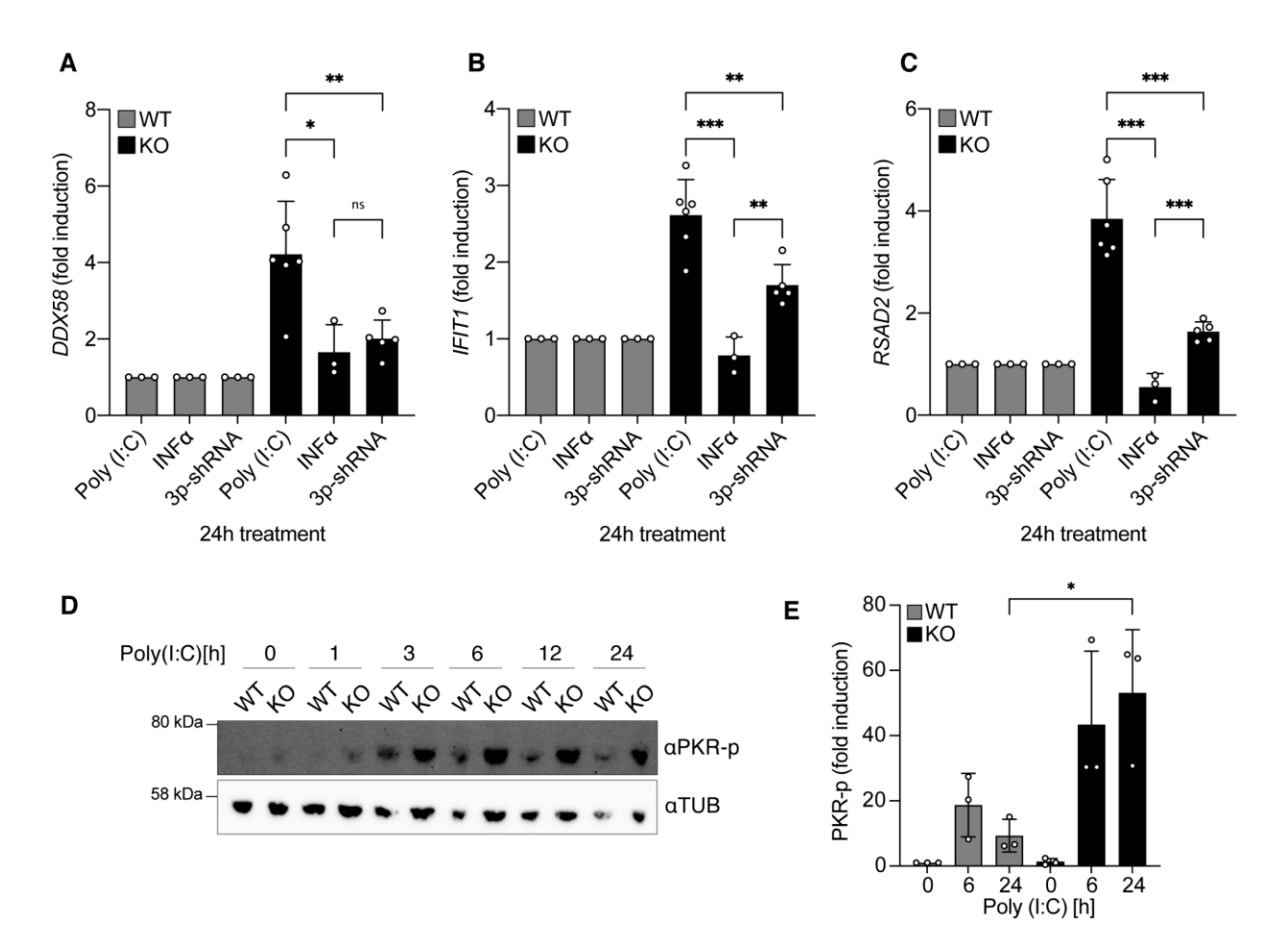


Figure 3.5.1 DHX36 acts early during anti-viral stress responses

A) – C) Analysis of the signaling cascade of DHX36 by the application of poly (I:C), INF-α, and 3p-shRNA for the stimulation of all PPRs, IFNAR1/2, and RIG-I, respectively. Transcript quantifications by RT-qPCR of the indicated ISGs after each 24 h treatments with the displayed compounds in WT and DXH36 KO cells are shown. All transcripts results are presented after normalization to mRNA levels of RNU6. Fold changes of each condition were calculated to the respective WT samples after the treatment. D) Immunoblot analysis of WT and DHX36 KO cells upon a timeline of poly (I:C) treatments using antibodies against phosphorylated PKR and α-tubulin after size separation via SDS-PAG. E) Protein signal intensities were quantified by measuring the densitometry using ImageJ and were normalized to the α-tubulin signal. Fold changes are displayed in comparison to WT untreated levels. Significances were determined by Students t-test (n≥3). Significance levels: *p < 0.05, **p < 0.01, ***p < 0.001, ns = not significant. Error bars represent standard deviations of at least 3 biological replicates.

The fact that the application of the RIG-I ligand resulted in only slightly increased ISG levels in the DHX36 KO cells and never reached the peaks observed upon poly (I:C) treatment led to the hypothesis that DHX36 fulfils its function at other steps. In line with this, the observed phenotype of constitutive PKR phosphorylation points to an implication of PKR in the DHX36 KO caused phenotype (Figure 3.1.1 C). To further examine if PKR is indeed involved in the signaling pathway of DHX36, a timeline of poly (I:C) treated cells was conducted and protein lysates were analyzed. The specific antibody against the phosphorylated version of PKR was used for the detection of its activation and signal intensities were normalized to the housekeeping gene α -Tubulin. The immune detection confirmed the constitutive phosphorylation in DHX36 KO cells without a viral trigger. Strikingly, the application of poly (I:C) for 1 to 3 h caused a massive phosphorylation in the DHX36 KO cells in comparison to WT cells and stayed high up to 24 h after the treatment (Figure 3.5.1 D). In contrast, the PKR phosphorylation in WT cells peaked at 6 h and showed a tendency of reduction after 24 h, even though not significantly (Figure 3.5.1 E).

These results strongly indicate that DHX36 functions already early in the type I IFN signaling pathways and is involved in the appropriate regulation of the viral RNA sensor PKR.

3.6 DHX36 negatively regulates PKR-induced type I IFN signaling

The observation of enhanced phosphorylation of PKR upon a viral trigger in the absence of *DHX36* was a clear indicator for a negative regulatory function of DHX36 on PKR (Figure 3.5.1 D-E). To rule out if the phenotype of increased ISG levels in poly (I:C) treated *DHX36* KO cells depends on PKR as well, a CRISPR/Cas9 mediated PKR knockout was performed in WT and the *DHX36* KO background. After viral transduction with the CRISPR/Cas9 plasmid containing a guide RNA designed against the PKR coding sequence, cells were single cell sorted by dilution and selected by antibiotic resistance. The absence of PKR in the *DHX36* KO background was confirmed by immunoblotting using an antibody against PKR (hereafter referred to as *DHX36/PKR* KO) (Figure 3.6.1 A). Unfortunately, a single PKR knockout in WT cells was not successful. First, the growth phenotype of all 3 different genetic conditions was analyzed by light microscopy after 24 h poly (I:C) treatment. WT cells as well as the *DHX36/PKR* KO showed typical cell growth in a stress-free environment, whereas the *DHX36* KO

displayed its typical growth retardation featured by clustering of cells (Figure 3.6.1 B). When poly (I:C) was applied for 24 h, the WT cells and DHX36/PKR KO cells showed again a similar phenotype with detached spherical cells in the supernatant. In contrast, the DHX36 KO cells stayed mostly adherent on the culture dish surface after 24 h poly (I:C) treatment (Figure 2 B). To further test the PKR dependency on the DHX36 KO evoked phenotype with regard to ISG expression, RNA samples of 24 h poly (I:C) treated WT, DHX36 KO, and DHX36/PKR KO cells were collected, reverse transcribed into cDNA and utilized for qPCR. The data is depicted as relative expression levels to the house keeping gene RNU6. A strong induction of DDX58, RSAD2, ADAR1 and IFIT1 after the application of poly (I:C) was observed for all 3 genetic conditions validating the previously described phenotype of increased levels in the DHX36 KO cells compared to WT cells. Interestingly, transcript levels of all tested genes in the DHX36/PKR KO background were similar to WT cell levels after the poly (I:C) treatment (Figure 3.6.1 C-F). This observation was validated by the fact that also immunoblotting under the same conditions showed the same trend on protein levels for IFIT1 (Figure 3.6.1 G). In addition to this, the levels of IFIT1 in the DHX36/PKR KO cells were even more decreased compared to the WT cells after 24 h poly (I:C) treatment (Figure 3.6.1 H). Additionally, the transcript levels of *ADAR1* in untreated conditions were restored to normal WT levels after the deletion of both DHX36 and PKR (Figure 3.6.1 E).

The collected data gives evidence that PKR is epistatic to DHX36, which leads to a negative regulation of PKR-induced type I IFN signaling by DHX36. Moreover, PKR acts as a positive regulator of ISG expression.

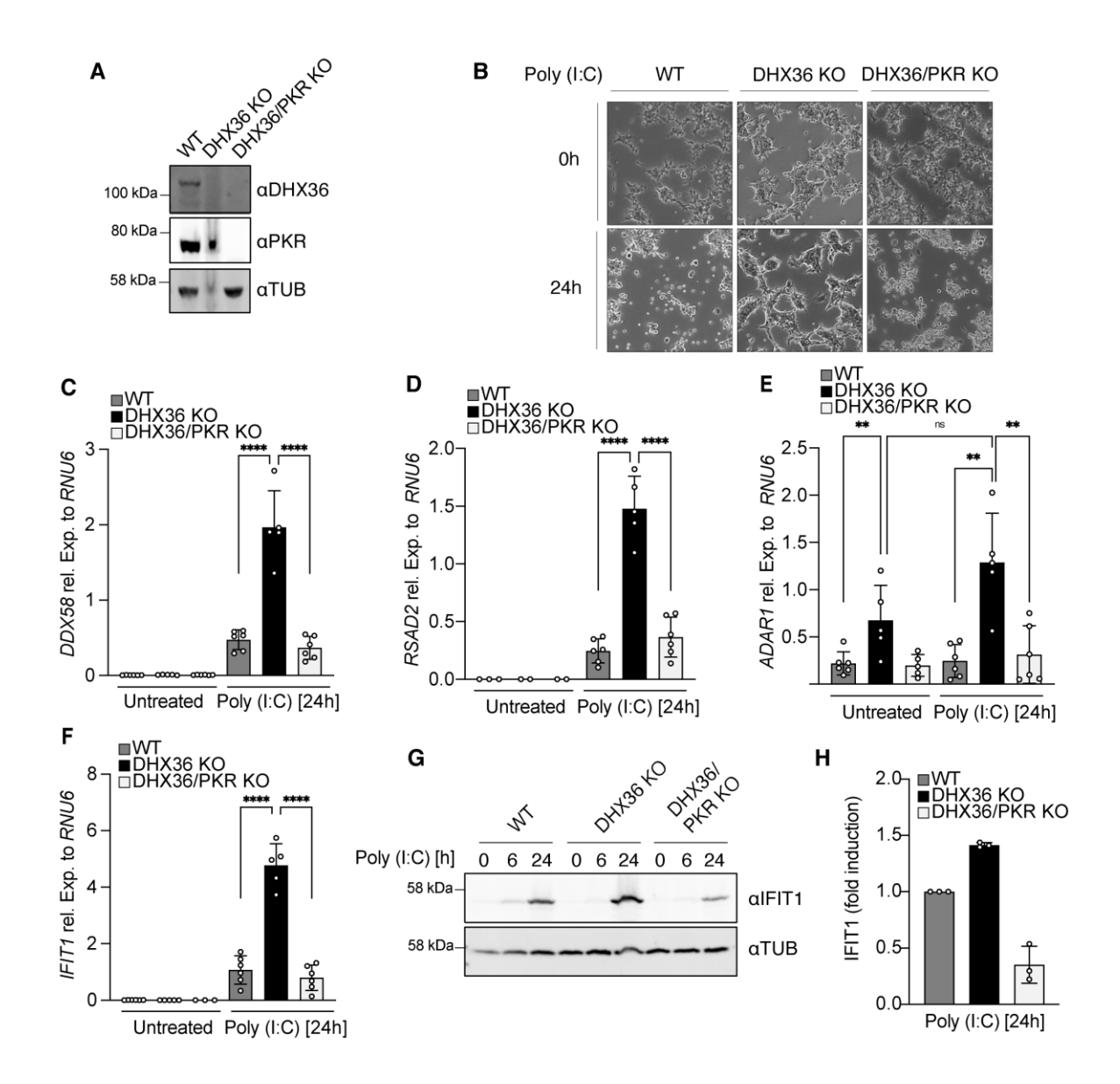


Figure 3.6.1 Negative regulation of type I IFN signaling by DHX36 depends on PKR A) Immunoblot verification of CRISPR/Cas9-mediated *DHX36* KO and *DHX36/PKR* double KO cells using antibodies against endogenous DHX36, PKR, and α-tubulin after size separation via SDS-PAG. B) Analysis of WT, *DHX36* and *DHX36/PKR* KO cells via light microscopy after the treatment with poly (I:C) for 24 h. C) - F) Transcript quantifications by RT-qPCR of the indicated ISG genes after 24 h poly (I:C) treatment comparing WT, *DHX36* KO, and *DHX36/PKR* KO cells. Gene transcripts were normalized to mRNA levels of *RNU6*. G) Immunoblot analysis of WT, *DHX36* KO, and *DHX36/PKR* KO cells upon 24 h poly (I:C) using antibodies against phosphorylated IFIT1 and α-tubulin after size separation via SDS-PAG. H) Protein signal intensities were quantified by measuring the densitometry using ImageJ and were normalized to the α-tubulin signal. Fold changes are shown relative to WT levels after 24 h poly (I:C) application. Significances were determined by Students t-test (n≥3). Significance levels: *p < 0.05, **p < 0.01, ***p < 0.001, ns = not significant. Error bars represent standard deviations of at least 3 biological replicates

3.7 The primed cell status upon the loss of *DHX36* is independent of PKR

The rescue of the ISG levels after the ablation of *PKR* in the *DHX36* KO cells suggests a reduction in the previously observed constitutive stressed and primed status of the cells as well (Figure 3.1-3.2, 3.6). To test this assumption, the same RNA/cDNA samples were analyzed by qPCR and tested for genes that are indicators of an ongoing type I IFN transfection. Both analyzed genes, *IFNB1* and *IRF7*, showed an increase of transcript levels in the *DHX36* KO cells compared to WT cells in untreated conditions. In contrast to the previously examined ISGs, the levels of *IFNB1* and *IRF7* remained high in the *DHX36/PKR* KO cells (Figure 3.7.1 A-B). The same trend was observed in the 24 h poly (I:C) treated samples, showing similar levels in the *DHX36* KO and *DHX36/PKR* KO cells that are significantly higher than in WT cells (Figure 3.7.1 A-B).

This interesting observation indicates an ongoing strong type I IFN response in the absence of *DHX36*, which could not be rescued by the loss of *PKR* as compared to the levels of ISGs. To further check this hypothesis, the RIG-I pathway that is also triggered by poly (I:C) was analyzed. Protein lysates previously collected from untreated and poly (I:C) stimulated samples were examined by immunoblotting, using a specific antibody that detects only the phosphorylated version of IRF3, which is an indicator of its activation downstream of for instance RIG-I. In untreated conditions, no phosphorylated IRF3 was detected in all tested genetic backgrounds (Figure 3.7.1 C). After 6 h of poly (I:C) treatment, the WT cells showed an increase of IRF3 phosphorylation that subsequently decreased by roughly 30% after 24 h poly (I:C) (Figure 3.7.1 D). On the other hand, the *DHX36* KO cells exhibited a stronger IRF3 phosphorylation after 6 h of treatment, which remained at similar levels after 24 h. Intriguingly, the *DHX36/PKR* mutant displayed highly increased phosphorylation levels of IRF3 after 6 and 24 h of poly (I:C) treatment resembling the *DHX36* KO phenotype (Figure 3.7.1 C-D).

The observed increased levels of type I IFN response genes and the elevated phosphorylation of IRF3 after poly (I:C) treatments upon the loss of *DHX36* alone or in combination with *PKR* indicates a separate function of DHX36 with regard to the priming effect and the type I IFN response (Figure 3.1-3.2, 3.6-3.7).

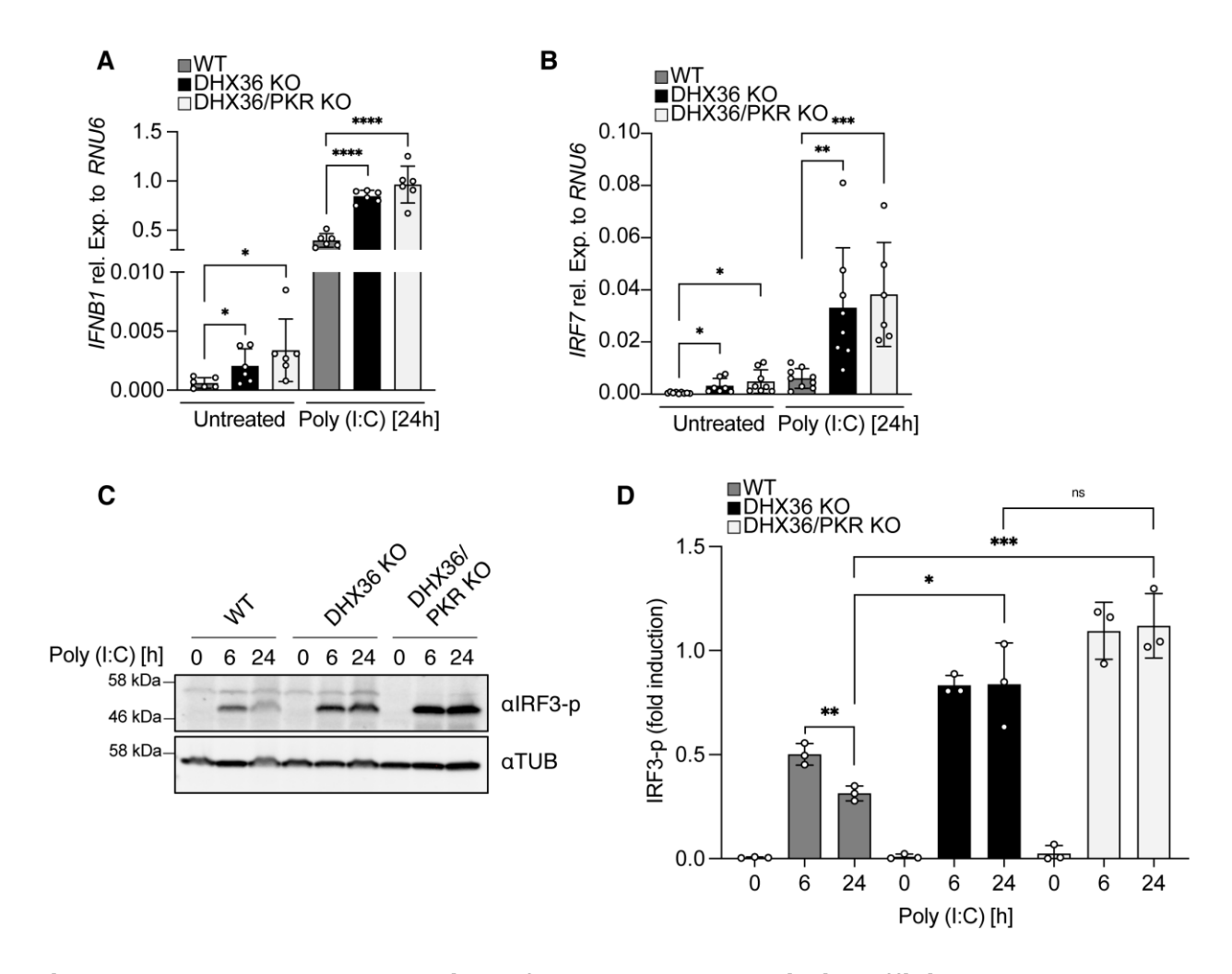


Figure 3.7.1 The double deletion of DHX36 and PKR is insufficient to reverse the primed status of the DHX36 KO cells

A) - B) Transcript quantifications by RT-qPCR of *IFNB1* and *IRF7* after 24 h poly (I:C) treatment comparing WT, *DHX36* KO, and *DHX36/PKR* KO cells. Gene transcripts are displayed as relative expression to *RNU6*. C) Immunoblot analysis of WT, *DHX36* KO, and *DHX36/PKR* KO cells upon 6 h and 24 h poly (I:C) using antibodies against phosphorylated IRF3 and α-tubulin after size separation via SDS-PAG. D) Protein signal intensities were quantified by calculating the densitometry using ImageJ and were normalized to the α-tubulin signal. Fold changes are shown relative to the α-tubulin signal. Significances were determined by Students t-test ($n \ge 3$). Significance levels: p < 0.05, p < 0.01, p < 0.001, p < 0.001,

3.8 DHX36 interacts with PKR and ADAR1 in an RNA-dependent manner

The identification of PKR as the prime cause of the observed phenotype of increased levels of ISGs seen upon the loss of *DHX36* suggests a more intimate interaction of both

proteins. In order to analyze possible protein interaction partners of DHX36, mass spectrometry method was applied. Since HEK cells are generally deprived of TLRs or only express them on a low basal level, the pFRT vector containing DHX36iso1 was stably integrated into HeLa (Flp-In™ System of Thermo Fisher Scientific) cells to encompass more possible interaction partners of DHX36 with regard to PRRs in the analysis. The expression of N-terminally FLAG tagged DHX36iso1 was induced by the application of tetracycline for 16 h. Additionally, untreated as well as poly (I:C) treated samples were collected in triplicates. After protein isolation and protein complex immunoprecipitation (Co-IP) using anti-FLAG magnetic beads, the samples were sent for mass spectrometry analysis. As a negative control, WT cells incubated with anti-FLAG beads was deployed to exclude possible leaky expressions of the pFRT construct that uses the strong cytomegalovirus promoter for protein expression. The data is depicted as a volcano plot showing differences in DHX36 binding of untreated and the poly (I:C) treated samples after excluding false negative hits found in the WT negative control samples. Dotted lines indicate significant changes in differences of untreated and poly (I:C) treatments as well as significances. Protein names are only indicated for DHX36 interaction candidates depicted for further analysis or in case of general relevance. In untreated conditions only DHX36 was found, whereas several formerly identified DHX36 interaction partners were detected including DHX9, ILF3, and DDX21 after the addition of poly (I:C) for 6 h^{253,289}. Interestingly, also ADAR1 was found in the mass spectrometry data after the poly (I:C) treatment (Figure 3.8.1 A).

Since the previous evidence of DHX36-dependent negative PKR regulation and ADAR1 interaction with DHX36 suggest a possible protein complex of these proteins to execute their function. This hypothesis was tested by reconfirming the mass spectrometry data via Co-IP in untreated and poly (I:C) treated conditions in the initial HEK OE cell line. N-terminal FLAG tagged DHX36iso1 expression was induced by adding tetracycline and poly (I:C) was transfected using Lipofectamine 2000. Importantly, all tested proteins are capable of binding to nucleic acids, more precise to endogenous and exogenous RNA. To test whether the protein interactions are of physical nature or dependent on RNA, an RNase A treatment was performed. To exclude any unspecific binding, the HEK OE cell line was used without prior induction of the transgene in the absence of tetracycline. After collecting protein lysates and anti-FLAG IP, the samples were separated by

SDS-PAGE and proteins were detected by immunoblotting using specific antibodies against ADAR1, FLAG, PKR, and α-Tubulin. The input samples of ADAR1, PKR, and α-tubulin showed clear bands at the respective sizes and all proteins showed similar signal intensities in untreated or poly (I:C) treated samples (Figure 3.8.1 B). On the other hand, the signal of the FLAG tagged DHX36iso1 in the input was less intense, however, detectable in the tetracycline induced samples and absent without induction. By contrast, a distinct and strong signal was observed after the IP for the FLAG detection at the size of DHX36iso1 only in the tetracycline induced samples. This signal remained unchanged regardless of the poly (I:C) or RNase A treatment. Intriguingly, both proteins, ADAR1 and PKR were detected in the IP independent of the poly (I:C) treatment (Figure 3.8.1 B). Moreover, the application of RNase A completely abolished the PKR signal in untreated and poly (I:C) treated conditions. Similarly, the ADAR1 detection after RNase A treatment was clearly diminished.

The RNA-dependent interaction of DHX36 with PKR and ADAR1 suggests that the nucleic acid unwinding function of DHX36 could play a role in its function as well. In order to analyze this hypothesis, the DHX36 KO cells were complemented with a catalytic dead version of DHX36 (referred to as DHX36 CD), which is still capable of binding to nucleic acids, however, loses the function of ATP-dependent nucleic acid unwinding. This was accomplished by a single base mutation in the catalytic walker B domain, which gave rise to an amino acid substitution from aspartic acid to alanine. Subsequently, WT, DHX36 KO, DHX36 RE and DHX36 CD cells were treated with poly (I:C) for 24 h and RNA samples were taken and reverse transcribed into cDNA. qPCR analysis was performed for the 3 ISGs DDX58, IFIT1, and RSAD2. Fold changes are shown compared to WT cells treated with poly (I:C) for 24 h. The DHX36 KO cells exhibited the previously described increase of transcript levels in all 3 tested genes. In line with this, the DHX36 RE cells showed a complete rescue with transcript levels of DDX58, IFIT1, and RSAD2 similar to WT cell conditions. In contrast, the levels of DDX58 and RSAD2 were significantly upregulated in the DXH36 CD cells in comparison to the DHX36 RE cells (Figure 3.8.1 C-E). Likewise, the levels of IFIT1 showed a similar trend, yet not in a significant manner (Figure 3.8.1 D).

72

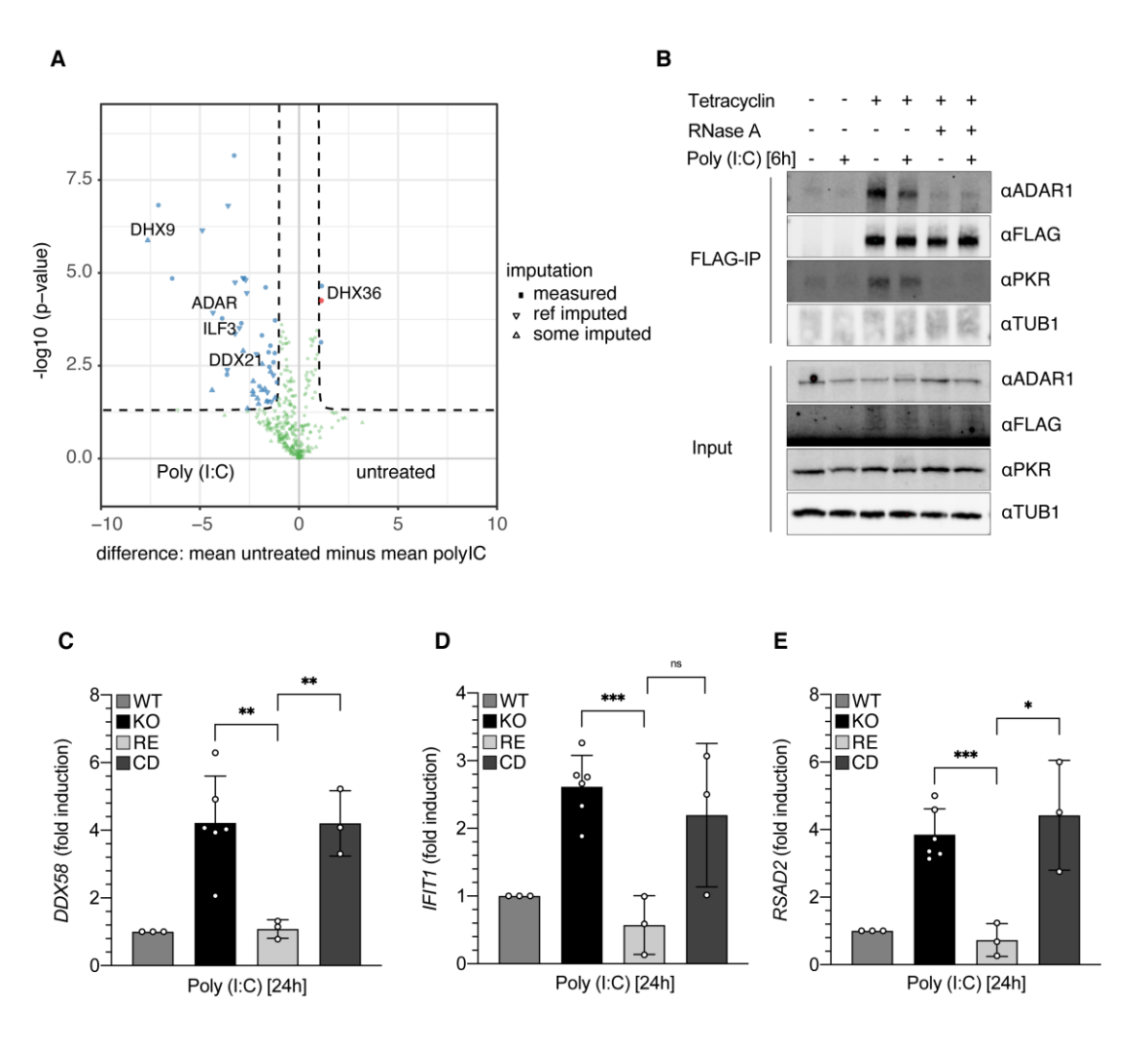


Figure 3.8.1 An RNA-dependent interaction of DHX36 with PKR and ADAR1

A) Mass spectrometry analysis after protein complex immunoprecipitation in untreated and 6 h poly (I:C) treated conditions in HeLa cells expressing the transgenic N-terminally FLAG tagged DHX36iso1. Depicted data is shown as difference between untreated and poly (I:C) treated samples after excluding false positive hits. Indicated significances are displayed as log₁₀ fold changes. B) Immunoblot of HEK *DHX36* OE cells untreated or 6 h poly (I:C) treated analyzed by protein complex immunoprecipitation with anti-FLAG magnetic beads and subsequent SDS-PAGE. Antibodies against ADAR1, FLAG, PKR, and α-tubulin were used for protein visualization in input and IP samples. C) − E) Transcript quantifications by RT-qPCR of the indicated ISG genes after 24 h poly (I:C) treatment comparing WT, *DHX36* KO, *DHX36* RE, and *DHX36* CD cells. Gene transcripts were normalized to mRNA levels of *RNU6*. Fold changes were calculated relatively to WT levels after 24 h poly (I:C) treatments. Significances were determined by Students t-test (n≥3). Significance levels: *p < 0.05, **p < 0.01, ***p < 0.001, ns = not significant. Error bars represent standard deviations of at least 3 biological replicates.

These results clearly demonstrate an RNA-dependent interaction of DHX36 with proteins of the type I IFN pathway, specifically PKR and ADAR1. Moreover, the observed phenotype of an increased amount of ISGs upon the loss of *DHX36* is solely dependent on the helicase catalytic domain of DHX36.

3.9 Increased type I IFN response is mediated by DHX36 rather than by rG4s

The observation that the catalytic domain of DHX36 is necessary for its inhibitory function suggested two scenarios. First, the domain functions as mediator for direct target protein repression as for instance PKR inhibition or second, it mediates rG4 resolution. To pinpoint the latter hypothesis, WT cells were treated for 24 h with the synthetic compound carboxypyridostatin (cPDS) to specifically stabilize rG4s and RNA samples were taken and reverse transcribed into cDNA. qPCR analysis was performed for the 3 ISGs *DDX58*, *IFIT1*, and *RSAD2*. Fold changes are shown compared to WT untreated cells. The transcript levels of *DDX58* and *IFIT1* were similar after cPDS treatment compared to unchallenged conditions (Figure 3.9.1 A-B). On the other hand, the amount of RSAD2 transcripts increased (Figure 3.9.1 C). To further investigate the possibility of rG4s functions during viral infections, the WT and DHX36 KO cells were incubated for 6 h with cPDS and afterwards treated with poly (I:C) for 24 h. RNA samples were taken and analyzed by qPCR for the transcripts of *DDX58*, *IFIT1*, and *RSAD2*. In all cases, the administration of cPDS to WT or DHX36 KO cells caused no changes in transcript levels after poly (I:C) treatment (Figure 3.9.1 D-E).

These results point to a DHX36 specific role in type I IFN signaling rather than a rG4-mediated function.

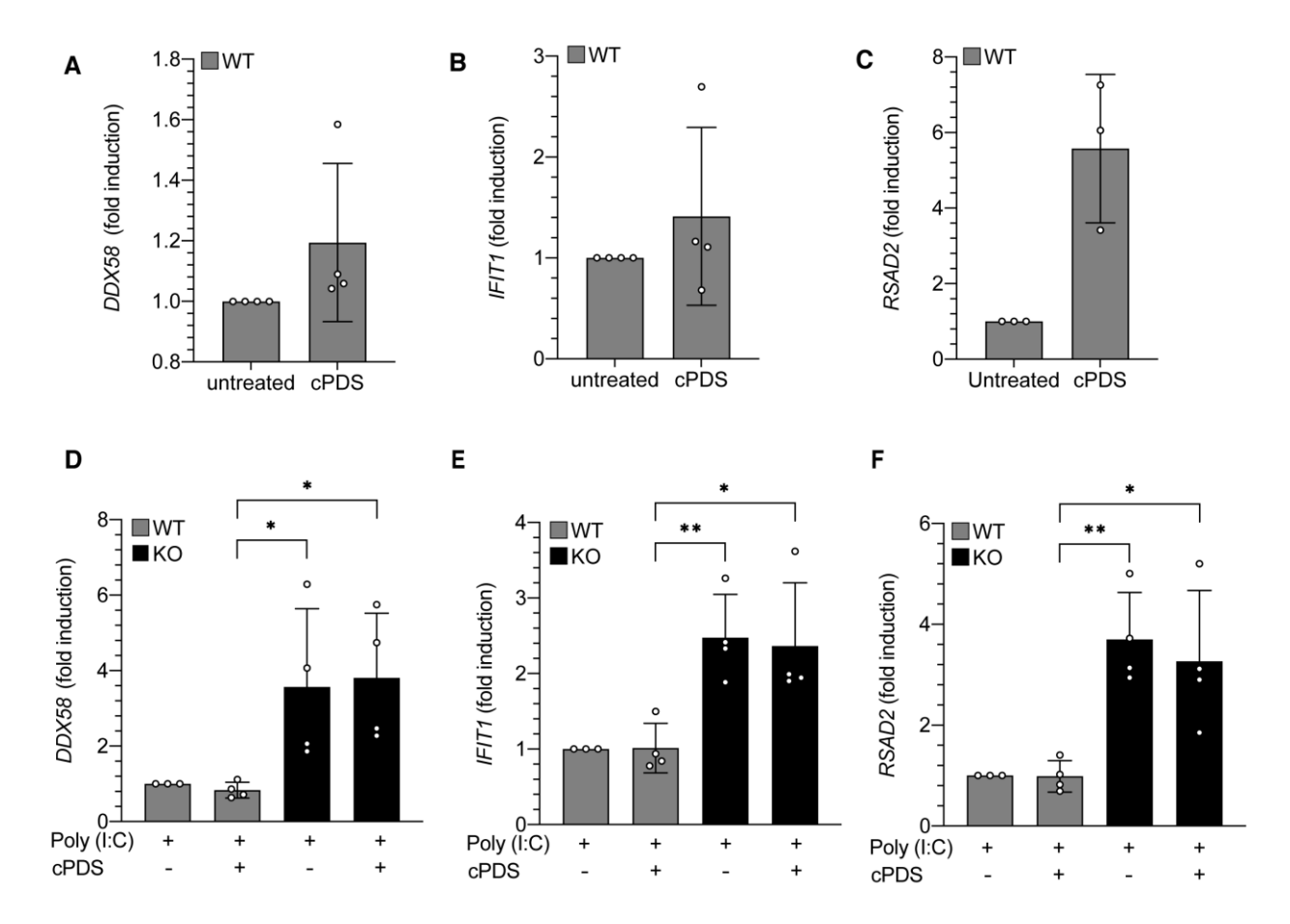


Figure 3.9.1 Increased type I IFN signaling is DHX36 mediated rather than rG4

A-C) Transcript quantifications by RT-qPCR of the indicated ISG genes after 24 h cPDS treatment of WT cells. Gene transcripts were normalized to mRNA levels of *RNU6*. Fold changes were calculated relative to WT levels. D-F) RT-qPCR analysis of the ISG genes after cPDS administration and additional poly (I:C) treatment for 24 h for WT and DHX36 KO cells. Gene transcripts were normalized to mRNA levels of *RNU6* and fold changes were calculated relatively to WT levels after 24 h poly (I:C) treatment. Significances were determined by Students t-test (n \geq 3). Significance levels: *p < 0.05, **p < 0.01, ***p < 0.001, ns = not significant. Error bars represent standard deviations of at least 3 biological replicates.

4. Discussion

Viral outbreaks and infections have been keeping the world in suspense. In order to face upcoming viral threats, the complete comprehension of the underlying molecular mechanisms is indispensable. The first line of defense against viruses is the innate immune system, especially the regulation of interferons (IFN) and their signaling cascades. This includes the appropriate detection of non-self characteristics such as viral RNA modifications referred to as pathogen associated molecular pattern (PAMPs) by intracellular pattern recognition receptors (PRRs). Even though interferon signaling has been studied over decades plenty of unsolved contradictions still exist and a clear view remains obscure. While the actual IFNs are mostly classified by their actions and downstream signaling, the investigation of viral RNA detection by PRRs continues and reveals a more elusive situation.

Initial studies proposed a specific function for PKR as a possible PRR, because of its ability to bind to dsRNA and inhibit translation to stop viral protein production as well as its capability to promote *IFNB1* expression^{157,158,169,160,161,163–168}. However, the discovery of RLRs showed that RIG-I and MDA5 are the major cytoplasmic receptors for dsRNA to drive type I IFN expression. Moreover, many other ribonucleic acid binding proteins with anti-viral activity have been discovered, especially helicases. Despite the RLRs, which all belong to the DExD/H-box helicases, other family members have been described to function as PRRs or play a specific role in the type I IFN response^{65,292}. Among them is the DEAH-box helicase DHX36, which is implicated in diverse cellular mechanism encompassing regulation of cellular homeostasis, resolution of secondary nucleic acid structures as well as control of anti-viral signaling^{228,253,255,277,288,289}. Even though the structure and action of DHX36 during G4-quadruplex (G4) unwinding is evidently clear, the role in viral RNA induced type I IFN signaling is less understood and many different functions of DXH36 are described. Additionally, a complete knockout study of *DHX36* with regard to type I IFN signaling in human cells is missing.

I speculated that a complete loss of *DHX36* influences the type I IFN signaling in several ways. Either by unspecific activation of PRRs caused by the accumulation of endogenous mRNA harboring RNA G4 (rG4) structures or by direct regulations of PRRs and thus, the involvement in their signaling cascades.

My thesis provides a system-wide analysis of transcriptomic changes upon the loss of DHX36 with regard to type I interferon signaling in human embryonic kidney cells (HEKs). Intriguingly, the ablation of DHX36 was accompanied by the accumulation of stress granules (SGs) and a constitutive autophosphorylation of PKR without viral triggers (Figure 1)²²⁸. In line with this, an increase of type I IFN genes as well as interferon stimulated genes (ISGs) was observed (Figure 3.1.1). These findings led to the hypothesis that DHX36 is involved in the negative regulation of type I IFNs and ISGs. To test whether the increase of type I IFNs and ISGs also lead to an enhanced anti-viral response the DHX36 KO cells were challenged with the viral RNA surrogate compound poly (I:C). This treatment gave rise to an upregulation of ISGs on transcript and protein levels in DHX36 KO cells compared to WT cells (Figure 3.2.1). To further confirm the negative regulatory role of DHX36 in the type I IFN response, a DXH36 overexpression experiment was conducted, which reversed the phenotype and decreased the amount of ISGs (Figure 3.3.1). These data support the idea of a negative regulation of type I IFNs and ISGs by DHX36. Furthermore, the observation of increased PKR phosphorylation in *DHX36* KO cells after the poly (I:C) treatment indicated that this could be the reason for the increased levels of type I IFNs and ISGs. To address this question, DHX36/PKR double-knockouts were generated and challenged with poly (I:C). The observation of diminished ISG levels after the double mutation of DHX36 and PKR showed that this phenotype completely depends on PKR (Figure 3.6.1). However, the primed state of increased IFNB1 and IRF7 levels still remained and thus, points to a dichotomy in PKR as well as DHX36 functions (Figure 3.7.1). This was in line with increased IRF3 phosphorylation levels observed in DHX36 KO and DHX36/PKR KO cells. The observation of the PKR dependency of the DHX36 KO phenotype indicated possible interaction of both proteins. To test this hypothesis a mass spectrometry analysis of DXH36 was conducted and subsequent CoIP experiments to confirm the results. An RNA-dependent interaction of DHX36 with PKR as well as the PKR inhibitory protein ADAR1 was observed and indicate actions of these proteins in close proximity (Figure 3.8.1). Finally, to check whether the increase of type I IFNs and ISGs was the direct result of the loss of DHX36 or indirect by elevated levels of rG4 the rG4 stabilizing compound cPDS was applied. The results point to an independent role of rG4s in this DHX36 induced phenotype (Figure 3.9.1).

In the following chapters, the newly obtained data will be compared to previous results and discussed in a scientific context to the published literature. To this end, this section is structured in several chapters, each focusing on a specific topic.

4.1 Loss of *DXH36* leads to an increased type I IFN signature

One of the key findings of this project was the increase of type I IFNs and ISGs induced by the loss of *DHX36* with and without a viral trigger. Several previous reports also indicated a role of DHX36 in type I IFN signaling, however, investigated its role mainly after a viral trigger induced by a virus or a synthetic compound. One study focused on mouse embryonic fibroblasts (MEFs) and utilized a Cre/loxP system, in which the loss of *DHX36* was induced by the application of tamoxifen for 72 h. The data showed no detection of IFN-β levels in the supernatant after 72 h tamoxifen treatment and the *IFNB1* mRNA levels visibly remained unchanged²⁸⁸. Moreover, other cytokines like interleukin 6 (*IL6*), *IL8*, or tumor necrosis factor alpha (*TNF*) remained at WT levels after siRNA-mediated knockdown of *DHX36* in MARC145 kidney cells isolated from monkeys²⁹⁰.

In contrast, my analysis of a complete *DHX36* knockout in HEK cells clearly showed a slight, however, significant upregulation of *IFNB1* transcript levels compared to WT cells (Figure 3.1.1 F). Concurrent with this, several ISGs such as *IFIT1*, *RSAD2*, and *ADAR1* as well as many genes of the JAK-STAT pathway as for example *JAK1*, *JAK2*, *STAT2*, *STAT5b* and the cytoplasmic receptors *IFNAR1* and *IFNAR2* showed increased mRNA levels upon the loss of *DHX36* (Figure 3.1.1 D-J). Moreover, the upregulation at the same time of several JAK-STAT inhibitor proteins such as *SOCS* in the *DHX36* knockout HEK cells suggests a feedback loop, in which the cells try to compensate the constant activation of the type I IFNs by the JAK-STAT pathway (Figure 3.1.1 D)^{293–295}.

Interestingly, the knockouts of other DEAD/DEAH-box helicases in bone marrow-derived dendritic cells (DCs) such as *DDX58* (RIG I) or *IFIH1* (MDA5) slightly diminished or unaltered *IFNB1* transcripts in unstressed conditions, respectively¹⁷¹. In line with this, the *IFNB1* mRNA levels after a knockdown of DDX46 in human THP1 cells or mouse macrophages remained unchanged²⁹⁶. The same was true for a *DDX60* knockdown in HeLa cells, in which the amount of *IFNB1*, *IFIT1*, and *CXCL10* transcripts were comparable to control treated cells²⁹⁷. In contrast, the siRNA mediated knockdown of the helicase DDX5 in mouse peritoneal macrophages showed an upregulation of the IFN-β

mRNA, even though not indicated as significant²⁹⁸. Moreover, the same study investigated the transcript levels of the ISG *Mx1* and the cytokine *CXCL10*, both with the same tendency.

The second major observation was that this primed phenotype in the HEK DHX36 KO cells (Figure 3.1.1) was accompanied by a massive increase of interferons and ISGs upon the treatment with the viral RNA analogue poly (I:C) in comparison to WT cells (Figure 3.2.1). In detail, the performed timeline of poly (I:C) treatment showed that DDX58 transcription started already 1 to 3 h after induction (Figure 3.1.1 C). This indicates that its transcription is regulated by other factors besides IFN-β, since IFNB1 transcription started between 3 and 6 h after poly (I:C) administration ((Figure 3.1.1 B). In line with this, starting points of the IFIT1 and RSAD2 transcription between 3 and 6 h are indicative of IFN-β independent initiation mechanisms, such as a direct IRF3mediated transcription (Figure 3.1.1 D-E). Noteworthy, even though DDX58 transcript levels peaked at 6 h after the poly (I:C) treatment, the protein levels were highest after 24 h, indicating a temporal delay of transcription to translation ((Figure 3.1.1 F). Interestingly, the DHX36 ablation gave rise to highest levels of IFIT1 on transcriptional as well as on protein level after 24 h poly (I:C) compared to WT conditions, thus differs in this regard from *DDX58* (Figure 3.1.1 E-F). However, the administration of poly (I:C) was verified only until 24 h post treatment, hence, the increase of transcript levels in the DHX36 KO cells to WT cells could be as well due to a temporal difference in the response. In detail, the primed status with already upregulated IRF7 and IFNB1 levels provoked by the DHX36 loss could accelerate the type I IFN response compared to WT conditions in the case of foreign RNA recognition⁹⁵. However, the PKR and IRF3 phosphorylation during the poly (I:C) treatment in WT cells increased only until 6 h and decreased later on (Figure 3.5.1 D and Figure 3.7.1 C). These two facts point to a completely accomplished anti-viral response within the first 24 h in HEK WT cells. Nevertheless, a prolonged monitoring after the viral trigger for both cellular conditions would clarify this issue. In total, these results clearly suggest a negative regulation of type I IFN signaling by DHX36, however, stays in contrast to several other studies.

In this regard, an siRNA mediated downregulation of DHX36 in bone marrow-derived DCs led to a reduction in released IFN- α and IFN- β levels upon the administration of short and long poly (I:C) compared to WT conditions²⁸⁹. Accordingly, another publication

showed that NF-κB levels in *DHX36* KO MARC145 cells were markedly reduced after poly (I:C) treatment or porcine reproductive and respiratory syndrome virus (PRRSV) infection²⁹⁰. In the same study, similar results were observed for transcript levels of IL 6, IL 8, and TNF-α after PRRSV attack. Likewise, the results of Yoo et al., 2014 revealed decreased transcripts of *IFNB1* as well as released IFN-β in the *DHX36* KO induced MEF cells after influenza A (IAV) virus or Newcastle disease virus (NDV) infection²⁸⁸. Since the origin of the used cells in these studies differ with regard to their species and

cell types, it could cause differences in the type I IFN response, as for instance HEK cells are generally deprived of most of the TLR receptors²⁹⁶. In this respect, the protein homology of the human and mouse DHX36 amounts to 92% identity, which could lead to subtle distinct functions (comparison of similarity by Clustal Omega). Additionally, the deployed HEK cells in this thesis originated from the kidney and thus, serving completely different functions as compared to bone marrow-derived DCs or MEFs. However, the greatest difference is the long-term perceived stress most likely caused by a constant DHX36 knockout in the HEK cells used in this thesis. This could have led to the observed differences in the anti-viral stress response compared to a knockdown after RNA interference or after a temporal induced knockout for 72 h. Especially, a complete knockout of DHX36 most likely gives rise to unviable conditions for many cell types, because of its implications in many diverse cellular functions as for instance genome integrity, transcription, splicing, or translation^{228,299}. Notwithstanding, the gathered data of a temporal knockdown compared to a conditional knockout can give important information on the same signaling cascades with regard to differences in the background, as for instance the long-term stress by a real knockout. In this context, the published results of Yoo et al., showed even differences in DHX36 behavior after treatment with different stimuli in the same cells. Interestingly, the treatment of poly (I:C) and a specific RIG-I ligand showed opposite effects. While the DHX36 ablated cells were accompanied by decreased IFNB1 transcripts after poly (I:C) treatment, the RIG-I ligand stimulation upregulated IFNB1 mRNA in the temporal tamoxifen induced DHX36 KO MEF²⁸⁸. This clearly indicates that the specific stimulus can cause differences in the overall type I IFN response.

Even though there are similar results observed for DHX36 in the literature indicating a positive effect on the anti-viral response, many other DEAD box helicases are described

as negative regulators. For example, the siRNA mediated knockdown of a set of helicases showed that DDX42 and DDX46 negatively regulate IFN-β expression after different virus infections such as vesicular stomatitis virus (VSV), Sendai virus (SeV), and herpes simplex virus (HSV)²⁹⁷. Similar results were shown for the knockdown of DDX5, DDX25, and DDX56 in three independent studies. The first study about DDX5 revealed an increase in IFNB1 expression and release as well as enhanced transcript levels of the ISG Mx1 and the cytokine CXCL10 upon VSV and HSV stimulation³⁰⁰. In the case of DDX25 or DDX56 knockdown in HEK cells, the expression of IFN-β was highly upregulated compared to WT cells after VSV and SeV or after encephalomyocarditis virus (EMCV) infection, respectively 301,302. These results again clearly pointing out the functional versatility of the DEAD/DEAH box helicases, especially with regard to the type of virus and the infected cell types. Moreover, it would be interesting to see if the loss of one helicase could be rescued by other helicases of the family. This goes in line with the observation that the DHX36 depletion in HEK cells in this thesis was accompanied by the upregulation of the aforementioned helicases DDX42 and DDX25 in RNA-seq data (Figure 6.1.1 C). Both are described as negative regulators of the type I IFN pathway such as DHX36 in this thesis, suggesting a compensatory role between the different members of the DEAD/DEAH box helicases. However, this hypothesis needs further verifications by rescue experiments.

These different results clearly show the versatility of DEAD/DEAH-box helicases and their functions in different species and cell types, especially in the case of DHX36.

4.2 DHX36 is a negative regulator of type I IFN signaling

The increase of type I IFN genes upon the loss of *DHX36* strongly implies a negative regulatory role of DHX36 in this regard. To verify this hypothesis, the level of *DHX36* during poly (I:C) administration were analyzed and revealed a downregulation in transcription after 3 to 6 h after the treatment (Figure 3.1.1 A). However, the detection of the DHX36 protein levels remained at a steady state until 6 h poly (I:C) application and started to decrease afterwards and were barely detectable after 24 h (Figure 3.1.1 B-C). The transcript levels increased after 12 h back to physiological unstressed conditions indicating a temporal delay for transcription and translation as well as a high half-life time of the DHX36 protein. Besides this, another publication showed that the binding of

DHX36 to specific mRNA targets is rG4-mediated and that a loss of DHX36 leads to an accumulation of those translational incompetent mRNAs and increased levels of cytoplasmic rG4 levels²²⁸. It would be of great interest whether WT cells after 24 h poly (I:C) treatment exhibit a similar phenotype compared to DHX36 KO cells caused by the strong DHX36 downregulation with regard to the accumulation of mRNA targets of DHX36 and if rG4s play a critical role in this context (further discussed in section 4.7). Additionally, the same study observed that DHX36 binds a rG4 structure in the coding sequence (CDS) of its own mRNA and possibly controls its own translation. Hence, a downregulation in DHX36 protein levels observed after poly (I:C) treatment suggests a sophisticated feedback loop and implies that, even though the *DHX36* mRNA is present, it is compromised in translation due to the rG4 formation in its CDS. As a consequence, other factors possibly drive the DHX36 translation after the stress is released. Accordingly, the conducted overexpression experiments of DHX36 showed that the observed downregulation during the type I IFN response is necessary for an appropriate expression of different ISGs such as DDX58, IFIT1, and RSAD2 after poly (I:C) treatment (Figure 3.1.1 D-F).

In contrast, Jing et al., 2017 showed that the infection of MARC145 cells from monkey or porcine primary pulmonary macrophages (PAMs) with PRRSV slightly induced the expression of DHX36 after 24 h by one to two fold²⁹⁰. Furthermore, the overexpression of DHX36 in MARC145 gave rise to increased levels of NF-kB levels after poly (I:C) treatment. In agreement with this, the upregulation of DHX36 after short and long poly (I:C) treatment in 929L mouse fibroblasts was accompanied by increased levels of IFN-β²⁸⁹. Another study showed a steady *DHX36* expression after poly (I:C) treatment in HEK293T cells, which are almost identical to the HEK Flp-InTM T-RexTM 293 cell line used in this thesis²⁸⁸. However, this study misses specific information about the used poly (I:C). Given the fact that the publication deals with RIG-I activation it is reasonable that they deployed short poly (I:C), because of its higher binding to RIG-I and not MDA5^{69–72}. Under these premises it is reasonable that short and long poly (I:C) type I IFN responses differ in the case of DHX36 expression. This would be in line with the observation in the same study where the administration of a specific RIG-I ligand caused increased levels of IFNB1 mRNA transcripts²⁸⁸. It would be interesting, whether DHX36 protein levels also differ after the RIG-I ligand treatment. Varying DHX36 expression

patterns induced by different stimuli were also demonstrated in ZF4 fibroblasts of zebrafish embryos. While the infection with spring viremia of carp virus (SVCV) caused a downregulation of *DHX36*, the treatment with Chum salmon reovirus (CSV) caused the opposite³⁰³.

Generally, the DHX36 downregulation described in this thesis and its negative regulatory role were confirmed by several different experiments. To further clarify the diverse expression of *DHX36* observed under different circumstances, the HEK *DHX36* KO cells could be tested with similar viruses or chemical compounds used in the other studies such as short poly (I:C).

4.3 DHX36, a negative regulator of PKR

In an effort to identify the potential signaling cascade in which DHX36 plays a regulatory role, the DHX36 KO cells were treated with different immunogenic compounds (Figure 5). The results showed no significant changes in ISG transcript levels for DDX58, IFIT1, and RSAD2 after IFN-α treatment indicating that DHX36 functions are upstream of IFNAR1 and IFNAR2 (Figure 3.5.1 A-C). A previous study showed that DHX36 and RIG-I stay in a complex to facilitate PKR phosphorylation²⁸⁸. Therefore, the DHX36 KO cells were treated with a RIG-I specific ligand. Interestingly, the levels of DDX58 were similar to WT transcripts after 24 h RIG-I ligand application. On the other hand, an increase of IFTI1 and RSAD2 levels in DHX36 KO cells was observed, however, was clearly diminished compared to the poly (I:C) treated samples (Figure 3.5.1 A-C). This could point to a contribution of DHX36 in RIG-I-dependent type I IFN signaling. Another explanation comes from observations of PKR. The loss of DHX36 was accompanied by a constitutive phosphorylation of PKR under normal conditions and a massive increase of its phosphorylation after poly (I:C) treatment compared to WT conditions (Figure 3.5.1 D). To identify possible epistatic regulations of both proteins, HEK double knockout cells of DHX36 and PKR were generated (Figue 3.6.1 A). The DHX36/PKR KO cells showed a complete abolishment of the DHX36 single KO phenotype, displaying DDX58, RSAD2, and ADAR1 transcript levels comparable to WT cells after 24 h poly (I:C) treatment (Figue 3.6.1 C-E). A similar observation was made for IFIT1 transcripts, however, the IFIT1 protein levels were even decreased in the DHX36/PKR KO cells in comparison to WT cells after the poly (I:C) administration (Figure 3.6.1 F-H). These results imply that PKR is the main contributor for the

increased ISG levels upon the loss of DHX36. Moreover, this is in line with observations of another study, in which the ablation of PKR in mouse bone marrow-derived DC reduced IFN-α and IFN-β levels upon the infection with several RNA viruses such as EMCV, Theiler's murine encephalomyelitis (TMEV), and Semliki Forest virus¹⁷⁰. Interestingly, even though the *PKR* knockout in the study reduced the IFN-α and IFN-β release, their mRNA levels were still upregulated. This IFN-β mRNA, however, was compromised in the poly A tail implicating a role of PKR in the maintenance of IFN-β mRNA integrity rather than in its transcription. Moreover, this phenotype was independent of eIF2-α phosphorylation, indicating a dichotomy of eIF2-α-dependent translation inhibition and IFN-B mRNA control by PKR. Taking this into account, the previously described observation of increased IFIT1 and RSAD2 transcript levels after specific RIG-I stimulation in this thesis could possibly be a side effect that derived from feedback loops. In this scenario, RIG-I activation leads to IFNB1 transcription and the higher activation of PKR in the DHX36 KO cells improves its integrity or stability compared to WT conditions. This would finally result in the observed slightly enhanced IFIT1 and RSAD2 expression. Since the DDX58 levels remained at WT levels after RIG-I ligand treatment, the major *DDX58* expression inducing compound would not be IFN-β-mediated, but rather controlled by other factors such as IRF3. This fits with the early upregulation of DDX58 after already 1 h poly (I:C) treatment in which IFNB1 levels were still low (Figure 3.2.1 C). However, the DHX36 KO cells exhibited an enhanced IRF3 phosphorylation after poly (I:C) treatment compared to WT cells and the IRF3 phosphorylation remained high in the DHX36/PKR double knockout (Figue 3.7.1 C-D). This clearly indicates that other PRRs, such as RIG-I, are most likely under negative regulation by DHX36 as well, which drive IRF3 phosphorylation. It would be interesting to test IRF3 phosphorylation levels after the administration of the RIG-I ligand in all three different cell lines. Consequently, these results give evidence that IRF3 activation alone without PKR takes place in HEK cells, but is not sufficient to drive the normal expression of ISGs such as DDX58, IFIT1, and RSAD2. Similar results were observed in PKR KO mouse fibroblasts, which were still capable of IRF3 and IRF7 phosphorylation and the production of IFNB1 mRNA after NDV infection¹⁶⁹. Nevertheless, the study missed to validate IFN-β release and thus, its functional capacity or later ISG expression in PKR null mutants. In contrast, another publication showed that the phosphorylation of IRF3 at

the C-terminus was slightly inhibited in *PKR* KO HeLa cells during ΔE3L vaccinia virus treatment compared to WT cells³⁰⁴. Since the antibody used in my thesis specifically detects phosphorylated IRF3 at serine position 386 it is possible that the position of IRF3 phosphorylation and activation depends on the type of virus. To further validate the aforementioned hypotheses, double knockouts of *DHX36/DDX58* or *DHX36/IRF3* and their responses to a viral trigger should be investigated.

Despite the fact that the *DHX36/PKR* double knockout reversed the levels of *DDX58*, *IFIT1*, *RSAD2*, and *ADAR1* to a similar or lower level compared to WT cells, the primed phenotype of increased *IFNB1* and *IRF7* transcript levels in untreated conditions was still present (Figure 7-8). This indicates that the loss of *DHX36* is the major driver of the upregulated *IFNB1* and *IRF7* transcripts and it is independent of PKR (further discussed in section 4.6).

In conclusion, my data gives evidence that DHX36 is a negative regulator of PKR and possibly of other PRRs such as RIG-I. Furthermore, PKR plays an important role in the regulation of ISG expression.

4.4 PKR and ADAR1, interaction partners of DHX36

In order to identify whether DHX36 physically interacts with PKR to fulfil its inhibitory function a co-immunoprecipitation with subsequent mass spectrometry analysis was performed (Figure 3.8.1 A). Previous studies showed the interaction of RIG-I, PKR, and DHX36, however, PKR was absent in my mass spectrometry data under normal conditions or after poly (I:C) treatment. These discrepancies could be the cause of very stringent washing steps with high salt concentration that could have led to the loss of weaker protein interactions. This would be in line with the observation that only DHX36 was detected in the mass spectrometry data in unstressed conditions after excluding false positive hits (data not shown). Interestingly, the PKR inhibitory protein ADAR1 was detected after poly (I:C) treatment. A subsequent Co-IP experiment in HEK cells was performed to verify the postulated interaction of PKR and ADAR1 (p150 long isoform) with DHX36, respectively. In contrast to the mass spectrometry data, the interaction of all proteins was detected under normal conditions as well under viral stress (Figure 3.8.1 B). This implies that those interactions are independent of viral RNA. However, the interaction of PKR and ADAR1 with DXH36 disappeared after the treatment with the ssRNA digesting enzyme RNase A indicating that the interaction is rather mediated by host cellular ssRNA than of physical nature. The previously mentioned study that described RIG-I and PKR interaction with DHX36 missed to investigate this possibility²⁸⁸. Moreover, another publication examined the interaction of PKR and ADAR1 in HEK293T cells and showed that both proteins interact in an dsRNA-independent manner using the digesting enzyme RNase V₁³⁰⁵. On the other hand, several other RNA-dependent DHX36 interactions were described, among them the binding of Human antigen R (HuR), the protein product of embryonic lethal and abnormal vision (ELAV)-like protein 1 (*ELAVL1*) or interleukin enhancer binding factor 3 (ILF3; other name NFAR1)²⁵³. The latter was detected in the mass spectrometry data after poly (I:C) treatment (Figure 3.8.1 A). Furthermore, the DEAD-box helicase DDX21 was found after viral stress in my mass spectrometry analysis, which was previously described to stay in a complex with DHX36 in myeloid dendritic cells (mDCs), however, also without a viral trigger²⁸⁹. Assuming that the interaction of both proteins intensifies under viral stress, the interaction could have been too weak for the harsh washing conditions of the immunoprecipitation before the mass spectrometry. Noteworthy, the RNase A treatment was performed according to other experimental setups in which the RNA-dependent interaction of DHX36 with ELAVL1 and ILF3 was investigated²⁵³. However, the lack of a real positive interaction control for DHX36 is missing.

Considering the RNA-dependent interaction of DHX36 with PKR and ADAR1 it is reasonable to ask whether this complex is necessary for the inhibitory function of DHX36. In this regard, another study showed that the interaction of ADAR1 with PKR leads to an inhibition of PKR phosphorylation in HEK293T cells³⁰⁵. Moreover, the overexpression of *ADAR1* was accompanied by an increase in VSV susceptibility in MEFs, which was lost upon the loss of *PKR*. This could explain the phenotype observed in the *DHX36* KO cells. The increased transcript levels of *ADAR1* could be an indicator of its inhibitory function to dampen the described PKR phosphorylation upon the *DHX36* ablation in unstressed conditions. Noteworthy, the appearance of a rG4 in the 5` untranslated region (UTR) of *ADAR1* could affect its mRNA abundancy and stability in an DHX36-dependent manner (analyzed by DHX36 PAR CLIP; data not shown). However, the enhanced *ADAR1* levels abolished in the *DHX36/PKR* KO, which implies that the PKR phosphorylation caused the upregulated transcript levels of *ADAR1* rather than the rG4 in the 5` UTR. To finally investigate if the complex of DHX36, PKR, and

ADAR1 is necessary to keep PKR in an inactive state under normal conditions, pull down experiments of PKR in *DHX36* KO cells should be performed and checked for the loss of ADAR1 interaction.

Combining these facts, it would be reasonable that both, DHX36 and ADAR1, play an essential role in the inhibition of PKR to maintain cellular homeostasis as well as orchestrating type I IFN signaling.

4.5 DHX36: Stress granule functions and anti-viral effects

The formation of anti-viral stress granules (avSG) is an important prerequisite for an appropriate immune response within cells²⁸⁵. It comes to no surprise that several viruses counteract this step during infection. Interestingly, a constitutive formation of SGs was observed upon the loss of DHX36 (Figure 3.1.1 A-B). In contrast, an siRNA-mediated downregulation of DHX36 in HeLa cells was not sufficient to cause any SG formation indicating that long term perceived stress induced by the permanent absence of DHX36 could be a reason for this²⁸⁸. The application of poly (I:C) to the HEK *DHX36* KO cells in my data, however, showed an attenuated formation of SGs compared to WT cells (Figure 3.4.1 E-F). Whether this effect is because of a temporal delay in the SG formation caused by the loss of DHX36 or due to other reasons should be investigated by a longer time course of viral stress. With regard to this, the SG positive cells in WT conditions reached a steady state after 6 to 24 h, which suggests a peak in SG formation at these times. Similar observations were published by another group, in which the SG formation was highly decreased in DHX36 knockdown HeLa cells after NDV infection²⁸⁸. However, the accumulation of NDV N gene RNA was similar in the DHX36 knockdown cells compared to WT cells suggesting that the reduced SG formation is independent of NDV replication. On the contrary, replication of the yellow fever virus (YFV) replicon in DHX36 KO HEK cells was clearly diminished after 24 h post application compared to WT conditions (Figure 3.4.1 D). This would be in line with the higher ISG response observed after 24 h poly (I:C) treatment in the DHX36 KO cells (Figure 3.1-3.2). To test this hypothesis, the ISG response after the YFV replicon transfection should be examined in WT and DHX36 KO cells. The observed discrepancy could be caused by the experimental setups. Yoo et al., 2014 used a viral strain, whereas only a replicon of the YFV was used in this thesis. Moreover, the two viruses belong to different families and even though both harbor a ssRNA genome, the NDV is

negative-sense and the YFV is positive-sense. Noteworthy, the presence of five *in silico* predicted rG4 sequences in the YFV genome could influence the replication in an unknown manner in cells devoid of *DHX36*.

Interestingly, the formation of SGs upon the infection with a measles virus (MV) mutant in HeLa cells was dependent on PKR, whereas negatively influenced by ADAR1306. Furthermore, ADAR1 impaired proper PKR activation and IFN-β induction upon MV infection suggesting that both proteins contribute to the dynamic oscillation of SG formation during type I IFN signaling. In context to the observed increase of PKR phosphorylation upon the loss of DHX36 in the HEK cells, one would expect increased SG formation during infection. However, the G3BP1 positive cells were reduced after poly (I:C) treatment (Figure 3.4.1 E-F). The concomitant upregulation of ADAR1 in the DHX36 KO HEK cells could be a counteract to decrease the SG formation (Figure 3.1.1. E and Figure 3.6.1 G). It would be interesting to see whether the additional PKR knockout in the DHX36 KO HEK cells would reverse the phenotype of increased SG formation since the ADAR1 transcript levels are comparable to WT levels again as well (Figure 3.6.1 G). Another reason for increased and uncontrolled PKR activation could be a change in localization of either PKR or ADAR1 after DHX36 loss, since both proteins show specific translocation into SGs upon MS infection³⁰⁷. This would be in line with the CoIP data of PKR and ADAR1 RNA-dependent interaction, indicating that these proteins are in close proximity in unstressed and stressed conditions. Further investigations should be performed, as previously discussed, in order to identify the cause of SG formation in DHX36 deficient cells.

In summary, the reduced SG formation in HEK cells upon the loss of *DHX36* as well as the DHX36 interaction with PKR and ADAR1 in an RNA-dependent manner indicates a positive regulatory role of DHX36 in SG regulation.

4.6 The role of rG4-dependent DHX36 functions in type I IFN responses

DHX36 is implicated in diverse cellular processes including the regulation of translation. In this regard, the formation rG4 structures in 5` and 3`UTRs or CDS of mature mRNA renders them translationally incompetent by blocking the accessibility to the ribosomal machinery. In order to regulate these fine-tuning modules of translation, DHX36 resolves the rG4s to drive the proper translation of the target mRNAs²²⁸. Interestingly, the loss of *DHX36* in HEK cells was accompanied by the accumulation of the DHX36 mRNA

binding targets as well as an enhancement of cytoplasmic G4 structures. As shown in my data, another consequence is the increase of IFNB1, IRF7 and the other ISG transcripts DDX58, IFIT1, RSAD2, and ADAR1 (Figure 3.1.1 E-J). Whereas IFNB1, DDX58, IFIT1, and RSAD2 mRNAs are depleted in rG4 structures, the IRF7 and ADAR1 transcripts possess an rG4 in the 5'UTR, respectively²⁴¹. Interestingly, the ADAR1 transcript was on the top 200 mRNA targets of DHX36 in the PAR CLIP data (data not shown), whereas IRF7 was a not bound. Hence, the increased transcript levels of ADAR1 in DHX36 KO cells could result from the stabilization of rG4s in in the 5`UTR and renders the mRNA more abundant but translationally incompetent. Measuring the protein levels by immunoblotting would clarify this question. In this context, ADAR1 is a potent binder of RNA polymerase II derived Alu repeat RNA, a class of repetitive SINEs (short interspaced elements) retroelements²²⁷. Due to its A-to-I editing property, ADAR1 destabilizes the Alu elements to maintain overall self-tolerance. In the case of ADAR1 depletion, Alu elements accumulate within the cell and activate the dsRNA recognizing PRRs PKR and MDA5, which triggers an uncontrolled immune response. In an effort to further describe this phenotype, the MDA5-mediated activation of PKR was demonstrated in ADAR1 KO neuronal progenitor cells (NPCs) with additional IFIH (MDA5) knockdown²²⁷. In contrast, the *DHX36/PKR* KO clearly rescued the increased levels of ISG transcripts after poly (I:C) treatment, however, the priming phenotype still remained with enhanced IFNB1 and IRF7 transcripts in unstressed conditions (Figure 3.7.1 A-B). It could be reasonable that PKR is the major driver of increased ISGs during the type I IFN response when DHX36 is absent. On the other hand, MDA5 could play a role in the elevated IFNB1 and IRF7 levels by still binding endogenous RNA as for instance Alu elements, which activates it and subsequent anti-viral responses³⁰⁸. Whether DHX36 is necessary for the proper processing of Alu elements and maybe acts in concert with ADAR1 to do so would be interesting to identify. In this line of thoughts, the upregulation of ADAR1 in DHX36 KO cells would be a sign of compensation, maybe because DHX36 is necessary for correct ADAR1 localization to RNA, which cannot be simply explained by increased ADAR1 levels. This would be congruent with the RNA-dependent interaction of DHX36 and ADAR1 observed in the CoIP data (Figure 3.8.1 A-B). As previously mentioned, this could be verified by more CoIP experiments as well as PAR CLIP analyzes of ADAR1 in DHX36 KO cells. Furthermore, PAR CLIP

analyzes of PKR or MDA5 would shed light on the fact of possible sequence specific interactions and whether DXH36 and the mentioned other proteins bind similar sequences of RNAs to fulfil their function. It would be interesting to know if rG4s are mediators of the assembly of such protein complexes.

However, the observation that the rG4 stabilizing ligand cPDS in WT cells could not induce the phenotype of increased ISGs as seen in the *DHX36* KO cells indicates an rG4-independent mechanism (Figure 3.9.1). Noteworthy, the presence and the fact that DHX36 is a potent rG4 unwinding helicase could negate the subtle changes in ISG transcript levels induced by cPDS. Another way to verify this hypothesis could be achieved by the use of a G4 disrupting small molecule referred to as phenylpyrrolocytosine (PhpC)-based G-clamp analog³⁰⁹. Introducing this compound into the *DHX36* KO cells would result in the resolution of the accumulated rG4s within the mRNAs of the cells and thus, would clarify whether the increased ISG primed phenotype is solely based on increased rG4 or due the real loss of *DHX36*. Furthermore, another interesting observation is that the ATP-dependent RNA unwinding catalytic domain of DHX36 is necessary for the negative regulation of type I IFN singaling (Figure 3.8.1 C-E). However, whether this function is needed for rG4 resolution with regard to viral stress or the described phosphorylation of PKR by another study is still elusive²⁸⁸.

In conclusion, the endogenous positive and negative effects of rG4s, their utilization by viruses as well as their regulation by DHX36 in type I IFN signaling still remains unknown and need further investigation.

4.7 DHX36, a possible target for cancer therapy

The implications of DHX36 in diverse processes are versatile and hence, it comes to no surprise that the loss of it impacts the overall cellular homeostasis. Changes of the general growth and clustering of cells are just two aspects beside the accumulation of translationally incompetent rG4 harboring mRNAs as well as constitutive stress with increased levels of type I IFNs (Figure 3.1.1, Figure 3.2.1, Figure 3.4.1). Interestingly, DHX36 protein levels decrease after viral stress and the overexpression of DHX36 in HEK cells showed a reduced response of several ISGs in comparison to WT conditions (Figure 3.3.1). These facts suggest that the temporary DHX36 downregulation, even though necessary for the proper type I IFN response, is a critical step for the cell, since it is accompanied by the impairment of cellular homeostasis. In the light of cancer

development, many different kinds of cancer display a constitutive upregulation of DHX36 as for instance observed in prostate cancer (The Cancer Genome Atlas; TCGA; cbioportal). It would be interesting to understand whether this is solely a correlation of other changes or a direct effect to cope with increased cellular mRNA and rG4s. Moreover, an upregulation of DHX36 could lead to a more inert anti-viral stress response and indirectly influence the overall behavior of cancer cells upon treatments with specific ligands or drugs.

Direct evidences of DHX36 actions with regard to hallmarks of cancer are still elusive, however, several interaction partners of DHX36 are known RNA binding proteins (RBPs) with implications in cancer disease states²⁵³. For instance, HuR is a posttranscriptional regulator of mRNAs and overexpressed as well as over-active in several cancer settings. It binds to AU-rich elements (AREs) in the 3` UTR of target mRNAs to protect them from ARE-mediated accelerated de-adenylation, which confers mRNA stability and proper translation³¹⁰. Interestingly, DHX36 was isolated in association with the ARE of urokinase plasminogen activator mRNA (ARE^{uPA}) and moreover, interacted with HuR in an RNA-dependent manner²⁵³. The binding of a catalytic dead variant of DHX36 to AREs was confirmed by another study via a global analysis of RNA binding sequences²²⁸. In this case, the majority of AU-rich binding sites of DHX36 were on mRNAs with G-rich binding motifs, which were capable of rG4 formation. It would be interesting to know whether HuR and DHX36 play synergistic or antagonistic roles in the regulation of mRNA stability and translation³¹¹. The same hypothesis is true for AREs and rG4s and if the binding of a protein to the nucleic acid sequence or structure influences the protein association to the other one. This would be of upmost importance for many transcripts bearing translation influencing rG4 structures, especially those that regulate disease related genes such as the angiogenic factor VEGFA, the proto-oncogene *NRAS* or the tumor suppressor *TP53*.

Another recent publication linked DHX36 to the DNA damage response of glioblastoma upon treatments such as radiotherapy or chemotherapy³¹². In this case, DHX36 binds to rG4 structures on mRNA on a global level and mediates their unwinding, which enables the association of heterogeneous nuclear ribonucleoproteins H and F (hnRNP H/F). In turn, the binding of hnRNP H/F keeps the rG4 structure resolved to facilitate its proper translation. The depletion of hnRNP H/F in the chemo- and radio-resistant human

glioblastoma cell line LN18 gave rise to an increased phosphorylation of the DNA damage marker γ-H2AX after ionizing radiation radiotherapy or temozolomide chemotherapy, whereas its overexpression attenuated it. This data was further confirmed by the binding of DHX36 and hnRNP H/F to the mRNA of the ubiquitin peptidase USP1, which has important functions in DNA damage repair and influenced its protein expression. Interestingly, the analysis of low-grade gliomas (LGG) and high-grade gliomas (HGG; also glioblastomas) patient tissue samples showed differential expression levels of DHX36 and hnRNP H/F. An increase of expression for each protein was observed in HGG samples, which have a faster growth and spread into normal brain tissues as compared to LGG. This could explain the correlation of upregulation of hnRNP H/F or other RBPs such as DHX36 observed in different cancer types and thus, makes them potential targets for treatments or early detection of diseases. However, bona fide effects or mere correlations need to be excluded.

4.8 A model for DHX36 functions during viral signaling in HEK cells

Taking the obtained and presented data of this thesis into consideration and combining it with the current state of research, a model of DHX36 for HEK cells and its function in type I IFN signaling can be proposed (Figure 4.9.1).

Healthy cells control transcription and translation in an orchestrated fashion. In this case, anti-viral proteins such as RIG-I, PKR, DHX36, and ADAR1 most likely reside in a complex mediated by their RNA-binding ability, which was also confirmed by other publications^{254,288,307}. The tolerance of PRRs like RIG-I and probably other RLRs as well as PKR to endogenous RNA is reduced and inhibited by DHX36 and ADAR1^{227,307}. Upon viral infections, the cytoplasmic foreign RNA is sensed by RIG-I and PKR, which leads to their activation^{64,288}. In the early stages of infection, virus RNA-mediated phosphorylated of PKR drives the overall translational shutdown via eIF2-α activation and results in the formation of avSGs¹⁶². I propose that within avSG, among other general proteins, RIG-I and PKR undergo increased activation after the graduate downregulation of their inhibitor DHX36 (Figure 3.3.1). Subsequently, the RIG-I signaling cascade results in the phosphorylation of IRF3 and its translocation into the nucleus to drive *IFNB1* transcription³¹³. While type I IFN signaling continues, PKR is necessary for the proper integrity of the 3' poly-A tail of the IFN-β mRNA to facilitate translation¹⁷⁰.

92

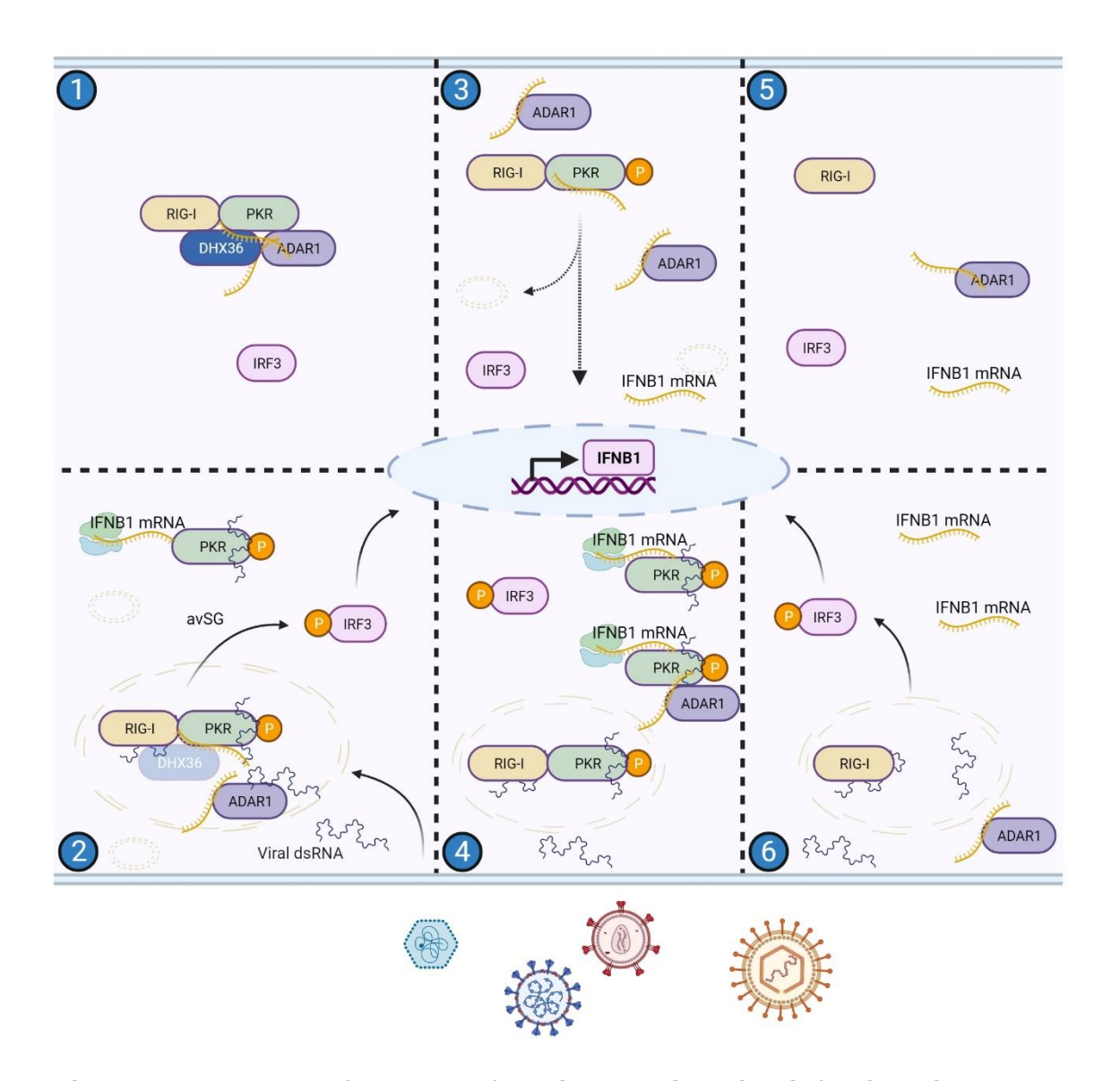


Figure 4.8.1 A model for DHX36 functions during viral infections in HEK cells

(1) In unchallenged conditions, RLRs and PKR bind similar endogenous RNA like DHX36 and ADAR1, which decrease their self-tolerance and inhibits autoactivation. (2) The sensing of viral RNA leads to a graduate downregulation of DHX36, which releases RLRs and PKR from its inhibition and activates the downstream signaling cascades involving IRF3 phosphorylation, eIF2 α -dependent translation inhibition (including SG formation), respectively. IFN- β mRNA transcription is induced and its integrity is PKR-dependent. The release of IFN- β induces type I IFN receptor-mediated JAK-STAT signaling ISG expression to hamper viral reproduction. (3) The loss of DHX36 leads to decreased inhibition of PKR and RIG-I and results in reduced self-tolerance to endogenous RNA. This induces a slight expression of IFN- β and other ISGs. (4) Diminished inhibition of PKR and RIG-I upon viral stress causes an overshoot of the signaling cascades without the inhibitory orchestrator DHX36. (6) The additional depletion of PKR reverses the increase in type I IFN signaling upon viral infection, however, (5) the self-tolerance of other PRRs still activates IFNB1 transcription. Figure created with BioRender.

Once released, IFN- β activates in an autocrine and paracrine fashion the interferon receptors IFNAR1 and IFNAR2, which eventually results in the JAK-STAT activation and the expression of ISGs³¹³. In situations of DHX36 depletion, PKR is constitutively active, which is accompanied by the upregulation of *IFNB1* and downstream factors such as *IRF7* as well as several ISGs (Figure 3.1.1). This increase of type I IFN signaling genes is concomitant with the formation of SGs (Figure 3.1.1). In cases of viral infections, PKR and maybe other RLRs are already in a primed state with decreased self-tolerance caused by the absence of their inhibitor DHX36. This leads to an overshoot of the signaling cascade, maybe by the PKR-mediated increased integrity and stability of the IFN- β mRNA (Figure 3.2.1).

The additional loss of *PKR* besides *DHX36* is still accompanied by increased *IFNB1* and *IRF7* transcripts, whereas the ISG levels upon viral infections are decreased (Figure 3.6.1 and Figure 3.7.1). Even though still massively abundant upon viral infection, the IFN- β mRNA is most likely inactive, because of the absence of PKR and the impaired 3 poly A tail. This impairs proper type I IFN signaling and results in decreased ISG levels, even though other mechanisms are functional such as IRF3 activation (Figure 3.7.1).

4.9 Concluding remarks

To finally conclude my thesis on the whole, I want to shortly address the relevance of DHX36 on an overall and broad scope and the remaining open questions.

The DEAH-box helicase DHX36 play important roles in many different cellular processes, among them RNA translation regulation and the topics of this thesis anti-viral responses and type I IFN signaling. Albeit the loss of *DHX36* is critical for cells, some cell-types survive its absence while others most likely not. All observations were made *in cellulo*, whereas a conditional *DHX36* knockout mouse model is embryonically lethal and tissue-specific ablations result in severe developmental defects in the affected organs. These facts underline the importance of DHX36 for the whole organism and its indispensable function.

In this context, several studies show increased levels of DHX36 in many cancer types, raising hopes as a potential anti-cancer drug target for this helicase of its rG4

modulation functions. On the same line of thoughts, the importance of DHX36 in anti-viral responses opens new fields for the development of vaccines against viruses.

My Data provides precious new insights into the function of DHX36 in HEK cells. While showing that DHX36 is a negative regulator of type I IFN signaling, this effect could be harnessed for a temporal boost of the signaling cascade to fight viral infections. Specific inhibitors of DHX36 could be developed and tested for such effects. Nevertheless, the mechanisms of rG4 mediated translation control and its effects in type I IFN signaling should be considered.

Moreover, the consideration of permanent DHX36 overexpression in many cancer types could point to another possible application. The immune incompetence of cancer cells could be connected to the increase in DHX36 levels and that those cells show less type I IFN signaling (Figure 3.3.1). If this is true, DHX36 inhibitors that specifically target cancer cells could modulate those cells to render them vulnerable for other treatments.

However, in order to fully understand the effects on type I IFN signaling by DHX36, the missing parts need further investigation. Among them are the contribution of other RLRs besides PKR for the observed primed phenotype such as MDA5 or RIG-I and their epistatic interactions. A special focus lies on ADAR1 and its ability to regulate self-tolerance by the modulation of RNAs. Moreover, the specific role of *IFNB1* transcripts and PKR-dependent ISG expression as well as the contradictory role of SG formations.

In summary, this thesis provides a detailed characterization of DHX36 and its functions in type I IFN signaling. The here presented data takes the properties of DHX36 with regard to anti-viral responses as well as its features of RNA homeostasis into account and thus, provides valuable information for basic and clinical research to better understand viral infections or cancer.

5. Abstract

The induction of type I interferons (IFN) is a hallmark of foreign nucleic acids immune sensing by the innate immune system. Based on the universal molecular structure of DNA and RNA throughout all kingdoms of life, the cell has to distinguish foreign nucleic acids from self-nucleic acids to properly respond to infecting pathogens. Thus, the orchestration of this crucial process, in which the cell has to balance the tolerance to endogenous nucleic acids, is achieved by a sophisticated network of receptor proteins as well as their negative and positive regulators.

A pivotal factor against viral RNA are cytoplasmic localized pattern recognition receptors (PRRs) as well as other proteins that detect specific structures of foreign RNA and induce a myriad of signaling cascades. The activation of PRRs upon viral RNA recognition results in the expression of IFNs and subsequently, the induction of interferon stimulated genes (ISGs) to impair viral spread.

One example of anti-viral proteins is the DEAH-box helicase DHX36. While described in several reports, the exact mechanism how and where this protein acts in the type I IFN signaling remains still elusive.

The here-presented doctoral thesis provides a detailed view on the specific function of the helicase DHX36 during viral stress in human embryonic kidney cells. The expression pattern of DHX36, its interactions to other proteins, as well as epistatic affiliations were analyzed. The sensing of viral RNA leads to the downregulation of DHX36 expression, which normally stays in an RNA-dependent complex with PKR and ADAR1. The loss of *DHX36* is accompanied by a slight increase in type I IFN genes and ISGs in unchallenged conditions, while a viral trigger massively induces their expression compared to WT cells. The positive effect of the *DHX36* depletion on increased ISGs is congruent with a decrease in yellow fever virus replicon replication and an enhanced cell metabolism during viral stress. Furthermore, the increase of ISGs during viral RNA recognition completely depends on PKR, while the enhanced type I IFN signaling is independent of PKR. I hypothesize that, DHX36 is a negative regulator of PKR and maybe other PRRs to control and orchestrate self-tolerance to endogenous RNA and correct activation of them during viral RNA detection.

6. Supplementary figures

6.1 Supplementary figures

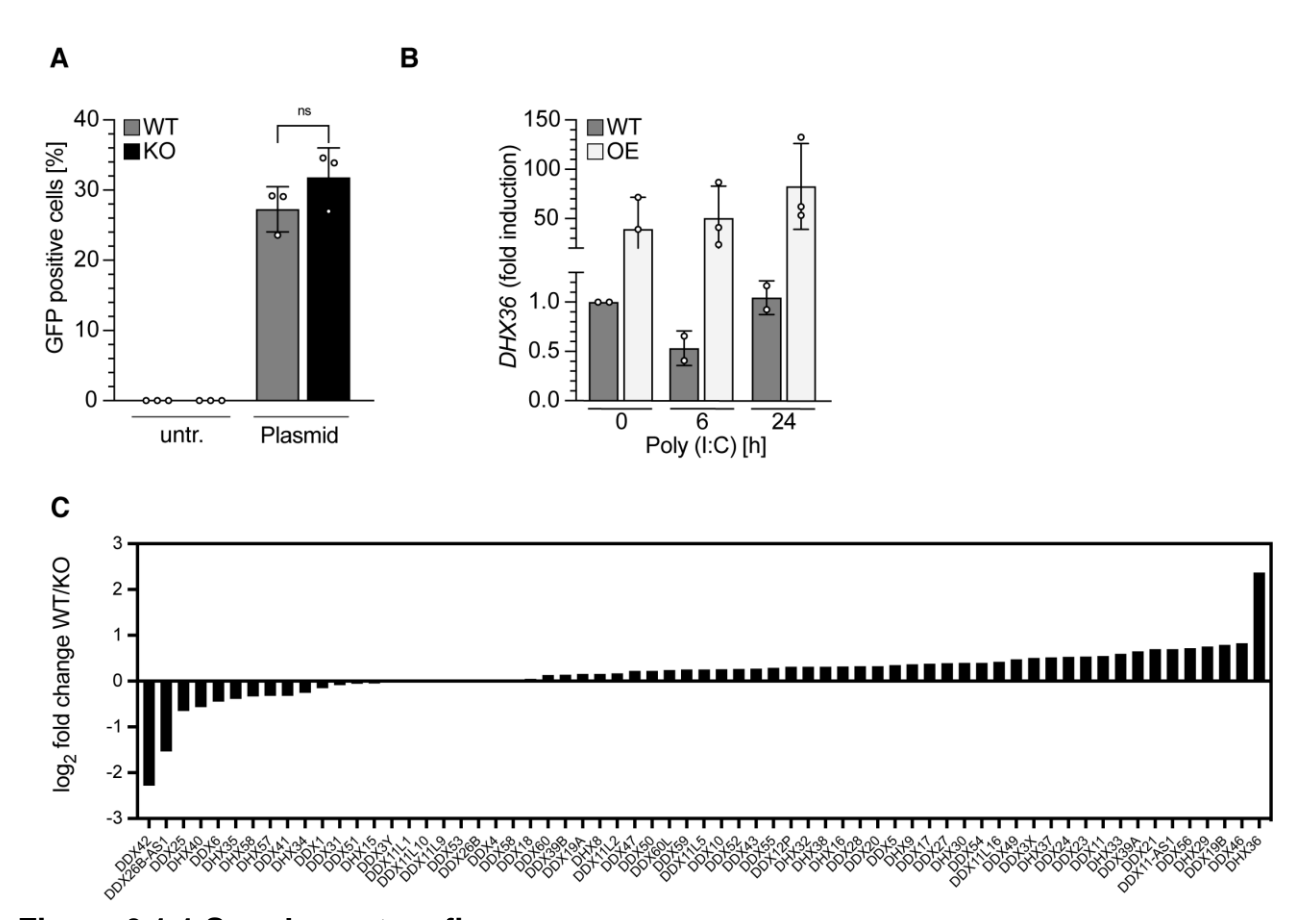


Figure 6.1.1 Supplementary figure

A) Quantifications of GFP-positive cells in WT and *DHX36* KO cells after Lipofectamine 2000 transfection of a GFP expressing plasmid. B) Transcript quantifications by RT-qPCR of the indicated genes comparing WT and *DHX36* OE cells after overexpression induction via tetracycline treatment. mRNA levels are normalized to *RNU6* and fold changes are displayed to WT untreated. C) RNA-seq analysis of DEAD/H-box helicases comparing transcript levels of WT and *DHX36* KO cells. Differences of gene transcript levels are indicated as log₂ fold changes of reads per kilobase of transcript per million mapped reads (RPKM). Significances were determined by Students t-test (n≥3). Significance levels: *p < 0.05, **p < 0.01, ***p < 0.001, ns = not significant. Error bars represent standard deviations of at least 3 biological replicates.

7. List of figures and tables

Figure 1.3.1 The type I interferon (IFN-I) response during RNA virus infection.	16
Figure 1.4.1 Cellular functions of RNA G quadruplexes (rG4s)	31
Figure 1.5.1 Schematic structure of DHX36	33
Figure 1.5.2 Innate immunity regulation by DHX36	38
Figure 3.1.1 The knockout of DHX36 induces anti-viral stress conditions	54
Figure 3.2.1 Loss of DHX36 increases type I IFN signaling upon a viral trigger	56
Figure 3.3.1 DHX36 regulation upon viral stimulation negatively regulates	type I IFN
signaling	58
Figure 3.4.1 Loss of DHX36 gives rise to enhanced anti-viral responses and	d increased
cell metabolism	61
Figure 3.5.1 DHX36 acts early during anti-viral stress responses	64
Figure 3.6.1 Negative regulation of type I IFN signaling by DHX36 depends or	n PKR 67
Figure 3.7.1 The double deletion of DHX36 and PKR is insufficient to reverse	the primed
status of the DHX36 KO cells	69
Figure 3.8.1 An RNA-dependent interaction of DHX36 with PKR and ADAR1.	72
Figure 3.9.1 Increased type I IFN signaling is DHX36 mediated rather than rG	474
Figure 4.9.1 A model for DHX36 functions during viral infections in HEK cells.	92
Figure 6.1.1 Supplementary figure	96
Table 1.1 Families of pattern-recognition receptors	18
Table 1.2 Adaptor proteins of PRRs	19
Table 8.1 Chemicals	99
Table 8.2 Commercial systems	99
Table 8.3 Bacterial strains	100
Table 8.4 Eukaryotic cell lines	100
Table 8.5 Antibodies	100
Table 8.6 Plasmids	101
Table 8.7 qPCR primer	101
Table 8.8 CRISPR/Cas9 guide RNAs	
Table 8.9 Buffers and solutions	102

8. Tables

Table 8.1 Chemicals

Chemicals	Identifier	Supplier
Carboxypyridostatin trifluoroacetate salt	SML1176	Sigma-Aldrich
Dynabeads Protein G	10003D	Thermo Fisher Scientific
Ethidium bromide solution (1%)	2218.1	Carl Roth GmbH
Fluoroshield with DAPI	F6057-20ML	Sigma-Aldrich
GeneRuler 1kb Plus DNA Ladder	SM1331	Thermo Fisher Scientific
GeneRuler Low Range DNA Ladder	SM1192	Thermo Fisher Scientific
Poly-D-Lysine	A-003-M	Sigma-Aldrich
Proteinmarker prestained (11 – 245 kDa)	1123YL500	BioLabs
Hoechst 33342 Ready Flow™ Reagent	R37165	Thermo Fisher Scientific
Fixable Viability Dye e Fluor 780	65-0865-14	eBioscience

Table 8.2 Commercial systems

Kit/System	Identifier	Supplier
CellTiter 96® Non-Radioactive Cell Proliferation	G4000	Promega
Assay (MTT)		
innuPREP Gel Extraction Kit	845-KS-5030250	Analytik Jena
innuPREP PCRpure Kit	845-KS-5010250	Analytik Jena
innuPREP Plasmid Mini Kit	845-KS-5041250	Analytik Jena
IQ SYBR Green	170-8885	BioRad
Lipofectamine 2000 Transfection Reagent	11668027	Thermo Fisher
		Scientific
Lipofectamine CRISPRMAX Cas9 Transfection	CMAX00015	Thermo Fisher
Reagent		Scientific
NuPAGE 4-12% Bis-Tris Protein Gels	NP0321BOX	Thermo Fisher
		Scientific
Superscript Reverse Transcriptase III	18080044	Thermo
QuantiTect Reverse Transcription Kit	205313	Qiagen

Table 8.3 Bacterial strains

Strain	Genotype	Supplier
DH5α	F- φ80 <i>lac</i> ZΔM15 Δ(<i>lac</i> ZYA- <i>arg</i> F)U169 <i>deo</i> R <i>rec</i> A1	Thermo Fisher
	endA1 hsdR17(rk-, mk+) phoA supE44 thi-1 gyrA96	Scientific
	relA1 λ ⁻	
DH5α	pFRT FlagHA-DHX36-1	Sauer et al.,2019
DH5α	pOG44	Sauer et al.,2019

Table 8.4 Eukaryotic cell lines

Cell line	Paternal cell line	Description	Origin
T-Rex [™] -		Identifier: R71007	Thermo Fisher
HEK 293			Scientific
MSC5	T-Rex [™] -HEK 293	Inducible expression of FH-DHX36-1	Sauer et al., 2019
MSC9	T-Rex [™] -HEK 293	DHX36-gene knock out by	Sauer et al., 2019
		CRISPR/Cas9	
MSC10	MSC9	Inducible overexpression of FH-	Sauer et al., 2019
		DHX36-1 in DHX36 KO cells	
MSC11	MSC9	Inducible overexpression of FH-	Sauer et al., 2019
		DHX36-1 E335A in DHX36 KO cells	
DH16	T-Rex [™] -HeLa	Inducible expression of FH-DHX36-1	This study
DH63	MSC9	DHX36/PKR double KO cells	This study

Table 8.5 Antibodies

Western blotting	Dilution	Identifier	Supplier
Anti-DHX36	1:500	sc-377485	Santa Cruz
			Biotechnology
Anti-FLAG	1:2000	F1804	Sigma-Aldrich
Anti-HA	1:2000	MMS-101R	Covance
Anti-PKR/EIF2AK2	1:1000	Ab32052	Abcam
Anti-PKR/EIF2AK2 (phospho T446)	1:1000	ab32036	Abcam
Anti-ADAR1	1:1000	ab126745	Abcam
Anti-IRF3 (phosphor S386)	1:1000	ab76493	Abcam

Immunofluorescence	Dilution	Identifier	Supplier
Anti-G3BP1	1:500	611126	BD Bioscience
Alexa Fluor 488 goat anti-mouse	1:5000	A11001	Thermo Fisher
IgG			Scientific
Cyanine 3 goat anti-rabbit IgG	1:5000	A10520	Thermo Fisher
			Scientific

Table 8.6 Plasmids

Plasmid name	Generated by	Marker	Origin
pFRT-Flag-HA		Amp	Spitzer et al. 2013
pFRT-FlagHA-DHX36-iso1	Restriction cloning	Amp	Sauer et al., 2019
pFRT-FlagHA-DHX36-iso1 E335A	Site-directed	Amp	Sauer et al., 2019
	mutagenesis		
pFRT-FlagHA-DHX36-iso2	Site-directed	Amp	Sauer et al., 2019
	mutagenesis		
pFRT-FlagHA-DHX36-iso2 E335A	Site-directed	Amp	Sauer et al., 2019
	mutagenesis		

Table 8.7 qPCR primer

For ADAR1 RT	TCCGTCTCCTGTCCAAAGAAGG
Rev ADAR1 RT	TTCTTGCTGGGAGCACTCACAC
For IRF7 RT	CCACGCTATACCATCTACCTGG
Rev IRF7 RT	GCTGCTATCCAGGGAAGACACA

Table 8.8 CRISPR/Cas9 guide RNAs

Guide RNA name	Sequence
For PKR KO	GTACTACTCCCTGCTTCTGA

Table 8.9 Buffers and solutions

Buffer	Composition	
DNA loading dye (6x)	48% (v/v) glycerol, 0.1% (v/v) bromphenol blue, 0.1% (v/v) xylene	
	cyanol	
TAE (10x)	40 mM Tris base, 20 mM acetic acid, 1 mM EDTA	
TBE (5x)	445 mM Tris base, 445 mM boric acid, 10 mM Na₂EDTA	
SDS loading dye (6x)	300 mM Tris-HCl pH 6.8, 120 mM DTT, 9% (w/v) SDS, 48% (v/v)	
	glycerol, 0.1% (v/v) bromphenol blue	
SDS running buffer (10x)	0.25 M Tris base, 1.92 M glycine, 1% (w/v) SDS	
Separating gel buffer (4x)	1.5 M Tris-HCl pH 8.8, 0.4% (w/v) SDS	
Stacking gel buffer (4x)	0.5 M Tris-HCl pH 6.8, 0.4% (w/v) SDS	
TBS-T	10 mM Tris-HCl pH 7.5, 150 mM NaCl, 0.05% (v/v) Tween20	
Western blotting buffer	50 mM Tris base, 50 mM glycine, 20% (v/v) methanol	
SOC	2% (w/v) tryptone, 10 mM NaCl, 0.5% (w/v) yeast extract, 10 mM	
	MgSO ₄ , 10 mM MgCl ₂ , 2.5 mM KCl, 2% (w/v) glucose	
NP40 Lysis Buffer	50 mM HEPES pH 7.5, 150 mM KCl, 2 mM Na ₂ EDTA, 0.5% (v/v)	
	NP-40 substitute, 1 mM NaF, freshly added: 0.5 mM DTT, 0.2 mM	
	PMSF, 1 mM LP, 1 mM AP, 0.1 mM AEBSF	
IP-Wash Buffer	50 mM Tris-HCl pH 7.5, 300 mM NaCl, 0.1% (v/v) NP-40	
	substitute, 5 mM Na₂EDTA	
Elution Buffer	10 mM Tris-HCl pH 7.5, 150 mM NaCl, 0.1 mg ml ⁻¹ FLAG peptide	
PCR Buffer for homemade	750 mM Tris-HCl pH 8.8, 200 mM (NH ₄) ₂ SO ₄ , 0.1% (v/v)	
Taq (10x)	Tween20, 25 mM MgCl ₂	

Table 8.10 Growth media and antibiotics

Solution	Identifier	Supplier
DPBS, no calcium, no magnesium	Cat#: 14190094	Thermo Fisher Scientific
DMEM, high glucose	Cat#: 41965039	Thermo Fisher Scientific
Fetal Bovine Serum (FBS)	Cat#: 10270106	Thermo Fisher Scientific
Trypsin-EDTA (0.25%), phenol red	Cat#: 25200056	Thermo Fisher Scientific
Penicillin-Streptomycin (10,000 U/ml)	Cat#: 15140122	Thermo Fisher Scientific
(PenStrep)		
Opti-MEM I Reduced Serum Medium	Cat#: 31985070	Thermo Fisher Scientific
Antibiotics	Identifier	Supplier
Ampicillin	Cat#: K029.5	Carl Roth GmbH
Blasticidin	Cat#: ant-bl-1	Invivogen
Hygromycin B	Cat#: ant-hg-5	Invivogen
Kanamycin	Cat#: T832.3	Carl Roth GmbH
Tetracycline	Cat#: 87128	Sigma-Aldrich

9. References

- 1. Khan, U., Mehta, R., Arif, M. A. & Lakhani, O. J. Pandemics of the past: A narrative review. *J. Pak. Med. Assoc.* **70(Suppl 3**, S34–S37 (2020).
- 2. Frith, J. The History of Plague Part 1. The Three Great Pandemics. *J. Mil. Veterans. Health* **20**, 11–16 (2012).
- 3. Valleron, A.-J. *et al.* Transmissibility and geographic spread of the 1889 influenza pandemic. *Proc. Natl. Acad. Sci. U. S. A.* **107**, 8778–8781 (2010).
- 4. Palese, P. Influenza: old and new threats. *Nat. Med.* **10**, S82-7 (2004).
- 5. Taubenberger, J. K. & Morens, D. M. 1918 Influenza: the mother of all pandemics. *Emerg. Infect. Dis.* **12**, 15–22 (2006).
- 6. Kaposi's sarcoma and Pneumocystis pneumonia among homosexual men--New York City and California. *MMWR. Morb. Mortal. Wkly. Rep.* **30**, 305–308 (1981).
- 7. Greene, W. C. A history of AIDS: looking back to see ahead. *Eur. J. Immunol.* **37 Suppl 1**, S94-102 (2007).
- 8. Weiss, R. A. HIV and AIDS in relation to other pandemics. Among the viruses plaguing humans, HIV is a recent acquisition. Its outstanding success as an infection poses immense scientific challenges to human health and raises the question 'What comes nest?'. *EMBO Rep.* **4 Spec No**, S10-4 (2003).
- 9. Kharsany, A. B. M. & Karim, Q. A. HIV Infection and AIDS in Sub-Saharan Africa: Current Status, Challenges and Opportunities. *Open AIDS J.* **10**, 34–48 (2016).
- 10. Becerra, J. C., Bildstein, L. S. & Gach, J. S. Recent Insights into the HIV/AIDS Pandemic. *Microb. cell (Graz, Austria)* **3**, 451–475 (2016).
- 11. Lee, N. et al. A major outbreak of severe acute respiratory syndrome in Hong Kong. N. Engl. J. Med. **348**, 1986–1994 (2003).
- 12. Rota, P. A. *et al.* Characterization of a novel coronavirus associated with severe acute respiratory syndrome. *Science* **300**, 1394–1399 (2003).
- 13. Skowronski, D. M. *et al.* Severe acute respiratory syndrome (SARS): a year in review. *Annu. Rev. Med.* **56**, 357–381 (2005).
- 14. The species Severe acute respiratory syndrome-related coronavirus: classifying 2019-nCoV and naming it SARS-CoV-2. *Nat. Microbiol.* **5**, 536–544 (2020).
- 15. Andersen, K. G., Rambaut, A., Lipkin, W. I., Holmes, E. C. & Garry, R. F. The proximal origin of SARS-CoV-2. *Nature medicine* vol. 26 450–452 (2020).
- 16. Zhou, P. et al. Addendum: A pneumonia outbreak associated with a new coronavirus of probable bat origin. *Nature* **588**, E6 (2020).
- 17. Rybicki, E. P. The classification of organisms at the edge of life or problems with virus systematics. *S. Afr. J. Sci.* **86**, 182–186 (1990).
- 18. Holmes, E. C. Viral Evolution in the Genomic Age. *PLOS Biol.* **5**, e278 (2007).
- 19. Pellett, P. E., Mitra, S. & Holland, T. C. Chapter 2 Basics of virology. in *Neurovirology* (eds. Tselis, A. C. & Booss, J.) vol. 123 45–66 (Elsevier, 2014).
- 20. Suomalainen, M. & Greber, U. F. Uncoating of non-enveloped viruses. *Curr. Opin. Virol.* **3**, 27–33 (2013).
- 21. Moyer, C. L. & Nemerow, G. R. Viral weapons of membrane destruction: variable modes of membrane penetration by non-enveloped viruses. *Curr. Opin. Virol.* **1**, 44–49 (2011).
- 22. Plemper, R. K. Cell entry of enveloped viruses. *Curr. Opin. Virol.* **1**, 92–100 (2011).
- 23. López-Lastra, M. et al. Translation initiation of viral mRNAs. Rev. Med. Virol. 20,

- 177-195 (2010).
- 24. Lee, K.-M., Chen, C.-J. & Shih, S.-R. Regulation Mechanisms of Viral IRES-Driven Translation. *Trends Microbiol.* **25**, 546–561 (2017).
- 25. Gupta, A. & Bansal, M. RNA-mediated translation regulation in viral genomes: computational advances in the recognition of sequences and structures. *Brief. Bioinform.* **21**, 1151–1163 (2020).
- 26. Jaafar, Z. A. & Kieft, J. S. Viral RNA structure-based strategies to manipulate translation. *Nat. Rev. Microbiol.* **17**, 110–123 (2019).
- 27. Mateu, M. G. Assembly, stability and dynamics of virus capsids. *Arch. Biochem. Biophys.* **531**, 65–79 (2013).
- 28. Perlmutter, J. D. & Hagan, M. F. Mechanisms of virus assembly. *Annu. Rev. Phys. Chem.* **66**, 217–239 (2015).
- 29. Lindenbach, B. D. Virion assembly and release. *Curr. Top. Microbiol. Immunol.* **369**, 199–218 (2013).
- 30. Parkin, J. & Cohen, B. An overview of the immune system. *Lancet (London, England)* **357**, 1777–1789 (2001).
- 31. Kaur, B. P. & Secord, E. Innate Immunity. *Pediatr. Clin. North Am.* **66**, 905–911 (2019).
- 32. Bonilla, F. A. & Oettgen, H. C. Adaptive immunity. *J. Allergy Clin. Immunol.* **125**, S33-40 (2010).
- 33. Riera Romo, M., Pérez-Martínez, D. & Castillo Ferrer, C. Innate immunity in vertebrates: an overview. *Immunology* **148**, 125–139 (2016).
- 34. Gourbal, B. *et al.* Innate immune memory: An evolutionary perspective. *Immunol. Rev.* **283**, 21–40 (2018).
- 35. Coates, M., Blanchard, S. & MacLeod, A. S. Innate antimicrobial immunity in the skin: A protective barrier against bacteria, viruses, and fungi. *PLoS Pathog.* **14**, e1007353 (2018).
- 36. Gadjeva, M. The complement system. Overview. *Methods Mol. Biol.* **1100**, 1–9 (2014).
- 37. Van Linthout, S., Miteva, K. & Tschöpe, C. Crosstalk between fibroblasts and inflammatory cells. *Cardiovasc. Res.* **102**, 258–269 (2014).
- 38. Hamada, A., Torre, C., Drancourt, M. & Ghigo, E. Trained Immunity Carried by Non-immune Cells. *Front. Microbiol.* **9**, 3225 (2018).
- 39. Palomino, D. C. T. & Marti, L. C. Chemokines and immunity. *Einstein (Sao Paulo)*. **13**, 469–473 (2015).
- 40. Chen, K., Liu, J. & Cao, X. Regulation of type I interferon signaling in immunity and inflammation: A comprehensive review. *J. Autoimmun.* **83**, 1–11 (2017).
- 41. Brubaker, S. W., Bonham, K. S., Zanoni, I. & Kagan, J. C. Innate immune pattern recognition: a cell biological perspective. *Annu. Rev. Immunol.* **33**, 257–290 (2015).
- 42. Takeda, K. & Akira, S. Toll-like receptors. *Curr. Protoc. Immunol.* **109**, 14.12.1-14.12.10 (2015).
- 43. Nikolakopoulou, C., Willment, J. A. & Brown, G. D. C-Type Lectin Receptors in Antifungal Immunity. *Adv. Exp. Med. Biol.* **1204**, 1–30 (2020).
- 44. Kim, Y. K., Shin, J. S. & Nahm, M. H. NOD-Like Receptors in Infection, Immunity, and Diseases. *Yonsei Med. J.* **57**, 5–14 (2016).
- 45. Sharma, B. R., Karki, R. & Kanneganti, T.-D. Role of AIM2 inflammasome in inflammatory diseases, cancer and infection. *Eur. J. Immunol.* **49**, 1998–2011

- (2019).
- 46. Rehwinkel, J. & Gack, M. U. RIG-I-like receptors: their regulation and roles in RNA sensing. *Nat. Rev. Immunol.* **20**, 537–551 (2020).
- 47. Beutler, B. Innate immunity: an overview. Mol. Immunol. 40, 845–859 (2004).
- 48. Deretic, V. Autophagy in inflammation, infection, and immunometabolism. *Immunity* **54**, 437–453 (2021).
- 49. Lamkanfi, M. & Dixit, V. M. Mechanisms and functions of inflammasomes. *Cell* **157**, 1013–1022 (2014).
- 50. Poltorak, A. *et al.* Defective LPS signaling in C3H/HeJ and C57BL/10ScCr mice: mutations in Tlr4 gene. *Science* **282**, 2085–2088 (1998).
- 51. Hoshino, K. *et al.* Cutting edge: Toll-like receptor 4 (TLR4)-deficient mice are hyporesponsive to lipopolysaccharide: evidence for TLR4 as the Lps gene product. *J. Immunol.* **162**, 3749–3752 (1999).
- 52. Matsumoto, M. *et al.* Subcellular localization of Toll-like receptor 3 in human dendritic cells. *J. Immunol.* **171**, 3154–3162 (2003).
- 53. Heil, F. *et al.* The Toll-like receptor 7 (TLR7)-specific stimulus loxoribine uncovers a strong relationship within the TLR7, 8 and 9 subfamily. *Eur. J. Immunol.* **33**, 2987–2997 (2003).
- 54. Ahmad-Nejad, P. *et al.* Bacterial CpG-DNA and lipopolysaccharides activate Toll-like receptors at distinct cellular compartments. *Eur. J. Immunol.* **32**, 1958–1968 (2002).
- 55. Latz, E. et al. TLR9 signals after translocating from the ER to CpG DNA in the lysosome. *Nat. Immunol.* **5**, 190–198 (2004).
- 56. Alexopoulou, L., Holt, A. C., Medzhitov, R. & Flavell, R. A. Recognition of double-stranded RNA and activation of NF-κB by Toll-like receptor 3. *Nature* **413**, 732–738 (2001).
- 57. Topping, K. D. & Kelly, D. G. Investigation of binding characteristics of immobilized toll-like receptor 3 with poly(I:C) for potential biosensor application. *Anal. Biochem.* **564–565**, 133–140 (2019).
- 58. Sato, S. *et al.* Toll/IL-1 Receptor Domain-Containing Adaptor Inducing IFN-β (TRIF) Associates with TNF Receptor-Associated Factor 6 and TANK-Binding Kinase 1, and Activates Two Distinct Transcription Factors, NF-κB and IFN-Regulatory Factor-3, in the Toll-Like Receptor S. *J. Immunol.* **171**, 4304 LP 4310 (2003).
- 59. Chen, Y., Lin, J., Zhao, Y., Ma, X. & Yi, H. Toll-like receptor 3 (TLR3) regulation mechanisms and roles in antiviral innate immune responses. *J. Zhejiang Univ. Sci. B* **22**, 609–632 (2021).
- 60. Meylan, E. *et al.* RIP1 is an essential mediator of Toll-like receptor 3-induced NF-kappa B activation. *Nat. Immunol.* **5**, 503–507 (2004).
- 61. Cusson-Hermance, N., Khurana, S., Lee, T. H., Fitzgerald, K. A. & Kelliher, M. A. Rip1 mediates the Trif-dependent toll-like receptor 3- and 4-induced NF-{kappa}B activation but does not contribute to interferon regulatory factor 3 activation. *J. Biol. Chem.* **280**, 36560–36566 (2005).
- 62. Sato, S. et al. Essential function for the kinase TAK1 in innate and adaptive immune responses. *Nat. Immunol.* **6**, 1087–1095 (2005).
- 63. Hornung, V., Barchet, W., Schlee, M. & Hartmann, G. RNA recognition via TLR7 and TLR8. *Handb. Exp. Pharmacol.* 71–86 (2008) doi:10.1007/978-3-540-72167-3_4.

- 64. Loo, Y.-M. & Gale, M. J. Immune signaling by RIG-I-like receptors. *Immunity* **34**, 680–692 (2011).
- 65. Taschuk, F. & Cherry, S. DEAD-Box Helicases: Sensors, Regulators, and Effectors for Antiviral Defense. *Viruses* **12**, (2020).
- 66. Luo, D. *et al.* Structural insights into RNA recognition by RIG-I. *Cell* **147**, 409–422 (2011).
- 67. Rothenfusser, S. *et al.* The RNA helicase Lgp2 inhibits TLR-independent sensing of viral replication by retinoic acid-inducible gene-I. *J. Immunol.* **175**, 5260–5268 (2005).
- 68. Quicke, K. M., Kim, K. Y., Horvath, C. M. & Suthar, M. S. RNA Helicase LGP2 Negatively Regulates RIG-I Signaling by Preventing TRIM25-Mediated Caspase Activation and Recruitment Domain Ubiquitination. *J. Interf. cytokine Res. Off. J. Int. Soc. Interf. Cytokine Res.* **39**, 669–683 (2019).
- 69. Hornung, V. et al. 5'-Triphosphate RNA is the ligand for RIG-I. Science **314**, 994–997 (2006).
- 70. Goubau, D. *et al.* Antiviral immunity via RIG-I-mediated recognition of RNA bearing 5'-diphosphates. *Nature* **514**, 372–375 (2014).
- 71. Schmidt, A. et al. 5'-triphosphate RNA requires base-paired structures to activate antiviral signaling via RIG-I. *Proc. Natl. Acad. Sci. U. S. A.* **106**, 12067–12072 (2009).
- 72. Pichlmair, A. *et al.* RIG-I-mediated antiviral responses to single-stranded RNA bearing 5'-phosphates. *Science* **314**, 997–1001 (2006).
- 73. Kato, H. *et al.* Differential roles of MDA5 and RIG-I helicases in the recognition of RNA viruses. *Nature* **441**, 101–105 (2006).
- 74. Lässig, C. *et al.* ATP hydrolysis by the viral RNA sensor RIG-I prevents unintentional recognition of self-RNA. *Elife* **4**, (2015).
- 75. Peisley, A., Wu, B., Yao, H., Walz, T. & Hur, S. RIG-I forms signaling-competent filaments in an ATP-dependent, ubiquitin-independent manner. *Mol. Cell* **51**, 573–583 (2013).
- 76. Berke, I. C. & Modis, Y. MDA5 cooperatively forms dimers and ATP-sensitive filaments upon binding double-stranded RNA. *EMBO J.* **31**, 1714–1726 (2012).
- 77. Wu, B. *et al.* Structural basis for dsRNA recognition, filament formation, and antiviral signal activation by MDA5. *Cell* **152**, 276–289 (2013).
- 78. Yu, Q., Qu, K. & Modis, Y. Cryo-EM Structures of MDA5-dsRNA Filaments at Different Stages of ATP Hydrolysis. *Mol. Cell* **72**, 999-1012.e6 (2018).
- 79. Allen, I. C. *et al.* NLRX1 protein attenuates inflammatory responses to infection by interfering with the RIG-I-MAVS and TRAF6-NF-κB signaling pathways. *Immunity* **34**, 854–865 (2011).
- 80. Lee, N.-R. *et al.* Activation of RIG-I-Mediated Antiviral Signaling Triggers Autophagy Through the MAVS-TRAF6-Beclin-1 Signaling Axis. *Front. Immunol.* **9**, 2096 (2018).
- 81. Hartmann, G. Nucleic Acid Immunity. Adv. Immunol. 133, 121–169 (2017).
- 82. Goubau, D., Deddouche, S. & Reis e Sousa, C. Cytosolic sensing of viruses. *Immunity* **38**, 855–869 (2013).
- 83. Honda, K., Takaoka, A. & Taniguchi, T. Type I interferon [corrected] gene induction by the interferon regulatory factor family of transcription factors. *Immunity* **25**, 349–360 (2006).
- 84. Veals, S. A. et al. Subunit of an alpha-interferon-responsive transcription factor is

- related to interferon regulatory factor and Myb families of DNA-binding proteins. *Mol. Cell. Biol.* **12**, 3315–3324 (1992).
- 85. Escalante, C. R., Yie, J., Thanos, D. & Aggarwal, A. K. Structure of IRF-1 with bound DNA reveals determinants of interferon regulation. *Nature* **391**, 103–106 (1998).
- 86. Fujii, Y. *et al.* Crystal structure of an IRF-DNA complex reveals novel DNA recognition and cooperative binding to a tandem repeat of core sequences. *EMBO J.* **18**, 5028–5041 (1999).
- 87. Sato, M. *et al.* Distinct and essential roles of transcription factors IRF-3 and IRF-7 in response to viruses for IFN-alpha/beta gene induction. *Immunity* **13**, 539–548 (2000).
- 88. Lin, R., Génin, P., Mamane, Y. & Hiscott, J. Selective DNA binding and association with the CREB binding protein coactivator contribute to differential activation of alpha/beta interferon genes by interferon regulatory factors 3 and 7. *Mol. Cell. Biol.* **20**, 6342–6353 (2000).
- 89. Chen, W. *et al.* Insights into interferon regulatory factor activation from the crystal structure of dimeric IRF5. *Nat. Struct. Mol. Biol.* **15**, 1213–1220 (2008).
- 90. Qin, B. Y. *et al.* Crystal structure of IRF-3 reveals mechanism of autoinhibition and virus-induced phosphoactivation. *Nat. Struct. Biol.* **10**, 913–921 (2003).
- 91. Lin, R., Mamane, Y. & Hiscott, J. Multiple regulatory domains control IRF-7 activity in response to virus infection. *J. Biol. Chem.* **275**, 34320–34327 (2000).
- 92. Wathelet, M. G. *et al.* Virus infection induces the assembly of coordinately activated transcription factors on the IFN-beta enhancer in vivo. *Mol. Cell* **1**, 507–518 (1998).
- 93. Au, W. C., Moore, P. A., Lowther, W., Juang, Y. T. & Pitha, P. M. Identification of a member of the interferon regulatory factor family that binds to the interferon-stimulated response element and activates expression of interferon-induced genes. *Proc. Natl. Acad. Sci. U. S. A.* **92**, 11657–11661 (1995).
- 94. Lin, R., Heylbroeck, C., Pitha, P. M. & Hiscott, J. Virus-dependent phosphorylation of the IRF-3 transcription factor regulates nuclear translocation, transactivation potential, and proteasome-mediated degradation. *Mol. Cell. Biol.* **18**, 2986–2996 (1998).
- 95. Marié, I., Durbin, J. E. & Levy, D. E. Differential viral induction of distinct interferon-alpha genes by positive feedback through interferon regulatory factor-7. *EMBO J.* **17**, 6660–6669 (1998).
- 96. Schmid, S., Mordstein, M., Kochs, G., García-Sastre, A. & Tenoever, B. R. Transcription factor redundancy ensures induction of the antiviral state. *J. Biol. Chem.* **285**, 42013–42022 (2010).
- 97. Panne, D., Maniatis, T. & Harrison, S. C. An atomic model of the interferon-beta enhanceosome. *Cell* **129**, 1111–1123 (2007).
- 98. Grandvaux, N. *et al.* Transcriptional profiling of interferon regulatory factor 3 target genes: direct involvement in the regulation of interferon-stimulated genes. *J. Virol.* **76**, 5532–5539 (2002).
- 99. Baldwin, A. S. J. The NF-kappa B and I kappa B proteins: new discoveries and insights. *Annu. Rev. Immunol.* **14**, 649–683 (1996).
- 100. Dev, A., Iyer, S., Razani, B. & Cheng, G. NF-κB and innate immunity. *Curr. Top. Microbiol. Immunol.* **349**, 115–143 (2011).
- 101. Sen, R. & Baltimore, D. Multiple nuclear factors interact with the immunoglobulin

- enhancer sequences. Cell 46, 705-716 (1986).
- 102. Liou, H. C. & Baltimore, D. Regulation of the NF-kappa B/rel transcription factor and I kappa B inhibitor system. *Curr. Opin. Cell Biol.* **5**, 477–487 (1993).
- 103. Grilli, M., Chiu, J. J. & Lenardo, M. J. NF-kappa B and Rel: participants in a multiform transcriptional regulatory system. *Int. Rev. Cytol.* **143**, 1–62 (1993).
- 104. Beg, A. A. & Baldwin, A. S. J. The I kappa B proteins: multifunctional regulators of Rel/NF-kappa B transcription factors. *Genes Dev.* **7**, 2064–2070 (1993).
- 105. Ryseck, R. P., Novotny, J. & Bravo, R. Characterization of elements determining the dimerization properties of RelB and p50. *Mol. Cell. Biol.* **15**, 3100–3109 (1995).
- 106. Kieran, M. et al. The DNA binding subunit of NF-kappa B is identical to factor KBF1 and homologous to the rel oncogene product. *Cell* **62**, 1007–1018 (1990).
- 107. Ghosh, S. *et al.* Cloning of the p50 DNA binding subunit of NF-kappa B: homology to rel and dorsal. *Cell* **62**, 1019–1029 (1990).
- 108. Bours, V., Villalobos, J., Burd, P. R., Kelly, K. & Siebenlist, U. Cloning of a mitogen-inducible gene encoding a kappa B DNA-binding protein with homology to the rel oncogene and to cell-cycle motifs. *Nature* 348, 76–80 (1990).
- 109. Haskill, S. *et al.* Characterization of an immediate-early gene induced in adherent monocytes that encodes I kappa B-like activity. *Cell* **65**, 1281–1289 (1991).
- 110. Dobrzanski, P., Ryseck, R. P. & Bravo, R. Differential interactions of Rel-NF-kappa B complexes with I kappa B alpha determine pools of constitutive and inducible NF-kappa B activity. *EMBO J.* **13**, 4608–4616 (1994).
- 111. Häcker, H. & Karin, M. Regulation and function of IKK and IKK-related kinases. *Sci. STKE* **2006**, re13 (2006).
- 112. Thanos, D. & Maniatis, T. Identification of the rel family members required for virus induction of the human beta interferon gene. *Mol. Cell. Biol.* **15**, 152–164 (1995).
- 113. ISAACS, A. & LINDENMANN, J. Virus interference. I. The interferon. *Proc. R. Soc. London. Ser. B, Biol. Sci.* **147**, 258–267 (1957).
- 114. Pestka, S., Krause, C. D. & Walter, M. R. Interferons, interferon-like cytokines, and their receptors. *Immunol. Rev.* **202**, 8–32 (2004).
- 115. Diaz, M. O., Bohlander, S. & Allen, G. Nomenclature of the human interferon genes. *J. Interferon Res.* **13**, 443 (1993).
- 116. Maeda, S. *et al.* Construction and identification of bacterial plasmids containing nucleotide sequence for human leukocyte interferon. *Proc. Natl. Acad. Sci. U. S. A.* **77**, 7010–7013 (1980).
- 117. Henco, K. et al. Structural relationship of human interferon alpha genes and pseudogenes. J. Mol. Biol. 185, 227–260 (1985).
- 118. Pestka, S. The human interferon-alpha species and hybrid proteins. *Semin. Oncol.* **24**, S9-4-S9-17 (1997).
- 119. Uzé, G., Lutfalla, G. & Gresser, I. Genetic transfer of a functional human interferon alpha receptor into mouse cells: cloning and expression of its cDNA. *Cell* **60**, 225–234 (1990).
- 120. Cleary, C. M., Donnelly, R. J., Soh, J., Mariano, T. M. & Pestka, S. Knockout and reconstitution of a functional human type I interferon receptor complex. *J. Biol. Chem.* **269**, 18747–18749 (1994).
- 121. Domanski, P. *et al.* Cloning and expression of a long form of the beta subunit of the interferon alpha beta receptor that is required for signaling. *J. Biol. Chem.* **270**, 21606–21611 (1995).

- 122. Soh, J. et al. Identification of a yeast artificial chromosome clone encoding an accessory factor for the human interferon gamma receptor: evidence for multiple accessory factors. *Proc. Natl. Acad. Sci. U. S. A.* **90**, 8737–8741 (1993).
- 123. Soh, J. et al. Identification and sequence of an accessory factor required for activation of the human interferon gamma receptor. *Cell* **76**, 793–802 (1994).
- 124. Hemmi, S., Böhni, R., Stark, G., Di Marco, F. & Aguet, M. A novel member of the interferon receptor family complements functionality of the murine interferon gamma receptor in human cells. *Cell* **76**, 803–810 (1994).
- 125. Uzé, G. & Monneron, D. IL-28 and IL-29: newcomers to the interferon family. *Biochimie* **89**, 729–734 (2007).
- 126. Agalioti, T. *et al.* Ordered recruitment of chromatin modifying and general transcription factors to the IFN-beta promoter. *Cell* **103**, 667–678 (2000).
- 127. Panne, D. The enhanceosome. Curr. Opin. Struct. Biol. 18, 236–242 (2008).
- 128. Escalante, C. R., Shen, L., Thanos, D. & Aggarwal, A. K. Structure of NF-kappaB p50/p65 heterodimer bound to the PRDII DNA element from the interferon-beta promoter. *Structure* **10**, 383–391 (2002).
- 129. Escalante, C. R., Nistal-Villán, E., Shen, L., García-Sastre, A. & Aggarwal, A. K. Structure of IRF-3 bound to the PRDIII-I regulatory element of the human interferon-beta enhancer. *Mol. Cell* **26**, 703–716 (2007).
- 130. Panne, D., Maniatis, T. & Harrison, S. C. Crystal structure of ATF-2/c-Jun and IRF-3 bound to the interferon-beta enhancer. *EMBO J.* **23**, 4384–4393 (2004).
- 131. Murray, P. J. The JAK-STAT signaling pathway: input and output integration. *J. Immunol.* **178**, 2623–2629 (2007).
- 132. Harpur, A. G., Andres, A. C., Ziemiecki, A., Aston, R. R. & Wilks, A. F. JAK2, a third member of the JAK family of protein tyrosine kinases. *Oncogene* **7**, 1347–1353 (1992).
- 133. Rane, S. G. & Reddy, E. P. JAK3: a novel JAK kinase associated with terminal differentiation of hematopoietic cells. *Oncogene* **9**, 2415–2423 (1994).
- 134. Guschin, D. *et al.* A major role for the protein tyrosine kinase JAK1 in the JAK/STAT signal transduction pathway in response to interleukin-6. *EMBO J.* **14**, 1421–1429 (1995).
- 135. Briscoe, J. *et al.* Kinase-negative mutants of JAK1 can sustain interferon-gamma-inducible gene expression but not an antiviral state. *EMBO J.* **15**, 799–809 (1996).
- 136. Fu, X. Y. A transcription factor with SH2 and SH3 domains is directly activated by an interferon alpha-induced cytoplasmic protein tyrosine kinase(s). *Cell* **70**, 323–335 (1992).
- 137. Fu, X. Y., Schindler, C., Improta, T., Aebersold, R. & Darnell, J. E. J. The proteins of ISGF-3, the interferon alpha-induced transcriptional activator, define a gene family involved in signal transduction. *Proc. Natl. Acad. Sci. U. S. A.* **89**, 7840–7843 (1992).
- 138. Zhong, Z., Wen, Z. & Darnell, J. E. J. Stat3: a STAT family member activated by tyrosine phosphorylation in response to epidermal growth factor and interleukin-6. *Science* **264**, 95–98 (1994).
- 139. Akira, S. *et al.* Molecular cloning of APRF, a novel IFN-stimulated gene factor 3 p91-related transcription factor involved in the gp130-mediated signaling pathway. *Cell* **77**, 63–71 (1994).
- 140. Yamamoto, K. et al. Stat4, a novel gamma interferon activation site-binding protein

- expressed in early myeloid differentiation. Mol. Cell. Biol. 14, 4342-4349 (1994).
- 141. Mui, A. L., Wakao, H., Harada, N., O'Farrell, A. M. & Miyajima, A. Interleukin-3, granulocyte-macrophage colony-stimulating factor, and interleukin-5 transduce signals through two forms of STAT5. J. Leukoc. Biol. 57, 799–803 (1995).
- 142. Greenlund, A. C., Farrar, M. A., Viviano, B. L. & Schreiber, R. D. Ligand-induced IFN gamma receptor tyrosine phosphorylation couples the receptor to its signal transduction system (p91). *EMBO J.* **13**, 1591–1600 (1994).
- 143. Qureshi, S. A., Salditt-Georgieff, M. & Darnell, J. E. J. Tyrosine-phosphorylated Stat1 and Stat2 plus a 48-kDa protein all contact DNA in forming interferon-stimulated-gene factor 3. *Proc. Natl. Acad. Sci. U. S. A.* **92**, 3829–3833 (1995).
- 144. Bluyssen, H. A. *et al.* Combinatorial association and abundance of components of interferon-stimulated gene factor 3 dictate the selectivity of interferon responses. *Proc. Natl. Acad. Sci. U. S. A.* **92**, 5645–5649 (1995).
- 145. Horvath, C. M., Stark, G. R., Kerr, I. M. & Darnell, J. E. J. Interactions between STAT and non-STAT proteins in the interferon-stimulated gene factor 3 transcription complex. *Mol. Cell. Biol.* **16**, 6957–6964 (1996).
- 146. Horvath, C. M., Wen, Z. & Darnell, J. E. J. A STAT protein domain that determines DNA sequence recognition suggests a novel DNA-binding domain. *Genes Dev.* **9**, 984–994 (1995).
- 147. Schneider, W. M., Chevillotte, M. D. & Rice, C. M. Interferon-stimulated genes: a complex web of host defenses. *Annu. Rev. Immunol.* **32**, 513–545 (2014).
- 148. Starr, R. *et al.* A family of cytokine-inducible inhibitors of signalling. *Nature* **387**, 917–921 (1997).
- 149. Endo, T. A. *et al.* A new protein containing an SH2 domain that inhibits JAK kinases. *Nature* **387**, 921–924 (1997).
- 150. Naka, T. *et al.* Structure and function of a new STAT-induced STAT inhibitor. *Nature* **387**, 924–929 (1997).
- 151. Der, S. D., Zhou, A., Williams, B. R. & Silverman, R. H. Identification of genes differentially regulated by interferon alpha, beta, or gamma using oligonucleotide arrays. *Proc. Natl. Acad. Sci. U. S. A.* **95**, 15623–15628 (1998).
- 152. de Veer, M. J. *et al.* Functional classification of interferon-stimulated genes identified using microarrays. *J. Leukoc. Biol.* **69**, 912–920 (2001).
- 153. Samarajiwa, S. A., Forster, S., Auchettl, K. & Hertzog, P. J. INTERFEROME: the database of interferon regulated genes. *Nucleic Acids Res.* **37**, D852-7 (2009).
- 154. Shaw, A. E. *et al.* Fundamental properties of the mammalian innate immune system revealed by multispecies comparison of type I interferon responses. *PLoS Biol.* **15**, e2004086 (2017).
- 155. Munir, M. & Berg, M. The multiple faces of proteinkinase R in antiviral defense. *Virulence* **4**, 85–89 (2013).
- 156. Feng, G. S., Chong, K., Kumar, A. & Williams, B. R. Identification of double-stranded RNA-binding domains in the interferon-induced double-stranded RNA-activated p68 kinase. *Proc. Natl. Acad. Sci. U. S. A.* 89, 5447–5451 (1992).
- 157. Dever, T. E. *et al.* Mammalian eukaryotic initiation factor 2 alpha kinases functionally substitute for GCN2 protein kinase in the GCN4 translational control mechanism of yeast. *Proc. Natl. Acad. Sci. U. S. A.* **90**, 4616–4620 (1993).
- 158. Chong, K. L. *et al.* Human p68 kinase exhibits growth suppression in yeast and homology to the translational regulator GCN2. *EMBO J.* **11**, 1553–1562 (1992).
- 159. Nanduri, S., Carpick, B. W., Yang, Y., Williams, B. R. & Qin, J. Structure of the

- double-stranded RNA-binding domain of the protein kinase PKR reveals the molecular basis of its dsRNA-mediated activation. *EMBO J.* **17**, 5458–5465 (1998).
- 160. Gordiyenko, Y., Llácer, J. L. & Ramakrishnan, V. Structural basis for the inhibition of translation through eIF2α phosphorylation. *Nat. Commun.* **10**, 2640 (2019).
- 161. Fernandez, J., Yaman, I., Sarnow, P., Snider, M. D. & Hatzoglou, M. Regulation of internal ribosomal entry site-mediated translation by phosphorylation of the translation initiation factor eIF2alpha. *J. Biol. Chem.* **277**, 19198–19205 (2002).
- 162. Williams, B. R. PKR; a sentinel kinase for cellular stress. *Oncogene* **18**, 6112–6120 (1999).
- 163. Williams, B. R. Signal integration via PKR. Sci. STKE 2001, re2 (2001).
- 164. Kumar, A., Haque, J., Lacoste, J., Hiscott, J. & Williams, B. R. Double-stranded RNA-dependent protein kinase activates transcription factor NF-kappa B by phosphorylating I kappa B. *Proc. Natl. Acad. Sci. U. S. A.* **91**, 6288–6292 (1994).
- 165. Koromilas, A. E. *et al.* The interferon-inducible protein kinase PKR modulates the transcriptional activation of immunoglobulin kappa gene. *J. Biol. Chem.* **270**, 25426–25434 (1995).
- 166. McAllister, C. S., Taghavi, N. & Samuel, C. E. Protein kinase PKR amplification of interferon β induction occurs through initiation factor eIF-2α-mediated translational control. *J. Biol. Chem.* **287**, 36384–36392 (2012).
- 167. Diebold, S. S. *et al.* Viral infection switches non-plasmacytoid dendritic cells into high interferon producers. *Nature* **424**, 324–328 (2003).
- 168. McAllister, C. S. & Samuel, C. E. The RNA-activated protein kinase enhances the induction of interferon-beta and apoptosis mediated by cytoplasmic RNA sensors. *J. Biol. Chem.* **284**, 1644–1651 (2009).
- 169. Smith, E. J., Marié, I., Prakash, A., García-Sastre, A. & Levy, D. E. IRF3 and IRF7 phosphorylation in virus-infected cells does not require double-stranded RNA-dependent protein kinase R or Ikappa B kinase but is blocked by Vaccinia virus E3L protein. *J. Biol. Chem.* 276, 8951–8957 (2001).
- 170. Schulz, O. *et al.* Protein kinase R contributes to immunity against specific viruses by regulating interferon mRNA integrity. *Cell Host Microbe* **7**, 354–361 (2010).
- 171. Takeuchi, O. & Akira, S. MDA5/RIG-I and virus recognition. *Curr. Opin. Immunol.* **20**, 17–22 (2008).
- 172. Kristiansen, H., Gad, H. H., Eskildsen-Larsen, S., Despres, P. & Hartmann, R. The oligoadenylate synthetase family: an ancient protein family with multiple antiviral activities. *J. Interf. cytokine Res. Off. J. Int. Soc. Interf. Cytokine Res.* **31**, 41–47 (2011).
- 173. Hovanessian, A. G., Brown, R. E. & Kerr, I. M. Synthesis of low molecular weight inhibitor of protein synthesis with enzyme from interferon-treated cells. *Nature* **268**, 537–540 (1977).
- 174. Slattery, E., Ghosh, N., Samanta, H. & Lengyel, P. Interferon, double-stranded RNA, and RNA degradation: activation of an endonuclease by (2'-5')An. *Proc. Natl. Acad. Sci. U. S. A.* **76**, 4778–4782 (1979).
- 175. Chebath, J., Benech, P., Hovanessian, A., Galabru, J. & Revel, M. Four different forms of interferon-induced 2',5'-oligo(A) synthetase identified by immunoblotting in human cells. *J. Biol. Chem.* **262**, 3852–3857 (1987).
- 176. Marié, I. & Hovanessian, A. G. The 69-kDa 2-5A synthetase is composed of two homologous and adjacent functional domains. *J. Biol. Chem.* **267**, 9933–9939

- (1992).
- 177. Coccia, E. M. *et al.* Activation and repression of the 2-5A synthetase and p21 gene promoters by IRF-1 and IRF-2. *Oncogene* **18**, 2129–2137 (1999).
- 178. Melchjorsen, J. *et al.* Differential regulation of the OASL and OAS1 genes in response to viral infections. *J. Interf. cytokine Res. Off. J. Int. Soc. Interf. Cytokine Res.* **29**, 199–207 (2009).
- 179. Hartmann, R., Justesen, J., Sarkar, S. N., Sen, G. C. & Yee, V. C. Crystal structure of the 2'-specific and double-stranded RNA-activated interferon-induced antiviral protein 2'-5'-oligoadenylate synthetase. *Mol. Cell* 12, 1173–1185 (2003).
- 180. Sarkar, S. N., Ghosh, A., Wang, H. W., Sung, S. S. & Sen, G. C. The nature of the catalytic domain of 2'-5'-oligoadenylate synthetases. *J. Biol. Chem.* **274**, 25535–25542 (1999).
- 181. Roberts, W. K., Hovanessian, A., Brown, R. E., Clemens, M. J. & Kerr, I. M. Interferon-mediated protein kinase and low-molecular-weight inhibitor of protein synthesis. *Nature* **264**, 477–480 (1976).
- 182. Kerr, I. M., Brown, R. E. & Hovanessian, A. G. Nature of inhibitor of cell-free protein synthesis formed in response to interferon and double-stranded RNA. *Nature* **268**, 540–542 (1977).
- 183. Baglioni, C., Minks, M. A. & Maroney, P. A. Interferon action may be mediated by activation of a nuclease by pppA2'p5'A2'p5'A. *Nature* **273**, 684–687 (1978).
- 184. Zhou, A. *et al.* Interferon action and apoptosis are defective in mice devoid of 2',5'-oligoadenylate-dependent RNase L. *EMBO J.* **16**, 6355–6363 (1997).
- 185. Marques, J. *et al.* The p59 oligoadenylate synthetase-like protein possesses antiviral activity that requires the C-terminal ubiquitin-like domain. *J. Gen. Virol.* **89**, 2767–2772 (2008).
- 186. Zhu, J. *et al.* Antiviral activity of human OASL protein is mediated by enhancing signaling of the RIG-I RNA sensor. *Immunity* **40**, 936–948 (2014).
- 187. Diamond, M. S. & Farzan, M. The broad-spectrum antiviral functions of IFIT and IFITM proteins. *Nat. Rev. Immunol.* **13**, 46–57 (2013).
- 188. Chebath, J., Merlin, G., Metz, R., Benech, P. & Revel, M. Interferon-induced 56,000 Mr protein and its mRNA in human cells: molecular cloning and partial sequence of the cDNA. *Nucleic Acids Res.* **11**, 1213–1226 (1983).
- 189. Kusari, J. & Sen, G. C. Transcriptional analyses of interferon-inducible mRNAs. *Mol. Cell. Biol.* **7**, 528–531 (1987).
- 190. Levy, D., Larner, A., Chaudhuri, A., Babiss, L. E. & Darnell, J. E. J. Interferon-stimulated transcription: isolation of an inducible gene and identification of its regulatory region. *Proc. Natl. Acad. Sci. U. S. A.* **83**, 8929–8933 (1986).
- 191. Wathelet, M. *et al.* Molecular cloning, full-length sequence and preliminary characterization of a 56-kDa protein induced by human interferons. *Eur. J. Biochem.* **155**, 11–17 (1986).
- 192. Smith, J. B. & Herschman, H. R. The glucocorticoid attenuated response genes GARG-16, GARG-39, and GARG-49/IRG2 encode inducible proteins containing multiple tetratricopeptide repeat domains. *Arch. Biochem. Biophys.* **330**, 290–300 (1996).
- 193. Niikura, T., Hirata, R. & Weil, S. C. A novel interferon-inducible gene expressed during myeloid differentiation. *Blood Cells. Mol. Dis.* **23**, 337–349 (1997).
- 194. Yu, M. et al. Cloning of a gene (RIG-G) associated with retinoic acid-induced differentiation of acute promyelocytic leukemia cells and representing a new

- member of a family of interferon-stimulated genes. *Proc. Natl. Acad. Sci. U. S. A.* **94**, 7406–7411 (1997).
- 195. Zhu, H., Cong, J. P. & Shenk, T. Use of differential display analysis to assess the effect of human cytomegalovirus infection on the accumulation of cellular RNAs: induction of interferon-responsive RNAs. *Proc. Natl. Acad. Sci. U. S. A.* **94**, 13985–13990 (1997).
- 196. Zhang, Y., Burke, C. W., Ryman, K. D. & Klimstra, W. B. Identification and characterization of interferon-induced proteins that inhibit alphavirus replication. *J. Virol.* **81**, 11246–11255 (2007).
- 197. Guo, J., Hui, D. J., Merrick, W. C. & Sen, G. C. A new pathway of translational regulation mediated by eukaryotic initiation factor 3. *EMBO J.* **19**, 6891–6899 (2000).
- 198. Daffis, S. *et al.* 2'-O methylation of the viral mRNA cap evades host restriction by IFIT family members. *Nature* **468**, 452–456 (2010).
- 199. Szretter, K. J. *et al.* 2'-O methylation of the viral mRNA cap by West Nile virus evades ifit1-dependent and -independent mechanisms of host restriction in vivo. *PLoS Pathog.* **8**, e1002698 (2012).
- 200. Züst, R. *et al.* Ribose 2'-O-methylation provides a molecular signature for the distinction of self and non-self mRNA dependent on the RNA sensor Mda5. *Nat. Immunol.* **12**, 137–143 (2011).
- 201. Indraccolo, S. *et al.* Identification of genes selectively regulated by IFNs in endothelial cells. *J. Immunol.* **178**, 1122–1135 (2007).
- 202. Zhou, Z. *et al.* Type III interferon (IFN) induces a type I IFN-like response in a restricted subset of cells through signaling pathways involving both the Jak-STAT pathway and the mitogen-activated protein kinases. *J. Virol.* **81**, 7749–7758 (2007).
- 203. Severa, M., Coccia, E. M. & Fitzgerald, K. A. Toll-like receptor-dependent and independent viperin gene expression and counter-regulation by PRDI-binding factor-1/BLIMP1. *J. Biol. Chem.* **281**, 26188–26195 (2006).
- 204. Chin, K. C. & Cresswell, P. Viperin (cig5), an IFN-inducible antiviral protein directly induced by human cytomegalovirus. *Proc. Natl. Acad. Sci. U. S. A.* **98**, 15125–15130 (2001).
- 205. Stirnweiss, A. *et al.* IFN regulatory factor-1 bypasses IFN-mediated antiviral effects through viperin gene induction. *J. Immunol.* **184**, 5179–5185 (2010).
- 206. DeFilippis, V. R. *et al.* Interferon regulatory factor 3 is necessary for induction of antiviral genes during human cytomegalovirus infection. *J. Virol.* **80**, 1032–1037 (2006).
- 207. Szretter, K. J. *et al.* The interferon-inducible gene viperin restricts West Nile virus pathogenesis. *J. Virol.* **85**, 11557–11566 (2011).
- 208. Wang, X., Hinson, E. R. & Cresswell, P. The interferon-inducible protein viperin inhibits influenza virus release by perturbing lipid rafts. *Cell Host Microbe* **2**, 96–105 (2007).
- 209. Nasr, N. et al. HIV-1 infection of human macrophages directly induces viperin which inhibits viral production. *Blood* **120**, 778–788 (2012).
- 210. Matikainen, S. *et al.* Tumor necrosis factor alpha enhances influenza A virusinduced expression of antiviral cytokines by activating RIG-I gene expression. *J. Virol.* **80**, 3515–3522 (2006).
- 211. Imaizumi, T. et al. Expression of retinoic acid-inducible gene-I (RIG-I) in

- macrophages: possible involvement of RIG-I in atherosclerosis. *J. Atheroscler. Thromb.* **14**, 51–55 (2007).
- 212. Matsumiya, T., Prescott, S. M. & Stafforini, D. M. IFN-epsilon mediates TNF-alpha-induced STAT1 phosphorylation and induction of retinoic acid-inducible gene-I in human cervical cancer cells. *J. Immunol.* **179**, 4542–4549 (2007).
- 213. Imaizumi, T. *et al.* Involvement of retinoic acid-inducible gene-I in the IFN-{gamma}/STAT1 signalling pathway in BEAS-2B cells. *Eur. Respir. J.* **25**, 1077–1083 (2005).
- 214. Schlee, M. & Hartmann, G. Discriminating self from non-self in nucleic acid sensing. *Nat. Rev. Immunol.* **16**, 566–580 (2016).
- 215. Weber, F., Wagner, V., Rasmussen, S. B., Hartmann, R. & Paludan, S. R. Double-stranded RNA is produced by positive-strand RNA viruses and DNA viruses but not in detectable amounts by negative-strand RNA viruses. *J. Virol.* **80**, 5059–5064 (2006).
- 216. Alexopoulou, L., Holt, A. C., Medzhitov, R. & Flavell, R. A. Recognition of double-stranded RNA and activation of NF-kappaB by Toll-like receptor 3. *Nature* **413**, 732–738 (2001).
- 217. Yoneyama, M. *et al.* The RNA helicase RIG-I has an essential function in double-stranded RNA-induced innate antiviral responses. *Nat. Immunol.* **5**, 730–737 (2004).
- 218. Kato, H. *et al.* Length-dependent recognition of double-stranded ribonucleic acids by retinoic acid-inducible gene-I and melanoma differentiation-associated gene 5. *J. Exp. Med.* **205**, 1601–1610 (2008).
- 219. Gitlin, L. *et al.* Essential role of mda-5 in type I IFN responses to polyriboinosinic:polyribocytidylic acid and encephalomyocarditis picornavirus. *Proc. Natl. Acad. Sci. U. S. A.* **103**, 8459–8464 (2006).
- 220. Dhir, A. *et al.* Mitochondrial double-stranded RNA triggers antiviral signalling in humans. *Nature* **560**, 238–242 (2018).
- 221. Lamers, M. M., van den Hoogen, B. G. & Haagmans, B. L. ADAR1: 'Editor-in-Chief' of Cytoplasmic Innate Immunity. *Front. Immunol.* **10**, 1763 (2019).
- 222. Bass, B. L. & Weintraub, H. A developmentally regulated activity that unwinds RNA duplexes. *Cell* **48**, 607–613 (1987).
- 223. Rebagliati, M. R. & Melton, D. A. Antisense RNA injections in fertilized frog eggs reveal an RNA duplex unwinding activity. *Cell* **48**, 599–605 (1987).
- 224. Wagner, R. W., Smith, J. E., Cooperman, B. S. & Nishikura, K. A double-stranded RNA unwinding activity introduces structural alterations by means of adenosine to inosine conversions in mammalian cells and Xenopus eggs. *Proc. Natl. Acad. Sci. U. S. A.* **86**, 2647–2651 (1989).
- 225. Hough, R. F. & Bass, B. L. Purification of the Xenopus laevis double-stranded RNA adenosine deaminase. *J. Biol. Chem.* **269**, 9933–9939 (1994).
- 226. BASILIO, C., WAHBA, A. J., LENGYEL, P., SPEYER, J. F. & OCHOA, S. Synthetic polynucleotides and the amino acid code. V. *Proc. Natl. Acad. Sci. U. S. A.* **48**, 613–616 (1962).
- 227. Chung, H. *et al.* Human ADAR1 Prevents Endogenous RNA from Triggering Translational Shutdown. *Cell* **172**, 811-824.e14 (2018).
- 228. Sauer, M. et al. DHX36 prevents the accumulation of translationally inactive mRNAs with G4-structures in untranslated regions. *Nat. Commun.* **10**, 2421 (2019).

- 229. GELLERT, M., LIPSETT, M. N. & DAVIES, D. R. Helix formation by guanylic acid. *Proc. Natl. Acad. Sci. U. S. A.* **48**, 2013–2018 (1962).
- 230. Arnott, S., Chandrasekaran, R. & Marttila, C. M. Structures for polyinosinic acid and polyguanylic acid. *Biochem. J.* **141**, 537–543 (1974).
- 231. Pan, B., Xiong, Y., Shi, K. & Sundaralingam, M. Crystal structure of a bulged RNA tetraplex at 1.1 a resolution: implications for a novel binding site in RNA tetraplex. *Structure* **11**, 1423–1430 (2003).
- 232. Tippana, R., Xiao, W. & Myong, S. G-quadruplex conformation and dynamics are determined by loop length and sequence. *Nucleic Acids Res.* **42**, 8106–8114 (2014).
- 233. Zhang, D.-H. *et al.* Monomorphic RNA G-quadruplex and polymorphic DNA G-quadruplex structures responding to cellular environmental factors. *Biochemistry* **49**, 4554–4563 (2010).
- 234. Williamson, J. R., Raghuraman, M. K. & Cech, T. R. Monovalent cation-induced structure of telomeric DNA: the G-quartet model. *Cell* **59**, 871–880 (1989).
- 235. Sen, D. & Gilbert, W. A sodium-potassium switch in the formation of four-stranded G4-DNA. *Nature* **344**, 410–414 (1990).
- 236. Chambers, V. S. *et al.* High-throughput sequencing of DNA G-quadruplex structures in the human genome. *Nat. Biotechnol.* **33**, 877–881 (2015).
- 237. Marsico, G. *et al.* Whole genome experimental maps of DNA G-quadruplexes in multiple species. *Nucleic Acids Res.* **47**, 3862–3874 (2019).
- 238. Huppert, J. L. & Balasubramanian, S. Prevalence of quadruplexes in the human genome. *Nucleic Acids Res.* **33**, 2908–2916 (2005).
- 239. Hänsel-Hertsch, R. *et al.* G-quadruplex structures mark human regulatory chromatin. *Nat. Genet.* **48**, 1267–1272 (2016).
- 240. Lyu, J., Shao, R., Kwong Yung, P. Y. & Elsässer, S. J. Genome-wide mapping of G-quadruplex structures with CUT&Tag. *Nucleic Acids Res.* **50**, e13 (2022).
- 241. Kwok, C. K., Marsico, G., Sahakyan, A. B., Chambers, V. S. & Balasubramanian, S. rG4-seq reveals widespread formation of G-quadruplex structures in the human transcriptome. *Nat. Methods* **13**, 841–844 (2016).
- 242. Guo, J. U. & Bartel, D. P. RNA G-quadruplexes are globally unfolded in eukaryotic cells and depleted in bacteria. *Science* **353**, (2016).
- 243. Huppert, J. L. & Balasubramanian, S. G-quadruplexes in promoters throughout the human genome. *Nucleic Acids Res.* **35**, 406–413 (2007).
- 244. Leppek, K., Das, R. & Barna, M. Functional 5' UTR mRNA structures in eukaryotic translation regulation and how to find them. *Nat. Rev. Mol. Cell Biol.* **19**, 158–174 (2018).
- 245. Liu, H., Matsugami, A., Katahira, M. & Uesugi, S. A dimeric RNA quadruplex architecture comprised of two G:G(:A):G:G(:A) hexads, G:G:G:G tetrads and UUUU loops. *J. Mol. Biol.* **322**, 955–970 (2002).
- 246. Christiansen, J., Kofod, M. & Nielsen, F. C. A guanosine quadruplex and two stable hairpins flank a major cleavage site in insulin-like growth factor II mRNA. *Nucleic Acids Res.* **22**, 5709–5716 (1994).
- 247. Bonnal, S. *et al.* A single internal ribosome entry site containing a G quartet RNA structure drives fibroblast growth factor 2 gene expression at four alternative translation initiation codons. *J. Biol. Chem.* **278**, 39330–39336 (2003).
- 248. Al-Zeer, M. A. & Kurreck, J. Deciphering the Enigmatic Biological Functions of RNA Guanine-Quadruplex Motifs in Human Cells. *Biochemistry* **58**, 305–311

- (2019).
- 249. Matsumura, K. *et al.* The novel G-quadruplex-containing long non-coding RNA GSEC antagonizes DHX36 and modulates colon cancer cell migration. *Oncogene* **36**, 1191–1199 (2017).
- 250. Singleton, M. R., Dillingham, M. S. & Wigley, D. B. Structure and mechanism of helicases and nucleic acid translocases. *Annu. Rev. Biochem.* **76**, 23–50 (2007).
- 251. Fairman-Williams, M. E., Guenther, U.-P. & Jankowsky, E. SF1 and SF2 helicases: family matters. *Curr. Opin. Struct. Biol.* **20**, 313–324 (2010).
- 252. Linder, P. et al. Birth of the D-E-A-D box. Nature vol. 337 121–122 (1989).
- 253. Tran, H., Schilling, M., Wirbelauer, C., Hess, D. & Nagamine, Y. Facilitation of mRNA deadenylation and decay by the exosome-bound, DExH protein RHAU. *Mol. Cell* **13**, 101–111 (2004).
- 254. Chalupníková, K. *et al.* Recruitment of the RNA helicase RHAU to stress granules via a unique RNA-binding domain. *J. Biol. Chem.* **283**, 35186–35198 (2008).
- 255. Vaughn, J. P. *et al.* The DEXH protein product of the DHX36 gene is the major source of tetramolecular quadruplex G4-DNA resolving activity in HeLa cell lysates. *J. Biol. Chem.* **280**, 38117–38120 (2005).
- 256. Booy, E. P. *et al.* The RNA helicase RHAU (DHX36) unwinds a G4-quadruplex in human telomerase RNA and promotes the formation of the P1 helix template boundary. *Nucleic Acids Res.* **40**, 4110–4124 (2012).
- 257. Chen, M. C. *et al.* Structural basis of G-quadruplex unfolding by the DEAH/RHA helicase DHX36. *Nature* **558**, 465–469 (2018).
- 258. Giri, B. *et al.* G4 resolvase 1 tightly binds and unwinds unimolecular G4-DNA. *Nucleic Acids Res.* **39**, 7161–7178 (2011).
- 259. Lattmann, S., Giri, B., Vaughn, J. P., Akman, S. A. & Nagamine, Y. Role of the amino terminal RHAU-specific motif in the recognition and resolution of guanine quadruplex-RNA by the DEAH-box RNA helicase RHAU. *Nucleic Acids Res.* **38**, 6219–6233 (2010).
- 260. Creacy, S. D. *et al.* G4 resolvase 1 binds both DNA and RNA tetramolecular quadruplex with high affinity and is the major source of tetramolecular quadruplex G4-DNA and G4-RNA resolving activity in HeLa cell lysates. *J. Biol. Chem.* **283**, 34626–34634 (2008).
- 261. Umate, P., Tuteja, N. & Tuteja, R. Genome-wide comprehensive analysis of human helicases. *Commun. Integr. Biol.* **4**, 118–137 (2011).
- 262. Heddi, B., Cheong, V. V., Martadinata, H. & Phan, A. T. Insights into G-quadruplex specific recognition by the DEAH-box helicase RHAU: Solution structure of a peptide-quadruplex complex. *Proc. Natl. Acad. Sci. U. S. A.* 112, 9608–9613 (2015).
- 263. Tippana, R., Hwang, H., Opresko, P. L., Bohr, V. A. & Myong, S. Single-molecule imaging reveals a common mechanism shared by G-quadruplex-resolving helicases. *Proc. Natl. Acad. Sci. U. S. A.* **113**, 8448–8453 (2016).
- 264. Yangyuoru, P. M., Bradburn, D. A., Liu, Z., Xiao, T. S. & Russell, R. The G-quadruplex (G4) resolvase DHX36 efficiently and specifically disrupts DNA G4s via a translocation-based helicase mechanism. *J. Biol. Chem.* 293, 1924–1932 (2018).
- 265. Gueddouda, N. M., Mendoza, O., Gomez, D., Bourdoncle, A. & Mergny, J.-L. G-quadruplexes unfolding by RHAU helicase. *Biochim. Biophys. acta. Gen. Subj.* **1861**, 1382–1388 (2017).

- 266. Tippana, R., Chen, M. C., Demeshkina, N. A., Ferré-D'Amaré, A. R. & Myong, S. RNA G-quadruplex is resolved by repetitive and ATP-dependent mechanism of DHX36. *Nat. Commun.* **10**, 1855 (2019).
- 267. Pipier, A. et al. Transcription-associated topoisomerase activities control DNA-breaks production by G-quadruplex ligands. bioRxiv 2020.02.18.953851 (2020) doi:10.1101/2020.02.18.953851.
- 268. Bossaert, M. *et al.* Transcription-associated topoisomerase 2α (TOP2A) activity is a major effector of cytotoxicity induced by G-quadruplex ligands. *Elife* **10**, (2021).
- 269. De Magis, A. *et al.* DNA damage and genome instability by G-quadruplex ligands are mediated by R loops in human cancer cells. *Proc. Natl. Acad. Sci. U. S. A.* **116**, 816–825 (2019).
- 270. Lai, J. C. *et al.* The DEAH-box helicase RHAU is an essential gene and critical for mouse hematopoiesis. *Blood* **119**, 4291–4300 (2012).
- 271. Gao, X. *et al.* A G-quadruplex DNA structure resolvase, RHAU, is essential for spermatogonia differentiation. *Cell Death Dis.* **6**, e1610 (2015).
- 272. Nie, J. *et al.* Post-transcriptional Regulation of Nkx2-5 by RHAU in Heart Development. *Cell Rep.* **13**, 723–732 (2015).
- 273. Williams, A. B. & Schumacher, B. p53 in the DNA-Damage-Repair Process. *Cold Spring Harb. Perspect. Med.* **6**, (2016).
- 274. Gros, J., Guédin, A., Mergny, J.-L. & Lacroix, L. G-Quadruplex formation interferes with P1 helix formation in the RNA component of telomerase hTERC. *Chembiochem* **9**, 2075–2079 (2008).
- 275. Li, X. et al. Structure, interactions and effects on activity of the 5'-terminal region of human telomerase RNA. *J. Biochem.* **141**, 755–765 (2007).
- 276. Sexton, A. N. & Collins, K. The 5' guanosine tracts of human telomerase RNA are recognized by the G-quadruplex binding domain of the RNA helicase DHX36 and function to increase RNA accumulation. *Mol. Cell. Biol.* **31**, 736–743 (2011).
- 277. Murat, P. *et al.* RNA G-quadruplexes at upstream open reading frames cause DHX36- and DHX9-dependent translation of human mRNAs. *Genome Biol.* **19**, 229 (2018).
- 278. Gao, J. *et al.* Integrative analysis of complex cancer genomics and clinical profiles using the cBioPortal. *Sci. Signal.* **6**, pl1 (2013).
- 279. Bohálová, N. *et al.* Analyses of viral genomes for G-quadruplex forming sequences reveal their correlation with the type of infection. *Biochimie* **186**, 13–27 (2021).
- 280. Cui, H. & Zhang, L. G-Quadruplexes Are Present in Human Coronaviruses Including SARS-CoV-2. *Front. Microbiol.* **11**, 567317 (2020).
- 281. Butovskaya, E., Soldà, P., Scalabrin, M., Nadai, M. & Richter, S. N. HIV-1 Nucleocapsid Protein Unfolds Stable RNA G-Quadruplexes in the Viral Genome and Is Inhibited by G-Quadruplex Ligands. *ACS Infect. Dis.* **5**, 2127–2135 (2019).
- 282. Calderone, A., Licata, L. & Cesareni, G. VirusMentha: a new resource for virus-host protein interactions. *Nucleic Acids Res.* **43**, D588-92 (2015).
- 283. Naji, S. *et al.* Host cell interactome of HIV-1 Rev includes RNA helicases involved in multiple facets of virus production. *Mol. Cell. Proteomics* **11**, M111.015313 (2012).
- 284. Wang, L. *et al.* Comparative influenza protein interactomes identify the role of plakophilin 2 in virus restriction. *Nat. Commun.* **8**, 13876 (2017).
- 285. Tsai, W.-C. & Lloyd, R. E. Cytoplasmic RNA Granules and Viral Infection. Annu.

- Rev. Virol. 1, 147-170 (2014).
- 286. Brangwynne, C. P. Phase transitions and size scaling of membrane-less organelles. *J. Cell Biol.* **203**, 875–881 (2013).
- 287. Brangwynne, C. P. *et al.* Germline P granules are liquid droplets that localize by controlled dissolution/condensation. *Science* **324**, 1729–1732 (2009).
- 288. Yoo, J.-S. *et al.* DHX36 enhances RIG-I signaling by facilitating PKR-mediated antiviral stress granule formation. *PLoS Pathog.* **10**, e1004012 (2014).
- 289. Zhang, Z. *et al.* DDX1, DDX21, and DHX36 helicases form a complex with the adaptor molecule TRIF to sense dsRNA in dendritic cells. *Immunity* **34**, 866–878 (2011).
- 290. Jing, H. *et al.* DExD/H-Box Helicase 36 Signaling via Myeloid Differentiation Primary Response Gene 88 Contributes to NF-κB Activation to Type 2 Porcine Reproductive and Respiratory Syndrome Virus Infection. *Front. Immunol.* **8**, 1365 (2017).
- 291. Trapnell, C. *et al.* Differential gene and transcript expression analysis of RNA-seq experiments with TopHat and Cufflinks. *Nat. Protoc.* **7**, 562–578 (2012).
- 292. Meier-Stephenson, V., Mrozowich, T., Pham, M. & Patel, T. R. DEAD-box helicases: the Yin and Yang roles in viral infections. *Biotechnol. Genet. Eng. Rev.* **34**, 3–32 (2018).
- 293. Schuringa, J. J., Wierenga, A. T., Kruijer, W. & Vellenga, E. Constitutive Stat3, Tyr705, and Ser727 phosphorylation in acute myeloid leukemia cells caused by the autocrine secretion of interleukin-6. *Blood* **95**, 3765–3770 (2000).
- 294. Brender, C. *et al.* STAT3-mediated constitutive expression of SOCS-3 in cutaneous T-cell lymphoma. *Blood* **97**, 1056–1062 (2001).
- 295. Sakai, I., Takeuchi, K., Yamauchi, H., Narumi, H. & Fujita, S. Constitutive expression of SOCS3 confers resistance to IFN-alpha in chronic myelogenous leukemia cells. *Blood* **100**, 2926–2931 (2002).
- 296. Hornung, V. *et al.* Quantitative expression of toll-like receptor 1-10 mRNA in cellular subsets of human peripheral blood mononuclear cells and sensitivity to CpG oligodeoxynucleotides. *J. Immunol.* **168**, 4531–4537 (2002).
- 297. Zheng, Q., Hou, J., Zhou, Y., Li, Z. & Cao, X. The RNA helicase DDX46 inhibits innate immunity by entrapping m(6)A-demethylated antiviral transcripts in the nucleus. *Nat. Immunol.* **18**, 1094–1103 (2017).
- 298. Miyashita, M., Oshiumi, H., Matsumoto, M. & Seya, T. DDX60, a DEXD/H box helicase, is a novel antiviral factor promoting RIG-I-like receptor-mediated signaling. *Mol. Cell. Biol.* **31**, 3802–3819 (2011).
- 299. Schult, P. & Paeschke, K. The DEAH helicase DHX36 and its role in G-quadruplex-dependent processes. *Biol. Chem.* **402**, 581–591 (2021).
- 300. Zan, J. *et al.* RNA helicase DDX5 suppresses IFN-I antiviral innate immune response by interacting with PP2A-Cβ to deactivate IRF3. *Exp. Cell Res.* **396**, 112332 (2020).
- 301. Xu, S. *et al.* DDX56 antagonizes IFN-β production to enhance EMCV replication by inhibiting IRF3 nuclear translocation. *Vet. Microbiol.* **264**, 109304 (2022).
- 302. Feng, T. *et al.* DEAD-Box Helicase DDX25 Is a Negative Regulator of Type I Interferon Pathway and Facilitates RNA Virus Infection. *Front. Cell. Infect. Microbiol.* **7**, 356 (2017).
- 303. Mojzesz, M. et al. Viral infection-induced changes in the expression profile of non-RLR DExD/H-box RNA helicases (DDX1, DDX3, DHX9, DDX21 and DHX36) in

- zebrafish and common carp. Fish Shellfish Immunol. 104, 62-73 (2020).
- 304. Zhang, P. & Samuel, C. E. Induction of protein kinase PKR-dependent activation of interferon regulatory factor 3 by vaccinia virus occurs through adapter IPS-1 signaling. *J. Biol. Chem.* **283**, 34580–34587 (2008).
- 305. Nie, Y., Hammond, G. L. & Yang, J.-H. Double-stranded RNA deaminase ADAR1 increases host susceptibility to virus infection. *J. Virol.* **81**, 917–923 (2007).
- 306. John, L. & Samuel, C. E. Induction of stress granules by interferon and down-regulation by the cellular RNA adenosine deaminase ADAR1. *Virology* **454–455**, 299–310 (2014).
- 307. Okonski, K. M. & Samuel, C. E. Stress granule formation induced by measles virus is protein kinase PKR dependent and impaired by RNA adenosine deaminase ADAR1. *J. Virol.* **87**, 756–766 (2013).
- 308. Ahmad, S. *et al.* Breaching Self-Tolerance to Alu Duplex RNA Underlies MDA5-Mediated Inflammation. *Cell* **172**, 797-810.e13 (2018).
- 309. Mitteaux, J. et al. Identifying G-Quadruplex-DNA-Disrupting Small Molecules. J. Am. Chem. Soc. 143, 12567–12577 (2021).
- 310. Ripin, N. *et al.* Molecular basis for AU-rich element recognition and dimerization by the HuR C-terminal RRM. *Proc. Natl. Acad. Sci. U. S. A.* **116**, 2935–2944 (2019).
- 311. Badawi, A., Hehlgans, S., Pfeilschifter, J., Rödel, F. & Eberhardt, W. Silencing of the mRNA-binding protein HuR increases the sensitivity of colorectal cancer cells to ionizing radiation through upregulation of caspase-2. *Cancer Lett.* 393, 103–112 (2017).
- 312. Herviou, P. *et al.* hnRNP H/F drive RNA G-quadruplex-mediated translation linked to genomic instability and therapy resistance in glioblastoma. *Nat. Commun.* **11**, 2661 (2020).
- 313. Yang, Q. & Shu, H.-B. Deciphering the pathways to antiviral innate immunity and inflammation. *Adv. Immunol.* **145**, 1–36 (2020).

10. Acknowledgements

"I know. It's all wrong. By rights we shouldn't even be here. But we are. It's like in the great stories. The ones that really mattered. Full of darkness and danger they were, and sometimes you didn't want to know the end. Because how could the end be happy. How could the world go back to the way it was when so much bad happened? But in the end, it's only a passing thing, this shadow. Even darkness must pass. A new day will come. And when the sun shines it will shine out the clearer. Those were the stories that stayed with you. That meant something. Even if you were too small to understand why. But I think, I do understand. I know now. Folk in those stories had lots of chances of turning back only they didn't. Because they were holding on to something. That there's some good in this world and it's worth fighting for."Samwise Gamgee

Don't do a PhD they said. It is stressful, time consuming and brings nothing than pain. For sure, I couldn't resist this bidding and started it almost 5 years ago. Admittedly, there were times of pure frustration and suffering. Experiments didn't work out the way they should and the days in the lab became longer and longer. However, the good and funny times were surpassing all this. It was absolutely worth it! All these decisions shaped me and gave rise to the person I am right now. And I am deeply grateful for this.

First and foremost, I would like to thank my supervisor and mentor Prof. Dr. Katrin Paeschke for giving me the opportunity to work and thrive in her lab, for every scientific discussion, all the support and the precious advices that lead me the right way through the PhD.

I am grateful to the members of my thesis committee, my second supervisor Prof. Dr. Oliver Gruss, my third supervisor Prof. Dr. Hiroki Kato and my fourth supervisor Prof. Dr. Matthias Geyer for critically reading and evaluating my thesis as well as all discussions and feedback.

A special thanks to Dr. Markus Hafner for bioinformatical, practical, and all advices. Especially for the opportunity to visit his lab at the National Institute of Health and to perform critical experiments of my PhD in his laboratory. Thanks to Dr. Dimitrios Anastasakis who helped me in the wet lab during this time.

I want to thank Dr. Stefan Juranek for all unofficial lectures he conducted in the kitchen and the scientific questions he asked me. It helped me a lot to learn all the things I sadly forgot and also what I simply didn't know.

To all the former and current members of the Paeschke lab: Thank you! You made the life in the lab easier and more enjoyable. The countless coffee breaks, long, nasty, dirty and without any restrains, helped me throughout the whole PhD time. For sure the scientific support, physically and psychologically by: Melanie, mother of organization; Michi the brave Bavarian (Franconian); Eike, the oblivious boulderer; Alessio, the loud and dirty fitness guy; small Philipp, the small sweet lab puppy; big Philipp, metal Viking; Rebecca, the cheeky upside down Australian; Theresa and Lea, the ones who keep things running. Thank you, that you took your time and spent it with me. Also thanks to all the other people of the Medical Clinic II and III: Nici, the indecisive; Denise, rider of Rohan; Pia, composed fish pain lady. Most special thanks to Mona, the keeper of balance. Things would have ended differently without your help! Providing a room and warm meals, endless coffee support, and discussions about life and pain. Helping me whenever I was too blinded to see through the things I did and wanted to do.

Ich möchte mich auch bei meiner Familie bedanken. Ohne euch wäre ich nicht da, wo ich jetzt bin. Ihr habt mich immer mit Liebe behandelt und mir gezeigt, worauf es im Leben ankommt. Mich unterstützt, wo immer es ging und mich auf den richtigen Weg gebracht. Danke.

Eric, Pascal, Matti und Norm. Ihr seid die besten Freunde, die es gibt. Wann immer ich euch brauchte wart ihr da und auch sonst gebt ihr mir immer alles, was man sich wünschen kann. Viel Freude, alles Vertrauen der Welt und jede Menge Spaß dieses Leben zu dem zu machen was es sein soll. Danke für eure Unterstützung.

Kathi, mein kleiner feiner Begleiter. Mit ein paar Memes in mein Leben gesnacked und es unglaublich bereichert. Mit all deiner Zuneigung, Lustigkeit und Liebe hast du hast es mir erleichtert diese Zeit zu bestehen.

Tüdelü

Presentations

Talks

Hilbig D., Paeschke K.," The functions of the DEAH-box helicase DHX36 in type I IFN signaling ". CRC/Transregio 237 General Symposium, Austria. (November 2020)

Poster Presentation

- ❖ Hilbig D., Paeschke K.," The functions of the DEAH-box helicase DHX36 in type I IFN signaling ". Cluster Science Days 2020.
- ❖ Hilbig D., Paeschke K.," The functions of the DEAH-box helicase DHX36 in type I IFN signaling ". Cluster Science Days 2021.

Honors and Awards

- Cluster Science Days 2020 poster prize.
- Cluster Science Days 2021 poster prize.

Publications

- ❖ Ökmen B, Kemmerich B, Hilbig D, Wemhöner R, Aschenbroich J, Perrar A, Huesgen PF, Schipper K, Doehlemann G. Dual function of a secreted fungalysin metalloprotease in Ustilago maydis. New Phytol. 2018 Oct;220(1):249-261. doi: 10.1111/nph.15265. Epub 2018 Jun 19. PMID: 29916208.
- ❖ Sauer M, Juranek SA, Marks J, De Magis A, Kazemier HG, Hilbig D, Benhalevy D, Wang X, Hafner M, Paeschke K. DHX36 prevents the accumulation of translationally inactive mRNAs with G4-structures in untranslated regions. Nat Commun. 2019 Jun 3;10(1):2421. doi: 10.1038/s41467-019-10432-5. PMID: 31160600; PMCID: PMC6547686.